


COMPUTERISED

FORM 'A'

CERTIFIED that the work incorporated in thesis
"STUDY OF ELECTRICAL STRUCTURAL AND OPTICAL PROPERTIES
OF THICK FILMS OF Cd_2SnO_4 " submitted by Shri M.S. Setty
was carried out by the candidate under my supervision.
Such material as has been obtained from other sources
has been duly acknowledged in the thesis.

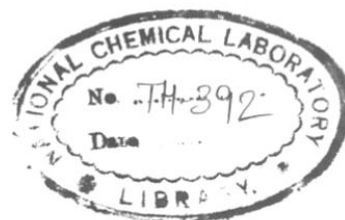

[A.P.B. Sinha]
Supervisor

STUDY OF ELECTRICAL, STRUCTURAL AND
OPTICAL PROPERTIES OF THICK FILMS OF Cd_2SnO_4

A Thesis
Submitted to
THE UNIVERSITY OF POONA
for
The Degree of
DOCTOR OF PHILOSOPHY
in Chemistry

By
M.S. SETTY, M.Sc.

COMPUTERISED



621.382:661.888.45(043)

SET

Physical Chemistry Division
National Chemical Laboratory
Poona-411008 (India)

*
1983

DEDICATED TO

MY

WIFE AND CHILDREN

ACKNOWLEDGEMENT

It gives me immense pleasure to express my indebtedness and to acknowledge my deep sense of gratitude to Dr. A.P.B. Sinha, F.N.A., Distinguished Scientist and Head, Physical Chemistry Division, National Chemical Laboratory, Pune, for suggesting this problem, inspiring guidance and keen interest throughout the course of this investigation.

My sincere thanks are due to all my colleagues for their wholehearted and ungrudging cooperation during the course of this work.

Finally, I am grateful to the Director, National Chemical Laboratory, Pune, for permitting me to submit this work in the form of a thesis.

M.S. Setty
[M.S. SETTY]

Poona
January 1983

C O N T E N T S

	Page No.
<u>CHAPTER - I : GENERAL INTRODUCTION</u>	1
<u>HISTORICAL SURVEY</u>	6
Structural properties	37
Burstein affect	54
Thick film technology	61
<u>CHAPTER - II : EXPERIMENTAL TECHNIQUES</u>	
2.1 Preparation of cadmium orthostannate	68
2.2 Formulation of the paste	71
2.3 Screen printing technique	77
2.4 Deposition of electrodes	90
2.5 Thermogravimetric analysis	90
2.6 X-ray analysis of PbO-doped Cd ₂ SnO ₄ thick films	92
2.7 Scanning electron microscope analysis	93
2.8 Electrical conductivity	94
2.9 Thermoemf measurements	95
2.10 Diffuse reflectance spectra	98
2.11 X-ray photoelectron spectroscopic analysis	99
2.12 Mossbauer spectroscopic analysis	100
<u>CHAPTER - III : RESULTS AND DISCUSSION</u>	
3.1 Thermogravimetric analysis	
1) 2 CdO + SnO ₂	102

	ii) Cd_2SnO_4	
	iii) 95 Cd_2SnO_4 + 5 glass	
3.2	X-ray diffraction	106
3.3	SEM results	124
3.4	Electrical conductivity (D.C.)	126
3.5	Thermoelectric measurements	145
3.6	Diffuse reflectance spectra results	148
3.7	X-ray photoelectron spectroscopic studies.	152
3.8	Mossbauer spectroscopic results.	158
<u>APPENDIX-I</u>	<u>A. I-V CHARACTERISTICS</u>	
A-1	Preparation of samples	161
A-2	Sample holder	161
A-3	Experimental set-up	161
A-4	Results and discussion	162
	<u>REFERENCES</u>	166
		175
<u>APPENDIX-II</u>	List of publications	184

CHAPTER - I : GENERAL INTRODUCTION
HISTORICAL SURVEY

General Introduction

Cd_2SnO_4 was first synthesised by Smith¹⁴ in 1960. Later, Nozik²³ characterised the semiconductor properties and predicted the possibility of using it as a transparent electrode.

Stannates were earlier used for colouring enamels¹ in ceramics and as additives in dielectric bodies¹¹ for decreasing the maturing temperature and improving the body density and the refractoriness.

Among the stannates, cadmium stannate has found wider applications in recent years. There are two distinct phases of CdO-SnO₂ system: cadmium metastannate (CdSnO₃) and cadmium orthostannate (Cd₂SnO₄). Both crystallise normally in orthorhombic structure.

Between the two stannates of cadmium, orthostannate phase has been more productive in its applications.

Cd₂SnO₄ is an n-type defect semiconductor^{23,72,77} which is transparent and highly conductive simultaneously. In most of the applications, thin films of Cd₂SnO₄ have been used. Oxygen vacancies provide donor states and are responsible for the high conductivity. Large Burstein shift²³ observed in the visible reflectance and transmission

spectra is the characteristic property of this transparent conductor.

Cd_2SnO_4 has been studied extensively for its electrical, structural and optical properties as thin film and as bulk material. Many methods of preparing thin films have been reported. Notable contributions have come chiefly from G. Haacke, A.J. Nozik and N. Miyata and their groups.

Vacuum evaporation,²⁴ d.c. reactive sputtering,^{63,64,75,81} rf sputtering,^{24,42,54,55,61,68,72,85} chemical vapour deposition²⁵, chemical spray deposition^{26,47,50,53,66}, dip coating⁷⁴ and ion plating⁸⁴ have been used for thin film preparation.

For many years, SnO_2 and $In_2O_3 \cdot SnO_2$ (ITO) were used as oxide transparent conductive coatings. Based on material property and economic factors, Cd_2SnO_4 was found to be more effective transparent electrode. Cadmium-tin oxide (CTO) has high figure of merit⁴³ as T.E. compared to ITO, SnO_2 or metal films.

The potential utility of Cd_2SnO_4 as T.E. material was first demonstrated in 1972.²³ Good conductor properties should occur in semiconductors with high mobilities and low effective mass for electrons.⁵²

There has been a big spurt of interest and activity in the study and applications of Cd_2SnO_4 films in the past 10 years or so as transparent conductor. This has resulted in a large number of publications in quick succession both as research papers and patents on the subject.

It has been used as transparent electrode for the back wall solar cells,^{26,41,45,59} electroluminescent devices,²⁴ as an ir window component for high power gas lasers,³⁹ electrochromic display devices^{40,82} and optoelectronic technology.⁵⁴ Thin films of Cd_2SnO_4 are transparent to solar radiation and reflective to thermal ir radiation.²⁴ This unique property has been made use of to augment solar thermal conversion efficiency^{47,49,50,54} in eye protective ir filters.⁴⁸ It is used for architectural window coatings,⁵¹ which transmit visible radiation but reflect ir portion of the incoming sunlight, Cd_2SnO_4 coatings are used in solar heat collectors.⁵⁶

Low resistance films are used in low voltage window de-misting and defrosting³⁰ of the aircraft. They are also used in photoconducting devices^{37,38} and in electrical heaters.⁶⁷ It has also been used as electrode in photogalvanic cells,⁵⁸ as anode for photoelectrolysis of water.⁷⁸

In spite of this impressive list of applications, the intrinsic properties of Cd_2SnO_4 have not been seriously studied. The fundamental properties like band gap and effective electron mass have not been clearly established. The effects of dopants on its properties have not been fully covered. There is, therefore, scope for basic studies to provide the needed scientific data.⁵²

It can also be seen that there is no reference in the literature about the study of Cd_2SnO_4 as thick films. Most of the work has been carried out on thin films or bulk material.

Thick film technology is a recent development. It is a new approach of fabricating components, devices and circuits in the field of hybrid microelectronics. There are certain advantages of the thick film technique which are explained in the body of the thesis. Dopant addition can closely be controlled. Stoichiometry of composition can be maintained. Processing of the material is easier. Very adherent films can be obtained. Being in between the thin film and bulk pellet as far as the thickness is concerned, the thick films provide interesting study.

In the light of the above observations, it was our endeavour to prepare highly conductive Cd_2SnO_4 thick films by chemical doping and offer plausible explanation for the conduction mechanism.

We have successfully adapted thick film technique for the preparation of the samples and their characterisation. The lead oxide dopant-induction is carried out subsequent to film deposition. This is done in a novel way. Doping is effected by including PbO with the other glass forming oxides which make the glass frit.

The results of our study are presented in three Chapters of the thesis. The first Chapter consists of the survey of literature. It includes general methods of preparation of Cd_2SnO_4 , structural disparities, transparent electrode characterisation and applications and Burstein effect. These have been described and discussed while reviewing the literature.

The second Chapter describes the preparation procedure of Cd_2SnO_4 . The X-ray data, thick film formulations, screen printing technique, thick film furnace fabrication, and experimental set ups for material characterisation are also included.

The third Chapter presents the results and discussion of thermogravimetric analysis, X-ray analysis, SEM, electrical conductivity, thermoemf, diffuse reflectance, ESCA and Mossbauer studies of the Cd_2SnO_4 thick films.

I. HISTORICAL SURVEY

Stannates were used in the dielectric bodies for the reasons that they were stable at ceramic temperatures and in the chemical environment. The earliest reference to the use of stannates in ceramics dates back to 1916.¹ Procedures for the preparation of stannates were available but not for their applications. Old English colour formulas are frequently referred to even to-day. Particular mention may be made to the calcium stannate in compounding chrome-tin reds. Because of the insoluble nature of the tin oxide in glass, it became a natural base, as an additive, for red and yellow glasses. Tin oxide produces opacity in glasses, glazes and enamels.

A series of patents were issued to Wainer²⁻⁵ and Wentworth⁶ for their work on stannates as ceramic dielectric bodies. As a matter of fact, Schusterius⁷ was the first to use tin compound in his development of dielectric material which had zero temperature coefficient^{of} capacitance. It was Kröger⁸ who described the cathodoluminescence of stannates in his book and has discussed the role of tin in phosphors. Kröger and Gerard⁹ patented the use of magnesium orthostannate as a phosphor base.

As the ionic radii of Ti^{4+} (0.68 \AA) and Sn^{4+} (0.71 \AA) are almost equal, and the analogous titanates and stannates

are isomorphous, there has been a big spurt in activity in this field.

Coffeen¹⁰ systematically studied a number of stannates as pure compounds for their dielectric properties. The precipitation method was chosen for their preparation because of better control of the stoichiometry. This was apparent in the case of the stannates of PbO (volatile nature) and Fe_2O_3 (variable valency). The hydrated stannates posed no problem in the studies. Thermal analysis provided information regarding the dehydration temperature, phase change, etc. It was particularly helpful to him in estimating the reaction temperature of a particular stannate. He presented the X-ray data for the hydrated and anhydrous stannates of Ba, Ca, Sr, Mg, Pb, Bi, Co, Ni, Cu, Zn, Cd, Fe(ous), Fe(ic) and Mn. He did not, however, index the interplanar distances. The electrical conductivity, dielectric and ceramic properties were measured at room temperature.

He¹¹ further studied these properties of binary systems of stannates of Mg, Pb, Bi, Zn, Ni, Cu, Cd, Co, Mn and Fe with barium titanate. Addition of these stannates had effectively decreased the maturing temperature and improved the body density and the refractoriness of BaTiO_3 .

Cadmium stannate (CdSnO_3) was first prepared by Naray Szabo¹² in 1943 by reacting CdO and SnO_2 (1:1 molar ratio). He assigned monoclinic distorted perovskite structure to this compound with lattice parameter $a = 7.80 \text{ \AA}$. But Megaw¹³ preferred to describe this stannate as belonging to the orthorhombic instead to monoclinic structure.

Smith¹⁴ is credited to have prepared Cd_2SnO_4 phase for the first time in 1960. He assigned orthorhombic crystal structure to this compound. He reported both meta (CdSnO_3) and ortho (Cd_2SnO_4) stannates by reacting CdCO_3 and SnO_2 at $1000-1100^\circ\text{C}$ in alumina boats in air. At these temperatures, he observed a small loss in weight due to volatilisation of CdO . He also prepared the stannates by treating a solution of potassium α -stannate with cadmium chloride and subsequently heating the white precipitate at ($600-800^\circ\text{C}$) to get a complex system. CdSnO_3 was found to have distorted perovskite structure with orthorhombic symmetry. The lattice constants were $a = 5.547 \text{ \AA}$, $b = 7.867 \text{ \AA}$ and $c = 5.577 \text{ \AA}$. The bright yellow product, Cd_2SnO_4 , was prepared with CdO and SnO_2 (2:1 mole ratio). Single crystals of Cd_2SnO_4 were prepared by the flux method using CdCl_2 flux and heating at $800^\circ\text{C}/7$ hours. The diffraction pattern was indexed on the basis of orthorhombic

cell and the lattice parameters were calculated.

Irene Margensterne et al.^{15,16} prepared cadmium metastannate by precipitation method by adding (a) Cd and Sn salt solutions to K_2CO_3 and (b) $CdCl_2$ solution to sodium α -stannate. The precipitate was calcined. Preparation conditions like solution concentration, pH, temperature etc. were reported to be controlling the crystallinity of the compound. X-ray analysis of both the hydrated and the calcined stannates was carried out. A new phase was reported corresponding to $CdSnO_3$ having the ilmenite instead of perovskite structure. This was reported to be the first meta-stannate having ilmenite structure. Phase transition occurred from ilmenite to perovskite at $1000^\circ C$ and was irreversible.

Therese Dupuis et al.¹⁷⁻²⁰ studied the IR absorption spectra of metastannate of bivalent metals (Cd, Zn, Cu, Ni, Co, Mn, Ca and Mg). The hexahydroxy stannates were calcined from $300-1300^\circ C$. The Cu and Mn metastannates were completely dissociated and others transformed into orthostannates. The IR spectra of all the metastannates showed a single strong absorption region, $490-570\text{ cm}^{-1}$ and a faint band occurred near 170 cm^{-1} . They observed that the presence of only two bands suggested an octahedral coordination in the crystal state although the mean Sn-O vibration frequency

was rather low. The IR spectra of the hydroxystannates confirmed a symmetrical S_6 structure of the complex ion $Sn(OH)_6^{--}$ in the crystalline state. All the (OH) groups were connected by the H bond.

Levy Clement²¹ claimed to have obtained a new structural variety of $CdSnO_3$ of spinel type with vacancies by heating hexahydroxy cadmium stannate $[CdSn(OH)_6]$ at $660^\circ C/10$ minutes. Thermal analysis of the mixed hydroxide revealed two endothermic peaks at 250 and $650^\circ C$ corresponding to dehydration and phase change from spinel to ilmenite structure. It is also mentioned that he obtained ilmenite phase after prolonged heating of the spinel type $CdSnO_3$ at $450^\circ C$. Crystallisation was associated with negligible enthalpy changes. X-ray diffraction studies showed the lattice to be fcc, space group $Fd\bar{3}m$ with $a = 9.15 \pm 0.003 \text{ \AA}$. Density determinations indicated $8Cd_{4/3}Sn_{4/3}O_4$ groups in the unit cell with $8/3$ cationic positions unoccupied. He assumed a statistical distribution of vacancies between octahedral and tetrahedral sites.

Nozik²² took a patent for the application of Cd_2SnO_4 as yellow pigment. He reported that this to have improved colour intensity, light fastness and heat stability. The colour saturation value was 83.

Nozik²³ was the first worker who seriously studied the semiconducting properties of Cd_2SnO_4 . Prior to 1972 this was largely unknown. He studied them both as crystalline material and as amorphous film. Cd_2SnO_4 was reported to be n-type defect semiconductor in which oxygen vacancies provided the donor states in the forbidden gap.

He prepared the crystalline Cd_2SnO_4 having orthorhombic structure by (1) solid state reaction between CdO and SnO_2 (2:1 mole ratio) at $1050^\circ C/6$ hours, (2) calcining the hydrous oxide obtained from metal chloride solutions and $NH_4OH/KOH/NaOH$. He also prepared Cd_2SnO_4 amorphous films by rf sputtering method.

Silver epoxy electrodes were used for pressed pellets and films. He measured electrical conductivity, thermoemf and Hall coefficients of the samples prepared under various conditions. Diffuse reflectance spectra of the samples presented in figure (1.1) showed a large shift in the fundamental optical absorption edge toward uv region, from 2.34 eV to 2.76 eV. This is the wellknown Burstein shift. His results are reproduced in the table (1.1). He pointed out that the reaction condition like oxygen deficient or reducing atmosphere or thermal quenching created high density of oxygen vacancies which was responsible for large conductivity values. He opined that ESR studies should determine the defect structure.

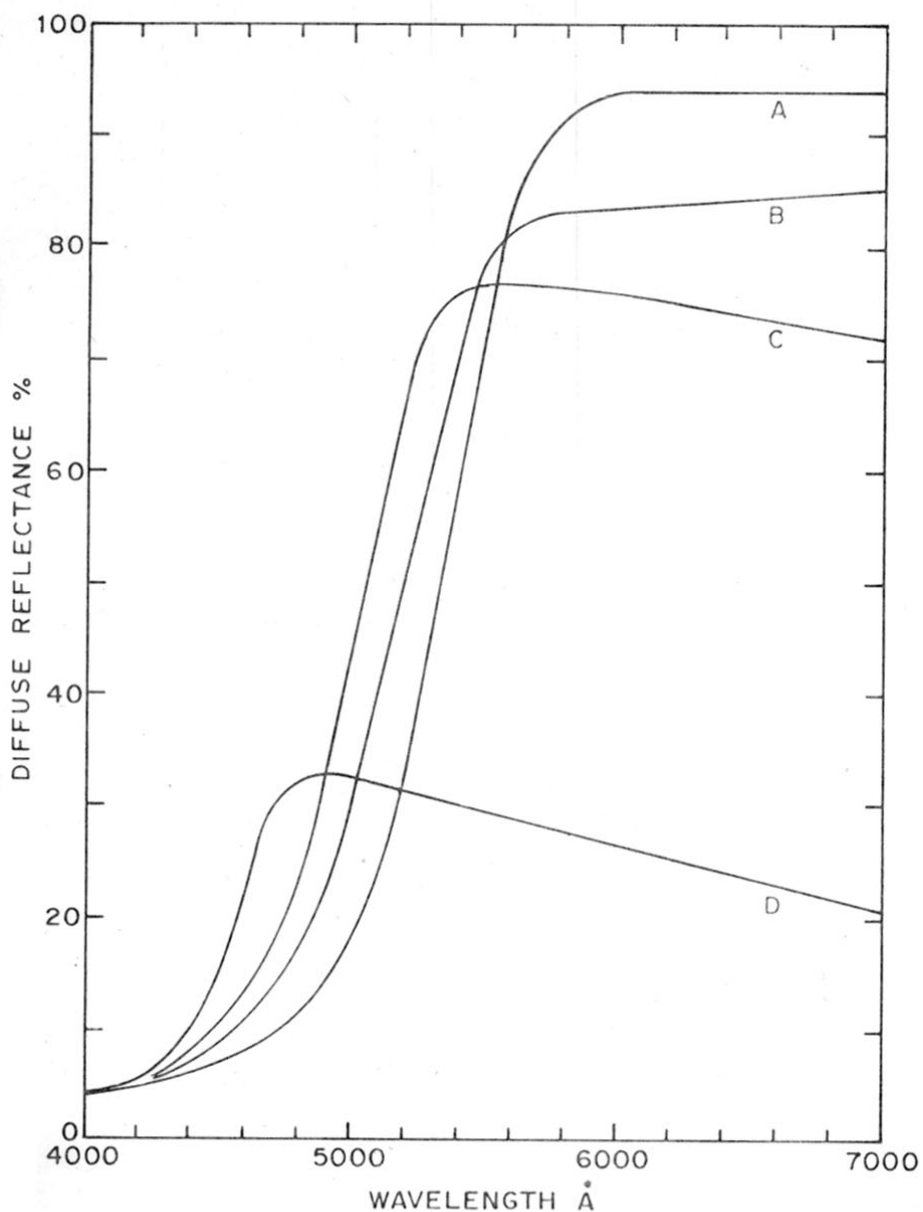


FIG. 1-1: DIFFUSE REFLECTION SPECTRA OF Cd_2SnO_4 POWDERS PREPARED UNDER VARIOUS CONDITIONS. A: PREPARED AND SLOW COOLED IN O_2 , $\sigma \sim 0.01 \Omega^{-1} \text{cm}^{-1}$; B: PREPARED AND QUENCHED IN AIR $\sigma \sim 0.5 \Omega^{-1} \text{cm}^{-1}$; C: PREPARED AND QUENCHED IN VACUUM $\sigma \sim 2.0 \Omega^{-1} \text{cm}^{-1}$; D: PREPARED AND QUENCHED IN VACUUM $\sigma \sim 6.0 \Omega^{-1} \text{cm}^{-1}$.

Table 1.1 - Effects of preparative conditions on the optical and electrical properties of crystalline Cd₂SnO₄ powder

Sample	Reaction atmosphere 1050°C, 6 hrs.	Cooling conditions	Colour	Approximate (a) absorption edge (Å)	Conductivity powder (Ω ⁻¹ cm ⁻¹)
C, D	Vacuum	Quench in air	Green	4500	2-10
B	Air	Quench in air	Yellow	5150	0.5
	Air	16 h in air (uncontrolled)	Bright yellow	5250	0.05
	Air	20 h in air (0.5-5°C/min)	Bright yellow	5250	0.02
A	O ₂	24 h in O ₂ (0.2-1°C/min)	Bright yellow	5300	0.001

(a) Defined as wavelength where the slope of diffuse reflectance spectrum is maximum.

The preparative conditions and properties of the sputtered films are reproduced in the table (1.2).

(a) All data obtained were at room temperature. All films were amorphous except the film F which was partially crystallised. (b) Substrate was water cooled except as noted. Sputtering atmosphere consisted of Ar and O_2 as noted. (c) Film was heated in H_2 at $280^\circ C$ for 10 minutes.

Visible and near-infrared transmission spectra of the films indicated a clear large Burstein shift. The effects of free-carrier absorption in the conductive film were apparent in its reduced transmission in the red and near-infrared. He calculated the absorption coefficient, α , from transmission spectra, refractive index and film thickness. The results of his studies on the spectral dependence of α for several films fitted in the equation.

$$\alpha = B (h\nu - E_0)^2 / h\nu \quad \dots \quad (1.1)$$

Optical band gap (E_0) was calculated from the plot $(\alpha h\nu)^{1/2}$ vs $h\nu$.

The crystal momentum (\vec{K}) is supposed to be conserved by the emission or absorption of phonons. But it was explained that in the case of amorphous films, the above equation was valid because the absence of

Table 1.2 - Electrical and optical properties of Cd₂SnO₄ films (a)

Sample	Sputtering (b) conditions (atm., power, time)	Thickness (μ)	Conducti- vity ($\Omega^{-1} \text{ cm}^{-1}$)	Sheet resistance Ω/\square	Hall coeffi- cient ($\text{cm}^2/\text{A sec}$)	Mobility ($\text{cm}^2/\text{V-sec}$)	Carrier Appa- rent density (cm^{-3})	Band gap (eV)
A	50% O ₂ 700 W, 6 $\frac{1}{4}$ h	2.9	0.098	35600	59.1	5.8	1.1x10 ¹⁷	2.06
B	20% O ₂ 600 W, 2 h	0.96	15.6	650	1.50	24	4.3x10 ¹⁸	2.28
C	100% Ar 100 W, 1 h	0.23	100	430	0.10	10	6.2x10 ¹⁹	2.81
D	100% Ar 200 W, 1 h	0.34	385	76	0.051	20	1.2x10 ²⁰	2.85
E	50% O ₂ 600 W, 6 $\frac{1}{2}$ h (c)	3.3	1330	2.3	-	-	-	2.51
F	20% O ₂ 700 W 2 h substrate temp. at 425°C	1.0	82	1200	1.1	100	5x10 ¹⁸	-

translational symmetry allowed relaxation of the requirement for conservation of (\vec{K}).

The author has thus observed some unusual electrical and optical properties which hitherto were not reported by earlier workers. Sputtered films had surprisingly high electron mobility and conductivity. The optical absorption edge shift is reflected in the optical band gap change from 2.06 to 2.85 eV. The effective electron mass was calculated to be $0.04 m_e$. This was reported to be very low for a wide-band-gap oxide. The author mentioned infrared reflection and magneto reflection studies to confirm the nature of the band gap.

He was the first to suggest the potentiality of Cd_2SnO_4 as transparent conductor because of large Burstein shift and high mobility.

Haacke^{25,26} took up the development of transparent conductors of Cd_2SnO_4 for solar energy applications. RF sputtering and spray deposition techniques were used for coatings. He used silica, sapphire, soda lime glass, chemcor glass, $Al_2O_3-SiO_2$ glass, stretched acrylic and polycarbonate materials as substrates. The films had high transparency and high ir reflectivity. He reported that interstitial Cd or oxygen vacancies essentially acted as dopants. In and Ta addition to Cd_2SnO_4 increased ir

reflectivity to 90% beyond 2μ . Modified post-deposition heat-treatment improved the conductivity ($0.7\Omega/\text{sq}$) and visible transmission value (80-85%). These coatings have been tried on CdS films and Si wafers.

Haacke⁴² further studied TE properties of Cd_2SnO_4 for the application in display technology, solar energy conversion. He found it to be an outstanding material compared to SnO_2 or ITO. He prepared the films by rf sputtering. In this paper, he mentioned that the substrate temperature, sputtering atmosphere and annealing temperature ($600\text{-}700^\circ\text{C}$) of the films influenced the conductivity. High conductivity was obtained in argon rich sputtering atmosphere.

A slight increase in lattice constant during the heat-treatment suggested the presence of interstitial cadmium creating additional donors. A shift from 2.0 to 2.9 eV in the absorption edge was noticed with a colour change from brownish to greenish grey in the films. Electrical conductivity increased to a great extent ($6000\Omega^{-1}\text{cm}^{-1}$). He also reported $n = 2 \times 10^{21}\text{cm}^{-3}$ and $\mu_H = 30\text{cm}^2/\text{V-sec}$.

Looking at the number of applications of T.Es, it was desirable to devise a method for meaningful comparison and evaluation of the potential materials.

The criterion for a good transparent electrode is the simultaneous occurrence of maximum transmission and conductivity. Haacke⁴³ derived a new figure of merit. The earlier figure of merit was defined by Frazer⁴⁴

$$F_{Tc} = \frac{T}{R_s} \quad \dots (1.2)$$

where $T = \frac{I}{I_0} = \exp(-at)$ and $\dots (1.3)$

$$R_s = \frac{1}{\sigma t} \quad \dots (1.4)$$

Here the weightage was put on R_s (sheet resistance) and for large film thickness (t). Haacke proved that such an assumption would lead to erroneous results.

Substituting the values for T and R_s , he obtained

$$F_{Tc} = \sigma t \exp(-at) \quad \dots (1.5)$$

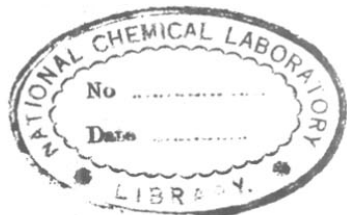
t_{max} was calculated from

$$\frac{\partial F_{Tc}}{\partial t} = \frac{a \exp(at) - \partial at \exp(at)}{\exp(2at)} = 0$$

$$t_{max} = \frac{1}{a}$$

Substituting t_{max} in the equation 3.1 gave

$$T = \frac{1}{e} = 0.37$$



621.382:661.888.45(043)

SET

indicating that the optical transmission was only 37%. This was too low a value for the T.E.

Therefore, he redefined the figure of merit to strike a better balance between transmission and film thickness, which although have opposing effects, as

$$\phi_{Tc} = \frac{T}{R_s} x \quad \dots (1.6)$$

Following the same procedure as before, he obtained

$$t_{\max} = \frac{1}{\alpha x} \quad \dots (1.7)$$

Assigning a value for $x = 10$, he obtained transmission = 90%. The new figure of merit was therefore

$$\phi_{Tc} = \frac{T}{R_s} 10 \quad \dots (1.8)$$

$$\text{or } \phi_{Tc} = t \exp(-10 \alpha t). \quad \dots (1.9)$$

where α = absorption coefficient (cm^{-1})
 σ = electrical conductivity ($\text{ohm}^{-1} \text{cm}^{-1}$)
 t = film thickness (cm).

He calculated ϕ_{Tc} values for Cu, Ag, Au, ITO and CTO. The results are reproduced in the figure (1.2). The author has thus proved that the semiconductors were superior transparent electrode materials compared to thin metal

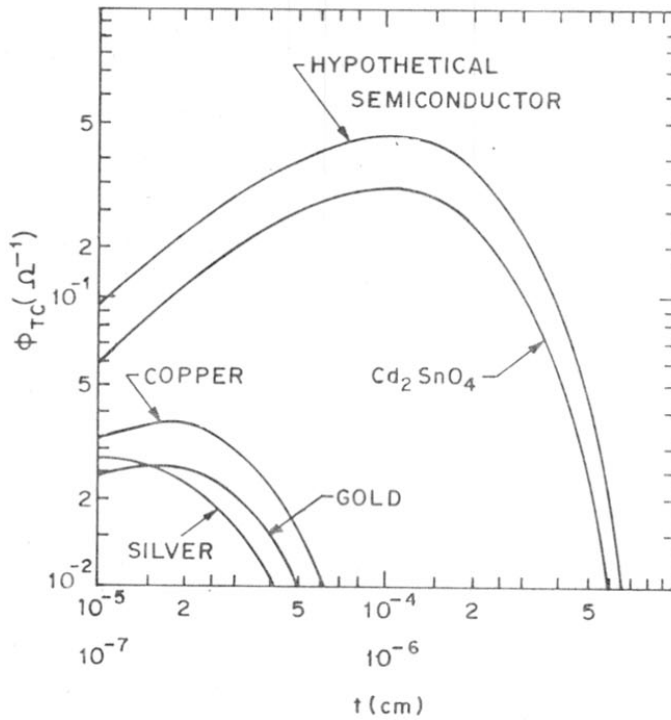


FIG. 1-2: CALCULATED FIGURE OF MERIT ϕ_{TC} Vs FILM THICKNESS AT 5500 Å WAVELENGTH FOR METAL AND SEMICONDUCTOR FILMS; UPPER ABSCISSA FOR SEMICONDUCTORS, LOWER ABSCISSA FOR METALS.

films. Cd_2SnO_4 emerged out as the one having the highest figure of merit for T.E.

Burton et al.⁴⁵ fabricated CdS-Cu₂S solar cells on Cd_2SnO_4 - coated silica substrates. This facilitated back wall operation. The light incident on the p-n junction interface through the wide gap material absorbed in the narrow gap layer.

They produced Cd_2SnO_4 crystalline films on hot substrates ($> 400^\circ\text{C}$) by rf sputtering. They obtained an n-type semiconductor with a band gap of 2.0 eV, $N = 10^{19} \text{ cm}^{-3}$ and $\mu_n = 10 \text{ cm}^2/\text{V-sec}$. X-ray analysis revealed the presence of a small percentage of CdO in the films. They reported the improvement in TE properties when the films were heat-treated at $600\text{-}700^\circ\text{C}/10$ minutes in Ar/CdS atmosphere. The optical absorption edge also shifted to 2.9 eV with the disappearance of CdO. This, they stated, resulted in the increase of free-electron density and mobility to 10^{21} cm^{-3} and $30 \text{ cm}^2/\text{V-sec}$. respectively. The cell characteristics were measured. Measurement of optical transmission as a function of wavelength revealed that the Cd_2SnO_4 films had maximum transmission in the wavelength region in which solar spectrum also had its highest intensity. The back wall response of the CdS/Cu₂S cells was reported to be not limited

by the short wavelength transmission characteristics of the Cd_2SnO_4 electrode. The adherence of CdS to Cd_2SnO_4 was excellent without cracking or peeling defects. It had ohmic contact as established by I-V results.

Nozik and Haacke⁴⁸ were issued a patent for the development of infrared attenuators with visible transparency by using Cd_2SnO_4 coatings. Eye protective IR filters (transmitting > 10% incident light of $\lambda > 0.65\mu$) were made by coating the substrate with a $3\mu\text{m}$ thick Cd_2SnO_4 layer.

They further patented^{49,50} the use of Cd_2SnO_4 coatings in solar thermal heat absorbing systems. The property of high transmittance for solar radiation and high reflectance for thermal radiation has been made use of by them. The absorbing system consisted of a steel pipe whose outer wall was coated with a high absorptivity material. It was surrounded by a glass tube, the inner wall of which was coated with Cd_2SnO_4 by spray technique of bromide solutions of Cd and Sn. The annular space was evacuated. The heat transfer medium passed through the steel pipe. This unit was located at the focal point of a parabolic reflecting trough. A flat plate coated with Cd_2SnO_4 could also be used for the purpose.

Haacke⁵¹ took another patent for the idea of using Cd_2SnO_4 coating for architectural windows. These transmit visible light but reflect IR portion of the solar radiation. He claimed to have increased the near IR-reflectivity by incorporating a small amount of Cu to produce $\text{Cd}_{2-x}\text{Cu}_x\text{SnO}_4$, where $x = 0.01$ to 0.3 .

Nozik⁴⁷ utilized the unique property of Cd_2SnO_4 films having conductivity $> 10^3 \text{ ohm}^{-1} \text{ cm}^{-1}$, being transparent to solar radiation and reflective to IR radiation. This enabled him to make a window of Cd_2SnO_4 film for solar heat collector by which its collection efficiency increased. He used spray technique (40% SnBr_4 + 30% CdBr_2 aqueous solutions and 30% H_2O_2 solution equal to half of the volume of the Cd-Sn bromide solutions). The substrate temperature was 950°C . He improved the properties by annealing at $280^\circ\text{C}/10$ minutes in H_2 atmosphere.

In his review paper⁵² on transparent conducting coatings, Haacke has exhaustively covered the subject. Metal and semiconductor films were considered for material evaluation. They included gold, SnO_2 , ITO, CdO and CTO films. Main uses and applications of these conductors mentioned are: heating elements on aircraft windows for de-icing and defogging, antistatic coating on instrument

panels, electrodes in electroluminescent lamps and displays, in imaging devices and ferroelectric memories, liquid crystals and electrochromic displays. The world-wide interest in solar energy conversion has enhanced the application limit of transparent electrodes. Cd_2SnO_4 was rated as a highly potential candidate for T.E.

Metal films recede to a second place on the basis of figure of merit for a T.E., although they have certain advantages like chemical compatibility, work function and fast deposition rate. Further, film strength, initial island formation, surface scattering render them less efficient as T.E. material. Gold, silver, copper and chromium films were considered.

Based on absorption processes, a good transparent electrode material should possess high carrier mobility and low effective electron mass. The useful transmission region is limited to wavelengths longer than the band gap energy and it should be around 3.0 eV to cover the full visible spectrum. Semiconductors were therefore found to be useful. InSb possessed the above properties, but it was not good because of the band gap restrictions.

The three semiconducting oxides SnO_2 , In_2O_3 and Cd_2SnO_4 possessed the required properties. CdO was also considered.

Table (1.3) presents the desired properties of the oxides for T.E.

Haacke et al.⁵³ reported a new method of preparing Cd_2SnO_4 by a simple spray deposition technique using a solution of CdCl_2 and SnCl_4 . The principle involved was the pyrolysis of a fine mist of a metal salt solution on a hot substrate. Both the phases of cadmium stannate were obtained. However, good transparency could be possible in single phase only. A number of deposition parameters were studied. At higher substrate temperatures ($> 800^\circ\text{C}$), Cd_2SnO_4 was formed and $< 800^\circ\text{C}$, CdSnO_3 phase was obtained. They obtained lowest R_s by fast deposition and immediate quenching of the sample. The best value they could achieve for was $500\text{-}1000 \Omega^{-1} \text{cm}^{-1}$ compared to $6500 \Omega^{-1} \text{cm}^{-1}$ by sputtering. The mobility was $1\text{-}5 \text{ cm}^2/\text{V}\text{-sec}$ only. The lower value was explained as due to the creation of lattice defects and grain boundary imperfections. They felt that σ and μ values could be improved. Impurity effect on σ has not been studied fully, although they mentioned the improvement of clarity of the films because of the dopants. The authors felt that the post deposition heat-treatment was not an intrinsic requirement except either to reduce or to remove the CdO phase.

Lloyd^{54,55} studied the properties of cadmium stannate films prepared by rf sputtering from powder targets. He

Table 1.3 - Transparent electrode properties of some oxide semiconductors

Material → Property ↓	CdO	SnO ₂	In ₂ O ₃	Cd ₂ SnO ₄
Polarity	n-type	n-type	n-type	n-type
Electron concentration (cm ⁻³)	5.10 ¹⁶ - 10 ²¹	10 ¹⁹	10 ¹⁷	10 ²⁰
Elec. cond. (Ω ⁻¹ cm ⁻¹)	2000	1200-1400	5600 (undoped)	6500
Carrier mobility (cm ² V ⁻¹ sec ⁻¹)	300 (crystalline) 120 (film)	10	55-60 (films) 75 (Sb doped) 125 (Ti doped) 170 (Zr doped)	30
Electron effective mass	-	0.275 m ₀	0.2-0.5 m ₀	0.04 m ₀
Optical absorption shift (Burstein shift) (eV)	2.3 - 2.7	3.57-3.93	2.6 - 3.75	2.34-2.76 (crystalline) 2.06-2.85 (films)
Visible transmission (%)	80 - 90	80 - 85	95	86 - 87
Sheet resistivity (Ω/sq)	220	100-200	1.6 - 3.0	1.05

measured film thickness, resistance, carrier concentration, Cd:Sn ratio, optical transmission and Hall effect. The results showed considerable scatter in the values of Cd:Sn ratio in the deposited films. This indicated the dissociation of the compound. The carrier density and the mobility values were higher for the heat-treated films as compared to the as-deposited films. Both the target and substrate temperatures played a decisive role in determining the Cd content and the oxidation state. It was reasoned that the carriers were liberated from the compensation traps in the structurally disordered as-deposited films during annealing. This was responsible for the carrier concentration increase from 4×10^{18} to $5 \times 10^{20} \text{ cm}^{-3}$. Increase in the mobility value (10 to $35 \text{ cm}^2/\text{V-sec}$) was attributed to the disappearance of the structural disorder during annealing. The transmission also improved (from 65 to 80%).

Haacke⁵⁶ evaluated the Cd_2SnO_4 films for solar heat collectors. He prepared the films by rf sputtering using silica, glass and single crystal silicon as substrates. The governing factors for a solar collector are total solar transmission (T_s) and infrared reflectivity (R_I). These depended on free carrier concentration (n) and film thickness (t) in the case of

a semiconductor. R_I increased with 'n' whereas T_S decreased due to free-carrier absorption. T_S required small 't', but R_I decreased with 't'. He reported, therefore, that T_S and R_I could not be maximised independently. These conditions should be optimised to get maximum $\frac{\alpha S}{\epsilon_T}$, where α was absorptivity and ϵ_T was total infrared emissivity. By adjusting the film thickness and annealing temperature, he obtained $\alpha > 0.9$ and $\epsilon_T \sim 0.1$, at 620°C annealing temperature, on Cd_2SnO_4 /silicon solar selective absorber.

Shannon et al.⁵⁷ synthesised single crystals of Cd_2SnO_4 , CdSnO_3 , In_2TeO_6 and CdIn_2O_4 either by the flux or the high pressure method. They studied the electrical and structural properties.

A mixture of CdSnO_3 and a $\text{Na}_2\text{B}_2\text{O}_7$ flux was melted in a platinum crucible at $1050^\circ\text{C}/4$ hours and cooled at $5^\circ\text{C}/\text{hr}$ to 650°C and then air quenched. A mixture of CdSnO_3 (rhombohedral and orthorhombic) and Cd_2SnO_4 (orthorhombic) single crystals was obtained. Cd_2SnO_4 was found to be not very conducting. Sb was added as dopant to enhance the conductivity.

The authors stated that conductivity of Cd_2SnO_4 could be increased by creating oxygen vacancies (reversible) or by chemical doping (irreversible). Undoped Cd_2SnO_4 was reported to be a semiconductor with $R_T = 10^3 \Omega \text{ cm}$ and $E_a = 0.15 \text{ eV}$.

They expressed continuous edge sharing of Cd^{2+} and Sn^{4+} octahedra was a necessary condition for a transparent conductor. The Seebeck coefficient for Cd_2SnO_4 ($\rho_{RT} = 10^3 \Omega\text{-cm}$) was reported to be $-170 \mu\text{V}/^\circ\text{C}$ whereas for $\text{Cd}_2\text{Sn}_{1-x}\text{Sb}_x\text{O}_4$ ($\rho = 10^{-1} \Omega\text{-cm}$) it was $-50 \mu\text{V}/^\circ\text{C}$. They opined that oxygen deficient conductor might have higher carrier mobility compared to chemically doped sample. But a doubt was also expressed that chemically doped system might also be oxygen deficient. The authors expressed the view that it would require further investigation to settle this point.

Hall⁵⁸ tried Cd_2SnO_4 as an optically transparent electrode for photoelectrochemical energy conversion using sulphuric acid as an electrolyte. The photogalvanic short-circuit currents and open circuit voltages were found to be comparable with other electrode materials. Cd_2SnO_4 films were used as underlays for SnO_2 anodes which produced higher power outputs. This also decreased overall resistance. He reported Cd_2SnO_4 to be n-type semiconductor having $E_g = 2.9 \text{ eV}$. He measured the electrical conductivity ($6 \times 10^3 \Omega^{-1} \text{ cm}^{-1}$) and carrier density (10^{21} cm^{-3}). The carriers were provided by oxygen vacancies and interstitial cadmium. The films were reported to be hydrophobic and wettability was found to increase with the contact time with the electrolyte.

This was attributed to the formation of surface hydroxyl groups as reported by Mollers and Memming.⁹⁰ He found the cadmium and oxygen to tin ratio was substantially lower, from his ESCA studies, after use in the electrochemical cell.

Cd_2SnO_4 cathode was also used in iron-thionine cell. It was not good due to the lack of Fe^{2+}/Fe^{3+} reactivity at Cd_2SnO_4 , for which no satisfactory explanation could be given. It would be interesting to explore why the redox couples react with difficulty at Cd_2SnO_4 cathode, although the flat band and redox potentials were favourably aligned inspite of it being a highly doped semiconductor.

Haacke et al.⁵⁹ developed Cd_2SnO_4 coatings with $1 \Omega/sq$ and 85-90% transmission for utilization in solar energy converters. They also evaluated them for high temperature green house window coatings and in selective absorbers. The backwall $Cd_2SnO_4/CdS/Cu_2S$ solar cell was reported to have $\sim 6\% \eta$.

Hici and Haacke⁶⁰ were issued a patent for depositing Cd_2SnO_4 films on plastics. The films were adherent and the optical transmission for 5500-10000 Å thick films was 80% with the sheet resistance of $26 \Omega/sq$.

Haacke et al.⁶¹ stressed the need in their paper to understand the influence of film structure and composition

on the conductivity and the optical absorption.

They prepared Cd_2SnO_4 films by reactive and bias (d.c. potential -200 V) sputtering. The films were reported to be amorphous when deposited at room temperature. However, they were crystalline on hot (400-500°C) substrates. It required only 150°C when single-crystal spinel substrates were used.

The disappearance of CdO phase improved the transparent electrode properties. The reason put forward for this was the dissociation of CdO and the Cd forming interstitial donors, resulting in the increase of lattice constant value (9.167 to 9.189 Å). A representative sample had $\sigma = 6700 \text{ } \Omega^{-1} \text{ cm}^{-1}$, $\mu_H = 40 \text{ cm}^2 \text{ V}^{-1} \text{ sec}^{-1}$ and $n = 10^{20} \text{ cm}^{-3}$ at $T_s = 690^\circ\text{C}$. The oxygen vacancies were also stated to be contributing to conductivity increase. Hall measurements revealed unexpected increase of μ with N which contradicted the semiconductor theory for homogeneous materials with high carrier concentrations. The mobility was found to be generally governed by the grain boundary, specimen inhomogeneity etc. Further studies of Hall measurements over a wide range of temperatures have been suggested.

Mass spectrometric analysis showed that Cd and Cd-O species left the samples during heat treatment. Ar or Ar-CdS

atmosphere for heat-treatment was reported to enhance the oxygen vacancies. However, the role of sulphur, supposed to be present, has not been explained.

Many dopants were tried (Ti, Zr, V, Nb, Mo, W, Rh, Cu, Ag, P, Bi and Th). They stated that detailed studies were required to understand fully the effect of the dopants. They never observed p-type conductivity. In the amorphous Cd_2SnO_4 films, the band edge shifted from 2.1 to 2.9 eV after heat-treatment. The large shift of optical absorption edge was presumably due to the presence of multiphase structure (CdO , CdSnO_3 and Cd_2SnO_4) of the specimens. Additive phenomenon has been suggested. However, for single phase Cd_2SnO_4 , the shift was from 2.34 to 2.76 eV only. Thus, the authors have posed more questions than providing adequate explanations for the results, ofcourse, suggesting more studies.

Miyata et al.^{63,64} studied the Cd-Sn oxide films made by diode DC reactive sputtering as transparent electrodes. The authors claimed that this method was an improvement over the previous sputtering methods. This did not require post heat-treatment of the films for getting highly conductive films. The sheet resistances were $40\ \Omega/\text{sq}$ and $180\ \Omega/\text{sq}$ for the film thicknesses of $0.3\ \mu\text{m}$ and $0.22\ \mu\text{m}$. The average transmission was 85% in the visible region. The absorption edge of the reactive sputtered films was 500 nm

and 480 nm compared to that of Nozik²³ (502 nm) for the films heattreated in the reduced atmosphere. They further claimed that the oxygen vacancies could be controlled. Miyata et al.⁶⁶ further prepared doped Cd_2SnO_4 films which were highly conductive and transparent. They obtained the films by chemical spray deposition technique on hot substrates (400-900°C) using aqueous solutions of Cd, Sn and In chlorides. The optical transmission of Cd-Sn-In films depended on In concentration. Post-deposition heattreatment at 200°C/30-120 minutes in oxygen atmosphere decreased the resistance by about 30% and improved the transmission from 70 to 80% in the visible and near infrared region.

Lloyd⁶⁸ was issued a patent for his work on the application of Cd_2SnO_4 as a resistor material. He deposited the films (0.9 μ thick) by rf sputtering in oxygen atmosphere. He could decrease the resistivity of the films from 2.2×10^{-2} to 4.5×10^{-4} Ω -cm by heating them in H_2 - N_2 atmosphere.

Agnihotri et al.⁶⁹⁻⁷¹ prepared selective coatings of cadmium stannate by pyrolytic decomposition of two parts of 0.2M $\text{CdCl}_2 \cdot 5\text{H}_2\text{O}$ and one part of 0.2M $\text{SnCl}_4 \cdot 3\text{H}_2\text{O}$ solutions in ethyl alcohol and acetic acid respectively on hot glass and quartz substrates. The films were

transparent to visible light. The thickness varied from a few tenths to nearly $1 \mu\text{m}$. The absorption data had been interpreted to an allowed direct transition of energy gap of 2.8 eV and an indirect interband transition of energy gap of 2.2 eV.

They calculated the band gap from plotting the values of $(\alpha\Delta d)^{1/2}$ vs $(h\nu)$ of the derived equation

$$\alpha\Delta d = \alpha_0 (h\nu - \Delta E)^x \quad \dots (1.10)$$

where $x = \frac{1}{2}$ for Cd_2SnO_4 .

The absorption coefficient reached values exceeding 10^5 cm^{-1} at the higher photon energy, same as in the case of allowed transitions.

For an indirect interband transition, the energy dependence of absorption coefficient, wherein the crystal momentum (\vec{k}) is conserved, they mentioned

$$\alpha = \alpha_0 (h\nu - \Delta E)^2 \quad \dots (1.11)$$

They derived $\Delta E = 2.2 \text{ eV}$ from $(\alpha h\nu)^{1/2}$ vs $(h\nu)$ graph. This was higher than 2.06 eV reported by Nozik²³ for amorphous Cd_2SnO_4 films. It is interpreted as to either the transition of electrons from the localized states at the valence band edge to the extended states in the conduction band or transition of electrons

from the extended states in the valence band to the localized states at the conduction band edge. They, therefore, stated that the amorphous material would have a shallower absorption edge because absorption started at lower energies.

Their results indicated that Cd_2SnO_4 films were transparent to sunlight (0.3 - 2.5 μm wavelength) but highly reflective beyond 2.5 μm . The films could be used as heat reflectors and therefore were useful in solar collectors. They obtained α_s (solar absorptivity) = 0.82 and ϵ_T (total infrared emissivity) = 0.09 at 5 μm .

Miyake and Miyata⁷³ patented the application of making transparent conducting layers for solar cells and display devices. The films were reported to be a mixture of CdSnO_3 and Cd_2SnO_4 with the electrical resistivity of 40^{-2} /sq and transmission of 85% in the visible region.

Dislich Helmit et al.⁷⁴ prepared Cd_2SnO_4 films by dip method. They dipped glass substrates in a solution containing $\text{Cd}(\text{OAc})_2$ in methanol and $\text{Sn}(\text{OBu})$ in ethanol along with the dopant $\text{Al}(\text{sec-Bu})_3$ (in the mole ratio 1.95:0.05:1 of Cd:Al:sn). Acetyl acetone was added to the system. The substrates were heated at 150°C/5 minutes and 640°C/15 minutes. They obtained a clear adherent and homogeneous layer whose electrical resistance was 30^{-7} /sq and a reflectivity of 74%.

74

Mackenzie et al.⁷⁷ studied the photoelectrochemical properties of polycrystalline pellets of sintered CdSnO_3 and Cd_2SnO_4 . They stated that CdSnO_3 gave a higher photocurrent (and background current) compared to that of Cd_2SnO_4 . They stated that both the stannates to be n-type semiconductors with a band gap of 2.3 eV, obtained from the wavelength dependence of photocurrent. They observed that the polycrystalline Cd_2SnO_4 was better for photoelectrochemical conversion than the single crystals. They reasoned that the latter might have had less 'O' vacancies.

However, Koffyberg et al.⁷⁸ stated that the band gap values, flat band potentials and the observed long term instability made the materials Cd_2SnO_4 , CdIn_2O_4 and CdGeO_4 unsuitable as electrodes in solar photoelectrolysis cells. The band gaps were calculated to be 2.12 (indirect), 2.23 (forbidden) and 3.15 eV (indirect) respectively for the materials.

Miyata et al.^{76,79,80} prepared Cd_2SnO_4 films by dc reactive sputtering from a Cd-Sn alloy and by rf sputtering of sintered CdO-SnO_2 targets in O_2 and Ar- O_2 atmospheres. They obtained high conductivity coupled with high optical transmission in the visible region. The additional work they carried out was to study the effect of O_2 concentration in the sputtering

atmosphere on the Cd_2SnO_4 properties. The lowest resistivity was $2.0 \times 10^{-4} \Omega\text{-cm}$ with 90% optical transmission at around 6% O_2 . Their results are tabulated in the table (1.4).

Howson et al.⁸³ deposited Cd_2SnO_4 films on glass substrate at room temperature by planar magnetron sputtering of Cd₂-Sn alloy in Ar- O_2 atmosphere. The sputtering atmosphere was activated by an rf discharge to give very high rates of deposition. Visual transparency, electrical conductivity, mobility and IR reflectance were measured and compared well with the films obtained by other methods. The advantage claimed by the authors was that the substrate was not required to be heated. They also deposited Cd_2SnO_4 by ion plating technique and obtained very good transparent electrode films.

Mitsunori et al.⁸⁶ prepared cadmium-tin and indium-tin oxide by thermal oxidation. The as-sputtered films of Cd-Sn or In-Sn alloy target were oxidised in Ar- O_2 by heating. They examined the dependence of electrical resistance and optical transmission on the thermal oxidation conditions. The resistivity and optical transmission values were $5.1 \times 10^{-4} \Omega\text{-cm}$ and ~ 90% in the visible region.

Jarzebski¹⁰² has briefly touched upon Cd_2SnO_4 in his review article on the preparation and physical

Table 1.4 - Effect of O₂ in the sputtering atmosphere on the electrical and optical properties of Cd₂SnO₄ films.

O ₂ % in Ar-O ₂	Resistivity Ω-cm	Carrier concentration cm ⁻³	Hall mobility cm ² V ⁻¹ sec ⁻¹	Average trans- mission (%)	Optical energy gap (eV)
0	6.2x10 ⁻⁴	5.0x10 ²⁰	22	93	2.71
2	4.4x10 ⁻³	1.5x10 ²⁰	11	87	2.45
4	-	3.3x10 ²⁰	-	-	2.50
6	2.5x10 ⁻⁴	6.0x10 ²⁰	-	-	2.55
8	-	4.6x10 ²⁰	-	-	2.30
13	-	2.0x10 ¹⁹	-	-	2.05
	1.8x10 ⁻²	8.8x10 ¹⁸	73	86	2.39
20	2.5x10 ⁻²	1.4x10 ¹⁹	-	-	2.05

properties of transparent conducting oxide films. He has dealt mostly on SnO_2 and ITO. He opined that the transparent conducting properties strongly depended on the preparation conditions and the current knowledge of physical properties of these films was limited. The reasons he mentioned were the technological difficulties in the deposition of the films and their complex structure, implying the need for exploring a suitable alternative method of preparation of the films. He further stated that there was scope for elucidating the conduction mechanism and band structure of Cd_2SnO_4 .

STRUCTURAL PROPERTIES

Smith¹⁴ was the first to prepare Cd_2SnO_4 and report its structure as orthorhombic.

The single crystals of Cd_2SnO_4 , yellow along and weakly birefringent, were used for X-ray analysis. Rotation and oscillation patterns taken for one of the crystals showed it to be orthorhombic with lattice parameters.

$$\begin{aligned} a &= 10.01 \pm 0.02 \text{ \AA} \\ b &= 5.55 \pm 0.01 \text{ \AA} \\ c &= 3.07 \pm 0.01 \text{ \AA} \end{aligned}$$

The diffraction patterns of Cd_2SnO_4 always showed weak lines due to the presence of CdO or CdSnO_3 or both.

Diffraction data for Cd_2SnO_4 of Smith are given in the table (1.5).

Hassanien³³ investigated the effect of substituting Cd in the place of Mg in the spinel structure of Mg_2SnO_4 . He stated that isomorphous substitution of cations in solid reactions led in some cases to the same structure as the host lattice and in others to a different one.

The author reported a gradual transformation from the spinel to the orthorhombic structure as x was increased from 0.01 to 2.0 in the system $x\text{CdO}(2-x)\text{MgO}\text{SnO}_4$. The compounds were prepared by solid state reaction of CdO , MgO and SnO_2 . The colour of the product changed from colourless to bright yellow. Many phases were identified between the two pure phases of spinel ($\text{Cd}_{0.1}\text{Mg}_{1.9}\text{SnO}_4$) and orthorhombic (Cd_2SnO_4) structures. The author did not index the 'd' values for Cd_2SnO_4 phase. He concluded that the CdSnO_3 phase was formed first and then on further reaction with CdO gave Cd_2SnO_4 . One feature of this work claimed was obtaining of Cd_2SnO_4 , free from CdO and CdSnO_3 .

Choisnet and Deschanvres³⁵ made a similar study. They substituted Zn by Cd in the spinel Zn_2SnO_4 which gave a cubic structure of spinel type. They reacted

Table 1.5 - X-ray diffraction data for Cd_2SnO_4
Cu $K\alpha$ radiation (Film 86)

No.	$\sin^2 \theta$	d	I_1/I	Reflecting planes (hkl)
1	0.0200	5.4468	1	010
2	0.0418	3.7676	1	210
3	0.0723	2.8665	8	310
4	0.0756	2.8016	2	020
5	0.0819	2.6916	10	011
6	0.1147	2.2745	2	410
7	0.1303	2.1339	2	320
8	0.1396	2.0616	4	021
9	0.1538	1.9642	2	CdSnO_3 line
10	0.1575	1.9409	7	401
11	0.1733	1.8504	1	030
12	0.1744	1.8289	1	411
13	0.1952	1.7435	2	321
14	0.2171	1.6532	3	CdO line
15	0.2251	1.6236	1	520
16	0.2278	1.6139	8	330
17	0.2307	1.6037	4	511
18	0.2317	1.6003	3	610
19	0.2348	1.5897	2	421
20	0.2525	1.5329	2	002
21	0.2683	1.4873	2	430

...contd.

Table 1.5 (contd)

No.	$\sin^2 \theta$	d	I_1/I	Reflecting planes (hkl)
22	0.2764	1.4652	1	601
23	0.2857	1.4411	1	521
24	0.2945	1.4194	3	611
25	0.3069	1.3945	6	302
26	0.3281	1.3448	2b	022
27	0.3486	1.3047	1b	402
28	0.3701	1.2662	2	711
29	0.3728	1.2616	2	041
30	0.3810	1.2479	2	322
31	0.3866	1.2388	2	630
32	0.4301	1.1746	3	721
33	0.4455	1.1541	2	-
34	0.4488	1.1498	3	631
35	0.4592	1.1367	3	811
36	0.5013	-	1	-
37	0.5095	-	1	-
38	0.5152	1.0732	1	CdO line
39	0.5217	1.0665	2	640
40	0.5262	1.0619	4	731
41	0.5466	1.0419	4	051
42	0.5606	1.0289	2	911
43	0.5751	1.0149	1	532
44	0.5915	1.0016	1	203
45	0.6048		2	-
46	0.6244		2	-
47	0.6338		2	-

CdO, ZnO and SnO₂ at 900-1050°C. The products had pale to brilliant yellow colour depending on the value of x (x = 0 to < 0.8) in the system 2xCdO 2(1-x)ZnO SnO₂. But when x > 0.8, a binary phase containing Cd₂SnO₄ and Zn_{0.4}Cd_{1.6}O₄ was obtained.

The distribution of Zn and Cd in the lattice was determined by the variation of F_{400}/F_{222} and F_{400}/F_{200} for different Cd contents. The line structure factor, F was determined by the intensity value (I). It was stated that the cation distribution in both the tetrahedral and the octahedral sites was given and Cd preferentially occupied the tetrahedral sites.

Tromel^{34,36} conducted the X-ray structural analysis of Sr₂PbO₄, Ca₂PbO₄, Ca₂SnO₄ and Cd₂SnO₄. He stated that all these compounds had the orthorhombic structure with space group D_{2h}^9 -Pbam and Z = 2. He prepared Cd₂SnO₄ by reacting CdCO₃ and SnO₂ at 900-950°C for several days. The colour of the compound was bright yellow.

The lattice parameters for the compounds were as shown in table (1.6).

He mentioned that the Cd₂SnO₄ contained chains of (SnO₄)⁴⁻ which were built by SnO₆ octahedra through the sharing of common edges similar to those in Pb₃O₄. The

Table 1.6 - Lattice parameters of the compounds

Compound	Lattice parameters (\AA)		
	a	b	c
Sr_2PbO_4	6.150	10.078	3.502
Ca_2PbO_4	5.836	9.745	3.381
Ca_2SnO_4	5.748	9.694	3.264
Cd_2SnO_4	5.546	9.888	3.193

bivalent atoms were between the chains and were surrounded by 7(O) atoms. The X-ray data for Cd_2SnO_4 is shown in the table (1.7). The crystal structure and edge sharing configuration of Cd_2SnO_4 are similar to figures (1.3) and (1.4).³⁶

Shannon et al.⁵⁷ synthesised and presented the crystallographic data for the crystals of $CdSnO_3$, Cd_2SnO_4 , In_2TeO_6 and $CdIn_2O_4$. The first two compounds were grown from $NaCl-Na_2CO_3-Na_2B_4O_7$ flux and $CdSnO_3$. They consisted of orange-brown octahedra (0.7 mm edge); yellow cubes (0.3 mm edge) and orange brown needles (0.2x1.0 mm) of rhombohedral $CdSnO_3$, orthorhombic $CdSnO_3$ and Cd_2SnO_4 respectively.

They obtained the X-ray diffraction pattern using $CuK\alpha$ radiation. The data are reproduced in table (1.8).

The cell dimensions obtained by them for Cd_2SnO_4 matched with those of Tromel^{34,36} but not with those of Smith.²³ All these three groups of workers mention that the compound contained octahedrally coordinated Sn^{4+} ions.

The table (1.9) gives the diffraction data for Cd_2SnO_4 .

Miyata et al.^{72,79} carried out X-ray analysis of the rf sputtered Cd_2SnO_4 thin films. They have noticed a broad peak (130) in the diffractograms for the films

Table 1.7 - X-ray powder pattern for Cd_2SnO_4 (FeK_{α} radiation)

No.	$\sin^2 \theta$	d	F	hkl
1	0.0385	4.9334	17	020
2	0.0399	4.8461	24	110
3	0.0687	3.6932	47	120
4	0.0918	3.1948	73	001
5	0.1166	2.8348	209	130
6	0.1213	2.7794		200
7	0.1310	2.6745		021
8	0.1321	2.6633		111
9	0.1534	2.4715	51	040
10	0.1605	2.4162		220
11	0.1837	2.2585	87	140
12	0.2087	2.1189		230
13	0.2227	2.0519	104	211
14	0.2456	1.9533	107	041
15	0.2517	1.9295	152	221
16	0.2757	1.8436		240
17	0.2825	1.8213	34	310
18	0.2993	1.7694	40	231
19	0.3111	1.7355	108	320
20	0.3452	1.6476	195	060
21	0.3590	1.6156		330
22	0.3622	1.6084	203	151

... contd

Table 1.7 (contd.)

No.	$\sin^2 \theta$	d	F	hkl
23	0.3677	1.5964		241
24	0.3741	1.5826		311
25	0.4031	1.5246	92	321
26	0.4372	1.4639		122
27	0.4528	1.4385		251
28	0.4662	1.4177		260
29	0.4846	1.3905		132
30	0.4890	1.3843		202
31	0.4941	1.3771		410
32	0.4988	1.3706		212
33	0.5180	1.3450		341
34	0.5201	1.3422		341
35	0.5223	1.3394		420
36	0.5519	1.3030		142
37	0.5858	1.2647		411
38	0.5915	1.2583		270
39	0.6041	1.2454		351
40	0.6149	1.2344		421
41	0.6169	1.2324		412
42	0.6380	1.2119		152
43	0.6502	1.2005	26	312
44	0.6633	1.1886	27	431
45	0.6787	1.1749		322
46	0.6821	1.1721		322

...contd.

Table 1.7 (contd)

No.	$\sin^2 \theta$	d	F	hkl
47	0.7056	1.1524		081
48	0.7083	1.1502		081
49	0.7129	1.1465		361
50	0.7268	1.1354		332
51	0.7287	1.1339		252
52	0.7419	1.1238		370
53	0.7660	1.1060	71	510
54	0.7937	1.0865		342
55	0.8064	1.0779	123	190
56	0.8159	1.0716	67	451
57	0.8264	1.0648		281
58	0.8295	1.0629		460
59	0.8336	1.0602		460
60	0.8428	1.0544		530
61	0.8519	1.0488	40	402
62	0.8578	1.0451		511
63	0.8615	1.0429		412
64	0.8670	1.0396		113
65	0.8862	1.0283		380
66	0.8899	1.0261		380
67	0.9092	1.0152		540
68	0.9207	1.0088	31	461

contd....

Table 1.7 (contd)

No.	$\sin^2 \theta$	d	F	hkl
69	0.9342	1.0015		531
70	0.9378	0.9996		432
71	0.9440	0.9963		133
72	0.9534	0.9914		470
73	0.9581	0.9889		470

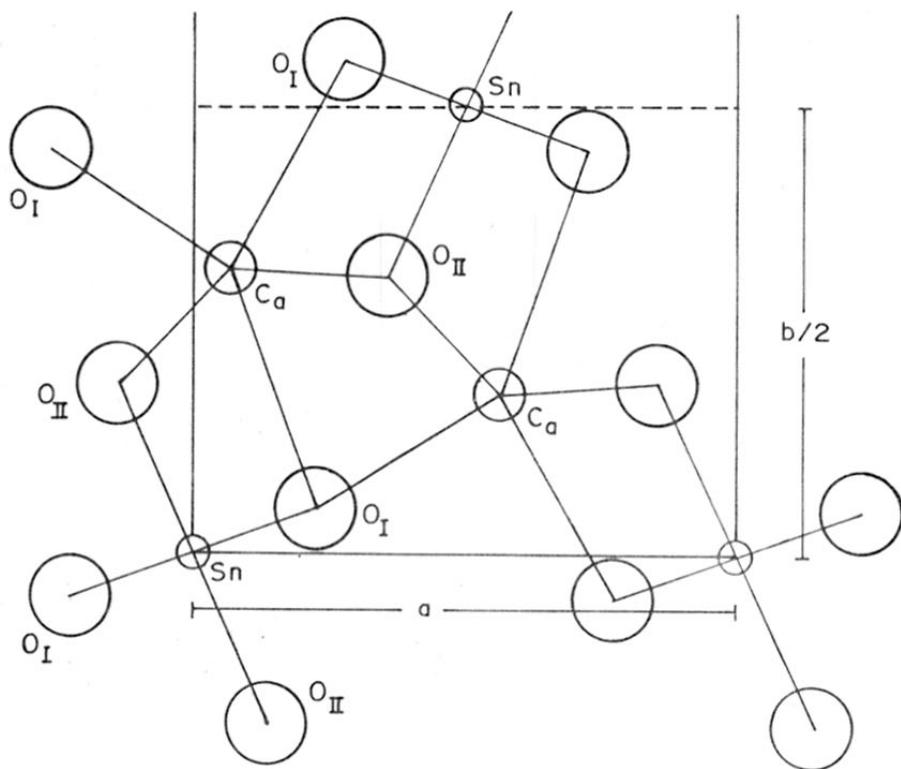


FIG. 1-3: Ca_2SnO_4 PROJECTION ON (001)

[Ref: (36)]

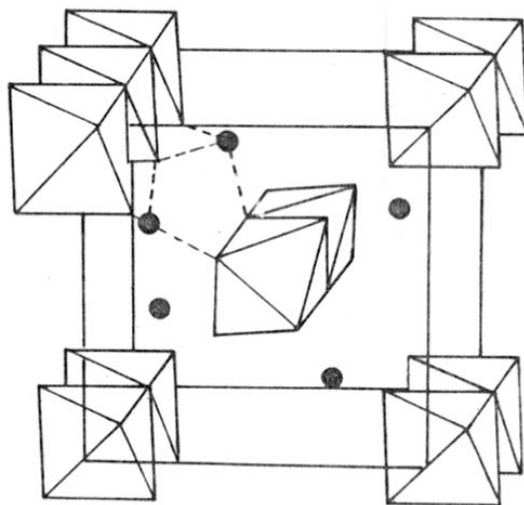


FIG. 1-4: α $[\text{Pb}_3\text{O}_4]^{4-}$ CHAINS IN Pb_3O_4 .

● → BIVALENT ATOMS

[Ref. No. 36]

Table 1.8 - Crystallographic data for transparent
conductive oxides

Compound	Structure type	Space group	Cell dimensions (Å)		
			a	b	c
SnO_2	Rutile	$P4_2/mnm$	4.737 ± 2	-	3.1861 ± 1
CdSnO_3	Ilmenite	$R\bar{3}$	5.4530 ± 3	-	14.960 ± 1
CdSnO_3	Perovskite	$Pbnm$	5.4578 ± 4	5.5773 ± 4	7.8741 ± 8
Cd_2SnO_4	SrPbO_4	$Pbam$	5.5684 ± 5	9.8871 ± 9	3.1923 ± 4
In_2O_3	C-rare earth	$Ia\bar{3}$	10.117 ± 1		
In_2TeO_6	Na_2SiF_6	$F\bar{3}m1$	8.8827 ± 3		4.8217 ± 3
CdIn_2O_4	Spinel	$Fd\bar{3}m$	9.1673 ± 5		

Table 1.9 - X-ray diffraction pattern of Cd₂SnO₄

No.	d _(obs)	I _(obs)	(hkl)
1	4.849	15	110
2	3.695	20	120
3	3.191	20	001
4	2.836	100	130
5	2.783	70	200
6	2.679	85	210
7	2.667	100	111
8	2.470	5	040
9	2.415	2	121
10	2.259	20	140
11	2.119	20	131
12	2.052	40	211
13	1.954	20	041
14	1.931	60	221
15	1.844	10	141
16	1.737	20	320
17	1.648	20	060
18	1.617	30	330
19	1.609	55	151
20	1.599	35	241
21	1.596	40	002

contd...

Table 1.9 (contd.)

No.	$d_{(\text{obs})}$	$I_{(\text{obs})}$	(hkl)
22	1.584	25	311
23	1.526	15	321
24	1.484	15	340
25	1.464	2	061
26	1.438	10	251
27	1.418	20	260
28	1.391	40	132
29	1.384	15	202
30	1.378	15	410
31	1.371	5	212
32	1.346	10	341
33	1.339	10	420
34	1.303	2	142

sputter-deposited in Ar and Ar-O₂ atmospheres. Heat-treatment of the films had no effect on the structural properties. The (hkl) values of the peak, incidentally matched with the results of Trömel^{34,36} and Shannon.⁵⁷

Siegel⁶⁵ reported a new structure for Cd₂SnO₄. He prepared it in three forms - sputtered thin films, precipitated mixed hydroxides, fired at 900°C and as fused material under high pressure and high temperature. All of them gave Cd₂SnO₄ with spinel structure. The interplanar distances naturally did not match with those reported by Trömel and Smith. However, Siegel found that the 'd' values and intensities of the reflections had substantial agreement with those reported for CdIn₂O₄ by Skribljak et al.³² The indate had been reported to have inverse spinel structure. The authors compared the scattering powers of Cd²⁺, In³⁺ and Sn⁴⁺ and their ionic radii. He then calculated the lattice parameter of the face-centred cubic cell to be 9.143 ± 0.001 Å. Following the discussion of Blasse⁸⁷, he stated that (8) Cd²⁺ ions occupied tetrahedral sites and (8) Cd²⁺ and (8) Sn⁴⁺ ions occupied octahedral sites.

The X-ray data of Siegel for Cd₂SnO₄ are reproduced in table (1.10).

Table 1.10 - X-ray powder diffraction data for
 Cd_2SnO_4

No.	$d(o)$	$I_1/I(o)$	hkl
1	5.25	10	111
2	3.22	40	220
3	2.74	100	311
4	2.63	30	222
5	2.28	25	400
6	1.858	30	422
7	1.754	70	{ 511 333
8	1.612	80	440
9	1.542	<10	531
10	1.1442	10	620
11	1.391	30	533
12	1.375	30	622
13	1.316	< 10	444
14	1.277	< 10	{ 711 551
15	1.220	20	642
16	1.188	60	{ 731 553
17	1.141	20	800
18	1.076	10	822
19	1.054	40	{ 751 555

contd....

Table 1.10 (contd.)

No.	$d_{(o)}$	$I_1/I_{(o)}$	hkl
20	1.048	20	662
21	1.020	10	840
22	0.9727	10	664
23	0.9577	40	931
24	0.9325	60	844
25	0.8964	10	[10,2,0 862
26	0.8834	50	[951 773
27	0.8793	20	[10,2,2 666
28	0.8343	20	10,4,2
29	0.8242	50	[11,1,1 775
30	0.8080	50	880
31	0.7840	30	[10,6,0 866
32	0.7755	70	[11,3,3 973

Haacke et al.⁶¹ reported that the Cd_2SnO_4 films obtained by sputtering Cd_2SnO_4 or Cd-Sn alloy targets crystallise in the spinel structure. They indicated the presence of CdO phase represented by 2.32 \AA line forming a shoulder on the 2.29 \AA Cd_2SnO_4 spinel line. When the films were heat-treated in argon atmosphere, the electrical conductivity was maximum. Incidentally, they found that this coincided with the disappearance of CdO shoulder as revealed by XRD patterns.

Nozik²³ reported that Cd_2SnO_4 prepared at above 900°C was orthorhombic and corresponded to the structure reported by Smith.¹⁴ He opined that the reaction temperature was critical because below 900°C the Cd_2SnO_4 possessed the cubic spinel structure. The amorphous films of Cd_2SnO_4 obtained by rf sputtering crystallised into cubic phase when heated to 700°C .

Miyata et al.⁷⁵ reported the Cd_2SnO_4 films obtained by dc reactive sputtering were amorphous. They observed $\text{Cd}_2\text{SnO}_4(001)$ and (130) peaks when the films were deposited at a substrate temperature of 200°C . These peaks suggested the orthorhombic structure for the material.

BURSTEIN EFFECT

The large shift of the fundamental optical absorption edge accompanied by large increase in conductivity in a

semiconductor is designated as "Burstein shift" after Elias Burstein. He interpreted this shift due to very small effective electron mass and not because of impurity effect.

This has been referred to by many workers while interpreting the transparent electrode properties of Cd_2SnO_4 . It is observed in CdO , In_2O_3 and ITO also. Stuke²⁹ is credited to have offered several interpretations for this unusual observation at the same time as Burstein.

Tanenbaum and Briggs²⁷ observed an anomalous dependence of optical absorption limit on the impurity content in InSb . They found the absorption limit was at $7.0 \mu\text{m}$ for an intrinsic sample whereas it was at $3.2 \mu\text{m}$ for a relatively impure sample. They, therefore, suggested that the transmission in the region, $3.2\text{-}7.0 \mu\text{m}$ was due to impurity effect. However, Elias Burstein²⁸ gave a different explanation. He believed that this was due to very small effective mass of the electrons in InSb and not due to any specific impurity effect.

He used the relation,

$$\left(\frac{\mu_n}{\mu_p} \right) L = \left(\frac{m_p}{m_n} \right)^{5/2} \quad \dots (1.12)$$

for calculating the effective masses of electrons and holes and obtained the values $m_n = 0.03 m$ and $m_p = 0.2 m$.

He stated that the very small effective mass of electrons was because of a sharp curvature at the bottom of the conduction band. It was associated with a small effective density of states and with a small degeneracy concentration ($N_c = 1.6 \times 10^{17} \text{ cm}^{-3}$ and $n_{\text{deg}} = 1.2 \times 10^{17} \text{ cm}^{-3}$ at 300°K). This rendered InSb to become degenerate at relatively low electron densities. Consequently, the height of the Fermi level, above the bottom of the conduction band increased rapidly with the increase in the electron density. It can be seen from the Fig. (1.5) that the optical absorption limit corresponded to the vertical transitions from the filled band to the lowest unfilled level, E_m in the conduction band. This level is $4kT$ below the E_F . The optical energy gap, E_o is between E_m and the corresponding level in the filled band which is $(m_n/m_p)E_m$ below the top of the filled band and $\neq E_G$.

Here, he assumed spherical energy surfaces. E_m is at the bottom of the conduction band at an electron density $n_m = 6.5 \times N_c = 1.0 \times 10^{18} \text{ cm}^{-3}$.

For n-type InSb,

$$E_o = E_G \quad \text{when e.d.} < n_m \quad \dots \quad (1.13)$$

$$\text{and } E_o \approx E_G + \left(1 + \frac{m_n}{m_p}\right) (E_F - E_c - 4KT) \quad \dots \quad (1.14)$$

when e.d. $> n_m$.

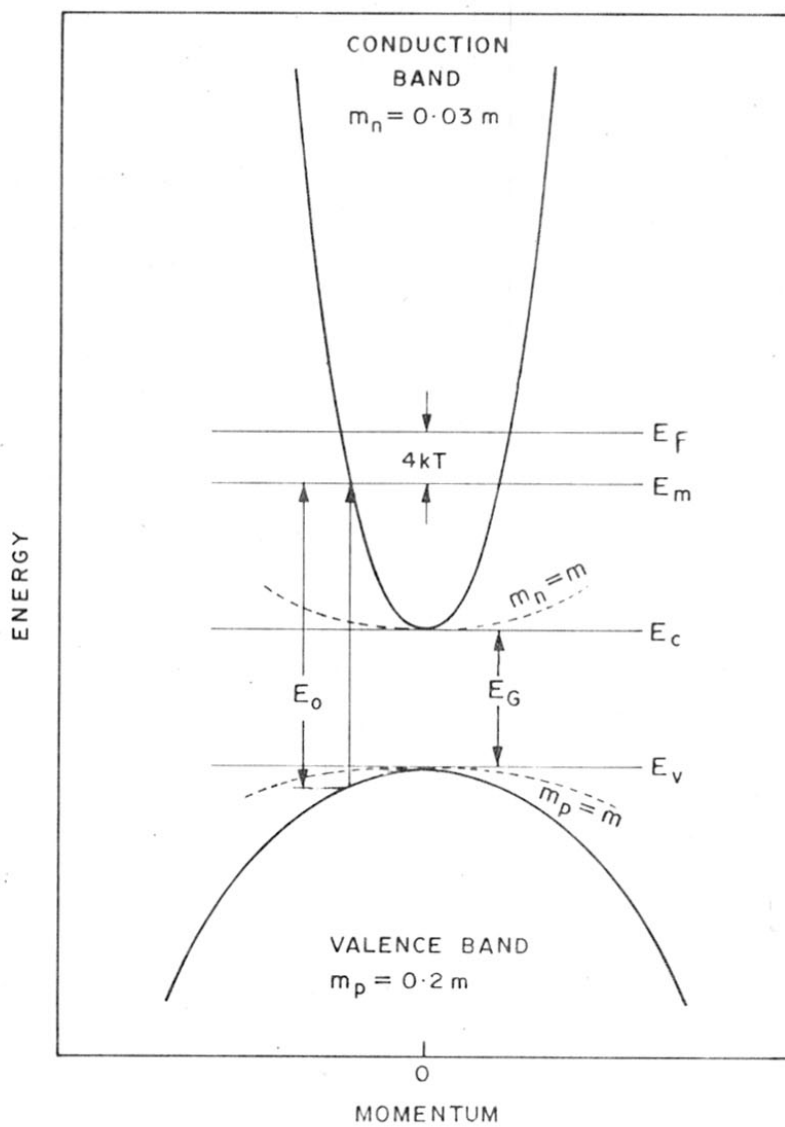


FIG. 1-5: ENERGY-MOMENTUM DIAGRAM OF InSb

For p-type InSb,

$$E_0 = E_G \quad \text{when h.d.} < 1.7 \times 10^{19} \text{ cm}^{-3} \quad \dots (1.15)$$

$$\text{and } E_0 = E_G + \left(1 + \frac{m_p}{m_n}\right) (E_V - E_F - 4KT) \quad \dots (1.16)$$

when h.d. > P_m .

From these calculations, he showed the optical energy gap 0.4 eV to be in agreement with 0.39 eV which corresponded to the absorption limit at $3.2 \mu\text{m}$. Moss³¹ estimated the small effective electron mass in support of the model proposed by Burstein in interpreting the observation of the shift in the optical absorption edge in InSb. This was done in three ways: (i) from the analysis of data on the temperature dependence of the absorption edge, (ii) from the relation between the effective mass and the variation of activation energy with impurity concentration and (iii) from the magnitude of the free-carrier absorption. The three estimates showed close agreement ($m_e/m = 0.034$, 0.028 and 0.032).

In CdO films, Stucke²⁹ found that the fundamental optical absorption edge shift was from 2.3 eV to 2.7 eV with the increase in carrier concentration. Large Burstein effect was caused by the high curvature of the conduction band which was associated with the small effective mass.

It was found to be $0.14 m$, a very small value for an oxide semiconductor. The observed relationship between the effective mass and the carrier concentration deviated from the square dependence of energy on the wave vector at higher energy states. It was therefore concluded that the conduction band must be non-parabolic. The low effective mass of the electrons indicate potentially high mobilities.

In the case of SnO_2 films, the Burstein shift was only 0.1 eV .⁵²

Nozik²³ observed a large Burstein shift in the optical spectra of Cd_2SnO_4 (crystalline and amorphous films). It was for the first time this was observed in the amorphous films. Electron mobility and conductivity increase in the samples was reflected in the large shift of the fundamental optical absorption edge towards uv. He reported a decreased reflectance because of free-carrier absorption in the case of crystalline sample. Visible and infrared transmission spectra of low and high conductivity films indicated large Burstein shift. There was reduced transmission in the red and infrared again because of free-carrier absorption.

He calculated the effective electron mass,

$$m^* = 0.04 m_e \text{ from}$$

$$N = \frac{8\pi}{3 h^3} (2m^* \Delta E_g)^{3/2} \quad \dots \quad (1.17)$$

As described earlier, the shift could be explained on the basis of low density of states at the bottom of the conduction band (low effective mass, deep parabola).

Miyata et al.⁷² earlier studied the optical properties of the rf sputtered Cd_2SnO_4 films and those annealed in Ar/Ar- O_2 atmosphere. They reported a drop in optical transmission in the near IR region and the shift of absorption edge toward uv from 2.23 to 2.53 eV. This corresponded in the carrier concentration change from 4.7×10^{19} to $2.0 \times 10^{21} \text{ cm}^{-3}$. The shift was reported to be due to Burstein-Moss effect. The values of electron effective mass were 0.11 m_e and 0.22 m_e at the above concentrations. They found these results to be similar to those of Nozik²³ but different from those for ITO with parabolic bands.⁸⁶

Mollwo and Stumpp⁸⁸ investigated the intrinsic absorption edge shift in CdO single crystals due to degeneration by high electron concentration in the conduction band. Their reflectivity measurements matched those of Finkenrath.⁸⁹

Haines and Bube⁶² reported the Burstein shift in indium-tin oxide. The optical band gap increased from 3.05 to 3.42 eV with the decrease in resistivity from

8.3×10^{-3} to 4.3×10^{-4} Ω -cm. There was also a decrease in transmission at larger wavelengths due to free-carrier absorption and dendritic precipitates.

Smith and Lyu¹⁰⁰ studied the effect of heat-treatment of the amorphous films of CdO-SnO₂ system in relation to the sputtering atmosphere and target composition. They optimised the preparation conditions: sputtering power (500 W, 1.6 W/cm²) target substrate spacing (3.5 cms), gas pressure (2×10^{-2} torr) and sputtering atmosphere (argon plus 0-10% oxygen). The CdO content in the target varied from 50, 67, 70 to 75 mole percent. The colour of the films varied from pale yellow (high SnO₂ content) to reddish (high CdO content) as against the highly conducting green films of Nozik²³ and Shannon.⁵⁷

The best values they obtained were conductivity ($300 \Omega^{-1} \text{cm}^{-1}$), mobility (15-50 cm²/V-sec), carrier concentration ($6.5 \times 10^{20} \text{cm}^{-3}$) and transmission (80-90%). The authors made some important observations. The decrease in resistivity was attributed to the heating effect on the films structure rather than on the composition of the film. The films annealed in nitrogen increased in large conductivity. However, it was not fully reversible when they were heated in oxygen. The increase in conductivity was related to the increased mobility. The authors opined

that the supposed to be amorphous films consisted of small crystallites ($< 20 \overset{\circ}{\text{Å}}$). Burstein shift was observed with the annealing of the samples.

Similar studies have been made by these authors on ITO.¹⁰¹

THICK FILM TECHNOLOGY¹¹⁸⁻¹²³

In a way, thick film technology has its origin in the development of proximity fuse in 1943 during world war II which heralded the advent of miniaturisation of electronic circuits.

The evolution of thick technology can be traced to the requirements of Aerospace Industry. The incorporated microelectronic circuitry demanded high functional capability, reduced weight, high rate of reliability and, ofcourse, environmental stability.

Thick film, in its present form, is comparatively a recent development. It connotes the deposition of paste materials by screen printing technique. This was developed as a commercially oriented field. More and more sophistication was pumped into its matrix. This particularly became attractive soon when it showed its capability to get resistors of desired specifications for high speed ICs and fast computers. Over years, with improved techniques and clear understanding of the

technology, it is now broad based and is being used in varied studies.^{91-97, 119-123}

The technology includes the sciences of solid state physics and chemistry, glass and ceramic technology, powder metallurgy and polymeric materials and adhesives.

The material reactions are complex and the results of research till recently were proprietary.⁹⁸

Thick film materials generally consist of finely divided, electrically active materials, insulating glass frits, organic fillers and vehicles. Each component has a definite role to play. The electronic conduction takes place in the active materials comprising metals, semiconductors and dielectrics. The glass frits provide good adhesion between the active particles and the substrate. They are based on Pb, Bi, Cd or Zn borosilicate glasses. The organic filler is ethyl cellulose and the vehicles are low vapour pressure organic solvents. Together, they control the viscosity of the paste materials and the useable components into position.

SCREEN PRINTING

It is a technique of depositing paste material on a substrate through a screen stencil using a squeegee to the desired shape and size.

Screen printing or mitography has been a vital tool in the development of THICK FILM TECHNOLOGY. It is the most practical way of making components and circuits compared to spraying, metallizing or die-stamping. 118

There are six basic factors⁹⁹ which influence the performance of screen printing. These, in essence, control the film thickness. Consequently, the electrical and other properties are tremendously affected.

1) SQUEEGEE

It is a blade which forces the paste to pass through the stencil. The squeegee material must be compatible with the resins and solvents used in the pastes. In literature, polyurethane, neoprene, viton are mentioned as popular materials. Table (1.11) shows the useful properties of the various squeegee materials. 119

Preferred hardness is from 80 to 90 on durometer. This is required to maintain constant attack angle ($45-60^{\circ}$), sharp cut off of the paste, clean surface and longer life of the screen. It provides line contact with the screen in operation. Squeegee pressures vary 1-10 pounds per linear inch. This depends on the paste viscosity, screen tension and breakaway distance. Excessive pressure results in coining of the screen. Squeegee motion is to be smooth and uniform.

Table 1.11 - Some significant properties of elastomeric materials

Material	Practical hardness (Durometer)	Abrasion resistance	Solvent resistance				Acid resistant
			Aliphatic Hydrocarbons	Aromatic Hydrocarbons	Oxygenated alcohols & ketones	Oils and gasoline	
Polyurethane	55-95	Outstanding	Excellent	Good	Poor	Excellent	Poor
Neoprene	40-95	Very good	Good	Fair	Poor	Good	Good
Nitrile	40-95	Good	Excellent	Good	Poor	Excellent	Fair
Butyl	80-90	Good	Poor	Poor	Very good	Poor	Very good
Silicone	40-85	Poor	Poor	Poor	Fair	Fair	Fair
Fluoro carbon	60-90	Good	Excellent	Excellent	Poor	Excellent	Very good

The ratio of the squeegee length to the screen size is very important. The thumb rule practice is to leave at least one inch border all around the pattern.

ii) INKS OR PASTE FORMULATIONS

This has been discussed earlier. Essentially, all the thick film materials should be thixotropic pastes. They must have high viscosity values at room temperature. The viscosity of the paste depends on the type of the solid material and its particulate size. Extreme care is taken to maintain constant viscosity value.

iii) SCREEN

The chief component of the screen printing equipment is the screen itself. It is a fine woven fabric made of silk, nylon or stainless steel. The thread can either be mono- or multifilament type. The general range of mesh count is from 120-400. The mesh count is defined as the number of openings per linear inch of the screen. Thicker prints are obtained with lower mesh number.

iv) SUBSTRATE

It is a support on which the prints are deposited. The high temperature process demands ceramic materials for substrates. Steatite, beryllia, barium titanate are mentioned in literature. The most widely used and

popularly accepted material is 96% alumina. The balance 4% is a binder. It is $MgSiO_3$ with American manufacturers and $CaSiO_3$ in the case of European makers. The important properties of the substrates are surface finish, flatness, permeability, flexural strength, compressive strength, camber, thermal coefficient of expansion, thermal conductivity, water absorption, volume resistivity and compatibility with thick film materials.

v) SCREEN PRINTER

Many types of screen printing machines are marketed now. Each has its individual specific processing advantages with the attached novel facilities. Substrate positioning is done by X-, Y- and θ -micrometer adjustments. The squeegee pressure and speed and breakaway distance of the stencil from the substrate are some of the important features which decide the selection of the printer.

vi) DRIER AND FURNACE

The prints are placed on a flat surface immediately after deposition. This is called settling step. Here the paste regains the viscosity fully and the mesh marks may get evened out.

The prints are then dried under a battery of infrared lamps in a clean chamber. The solvents volatilise out. The drying is carried out at 125-150°C/15 minutes.

The final stage is firing. This is a complex operation and calls for extreme care. It is carried out in a multi-zone, continuous and belt-driven tunnel furnace. The temperature in each zone is precisely controlled. The prints are passed through the furnace at the desired speed.

In the pre-peak firing zone the organic matter burns out and the glass frit softens at a steady rate. Metal/metal oxides start sintering, chemical changes take place and attain the desired electrical properties. The molten glass anchors the film to the substrate and provides a vitreous bond. The period for which the prints remain at peak temperature is known as dwell time. The cooling rate is also controlled. A slow-cool down of the prints prevents thermal shocks of the glass phase. A fast rate may impart microcracks in the body matrix and disadvantageously influence the properties.

CHAPTER - II : EXPERIMENTAL TECHNIQUES

II. EXPERIMENTAL TECHNIQUES

2.1 PREPARATION OF CADMIUM ORTHOSTANNATE

The Cd_2SnO_4 was prepared by high temperature solid-state reaction between reagent grade cadmium oxide (brown) and tin oxide (white) taken in the 2:1 mole ratio. Proper care was taken with regards to moisture by drying the oxides at $120^\circ\text{C}/2$ hours. They were mixed thoroughly in an agate mortar under the medium of distilled acetone. The dried mixture was transferred to a platinum crucible and was covered with a platinum lid. The sample was fired in a muffle furnace in air at $1050^\circ\text{C}/6$ hours. Platinum - 10% rhodium-platinum thermocouple measured the temperature within $\pm 5^\circ\text{C}$. The material was then furnace cooled. The product of the solid state reaction was bright yellow. The loosely bound lumps were finely powdered.

2.1.1 X-RAY ANALYSIS OF Cd_2SnO_4

The sample was analysed by X-ray diffractometer (Philips PW1730, Holland) for its compound formation. Cu K α radiation was used. The diffractogram covered angles of 2θ between 15 and 75° . It is shown in figure (2.1) and the structural data is presented in the table (2.1). The ' d '_{obs} values were calculated using Bragg's relation,

$$n\lambda = 2d\sin\theta \quad \dots (2.1)$$

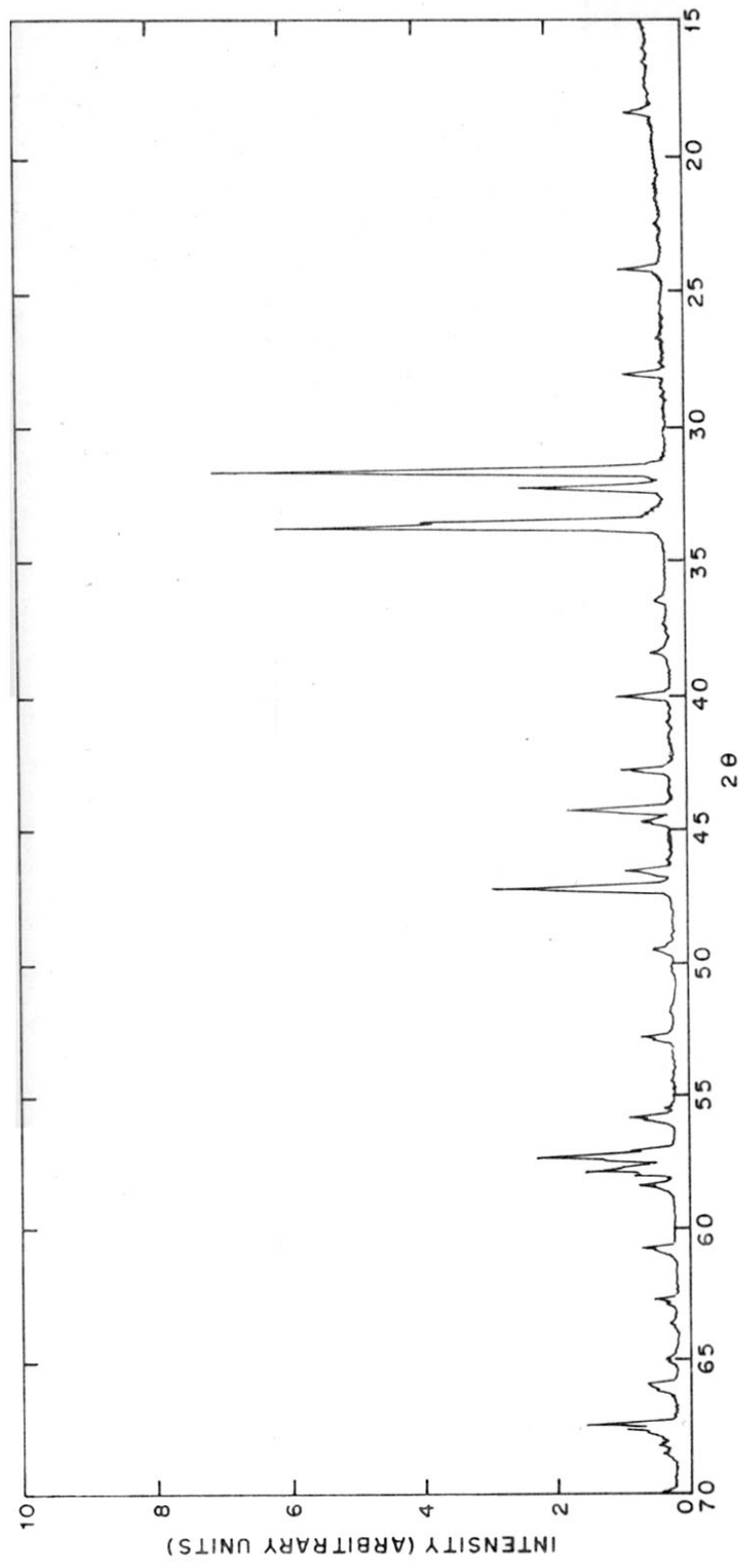


FIG. 2·1: X-RAY DIFFRACTOGRAM OF Cd_2SnO_4

Table 2.1 - Structural data for Cd₂SnO₄

No.	2θ	d_{obs}	d_{cal}	I/I _o	(hkl)
1	18.40	4.8176	4.8280	6	110
2	24.18	3.6775	3.6810	10	120
3	28.04	3.1794	3.1879	9	001
4	31.65	2.8246	2.8250	100	130
5	32.25	2.7729	2.7692	30	200
6	33.56	2.6680	2.6659	54	210
7	33.70	2.6572	2.6603	86	111
8	36.44	2.4635	2.4633	3	040
9	38.40	2.3421		4	
10	39.98	2.2531	2.2507	11	140
11	42.70	2.1157	2.1143	12	131
12	44.20	2.0473	2.0451	22	211
13	44.66	2.0273		7	
14	46.50	1.9513	1.9492	11	041
15	47.16	1.9255	1.9245	40	221
16	49.50	1.8754		4	
17	52.76	1.7335	1.7288	7	320
18	55.76	1.6472	1.6422	10	060
19	57.00	1.6142	1.6093	10	330
20	57.25	1.6077	1.6043	31	151

Table 2.1 (contd.)

21	57.40	1.6039	1.5939	15	241
22	57.78	1.5943	1.5939	19	002
23	58.30	1.5813	1.5770	9	311
24	60.70	1.5244	1.5196	7	321
25	62.60	1.4826	1.4773	5	340
26	63.52	1.4633	1.4599	1	061
27	64.80	1.4375	1.4339	2	251
28	65.90	1.4161	1.4125	7	260
29	66.00	1.4142	-	5	-
30	67.30	1.3900	1.3882	19	132
31	67.52	1.3860	1.3814	11	202
32	67.70	1.3828	1.3712	7	410
33	68.02	1.3771			
34	68.42	1.3700	1.3681	4	212
35	69.90	1.3446	1.3416	4	341
36	72.50	1.3026	1.3008	2	142

These values compared well with those reported by Shannon et al⁵⁷ (table 1.8). The relative intensity values were obtained from the peak heights. Corresponding reflecting planes (hkl) were taken from Shannon et al data (table 1.8) for calculating the lattice parameters, a, b and c using the formula,

$$\frac{1}{d^2} = \frac{h^2}{a^2} + \frac{k^2}{b^2} + \frac{l^2}{c^2} \quad \dots \quad (2.2)$$

'd'_{cal} values were calculated from the above cell dimensions and the (hkl) values. They matched with 'd'_{obs} values very closely.

The X-ray analysis and the colour of the sample confirmed that the reaction product was Cd₂SnO₄ as reported by others.^{23,33,52,57} The particle size of the Cd₂SnO₄ was checked by SEM and was found to be 2-3 μm in size. Figure (2.2) shows the photomicrograph of Cd₂SnO₄ particles.

This was the basic material used for further studies.

2.2 FORMULATION OF THE PASTE

2.2.1 GLASS FRIT

The properties of the glasses control the film

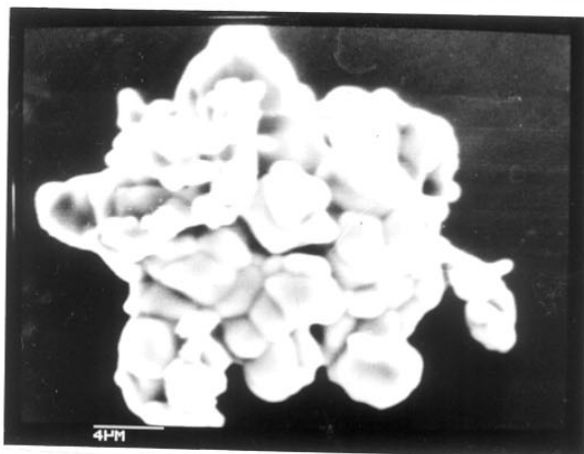


FIG. 2.2. SEM PHOTOMICROGRAPH
 Cd_2SnO_4 PARTICLES



FIG. 2.4. SEM PHOTOMICROGRAPH
GLASS POWDER.

properties to a large extent.

<u>Property of glass</u>	<u>How it influences the film property</u>
i) Temperature-viscosity relation	Determines the film firing temperature.
ii) Surface tension	Controls the mechanical properties of the films
iii) Chemical reactivity	Affects the electrical properties of the films.
iv) Coefficient of thermal expansion	Affects the bondability and the surface structure.

Based on the above observations and on our own experience, we selected lead oxide based glass. The composition of the glass consisted of PbO , B_2O_3 , SiO_2 , ZnO and ZrO_2 in the ratio 66:10:16:5:3. respectively. The ingredient oxides taken were chemically pure. Boron trioxide is highly hygroscopic and is difficult to handle for accurate weighings. Corresponding weight of boric acid was therefore used. The required silicon dioxide was prepared by freshly precipitating it from silicon tetrachloride. It is carried out by the hydrolysis of the distilled, chemically pure $SiCl_4$ prepared in the laboratory. ¹⁰³

Liquor ammonia (1:1) was added to the cooled SiCl_4 at a slow rate, keeping the contents always stirred. After completing the hydrolysis, the silica gel was slurried to get a homogeneous mass and filtered through the Buchner funnel. The solid was washed thoroughly using hot, distilled water to remove all the soluble salts. The filtrate was tested for the absence of Cl^- ion with the AgNO_3 solution. The silica gel cake was dried in an electric oven at 110°C . After complete drying, it was heated at $600^\circ\text{C}/2$ hours in a high temperature muffle furnace to remove the last traces of adsorbed moisture. This silica was used for making the glass frit.

The component oxides were mixed by wet milling in a ball-mill using acetone as medium. The ball-mill is shown in the figure (2.3). The roller speed was adjusted at 40-45 rpm. Mixing was carried out for one hour.

The slurry was filtered through a Buchner funnel. The cake was dried and was transferred to a clean platinum crucible. This was introduced into a muffle furnace at $800-850^\circ\text{C}$ and allowed to remain at that temperature for 15-20 minutes. The oxide mixture was melted and it resulted in a clear light brownish-yellow liquid. The molten glass was quickly poured into

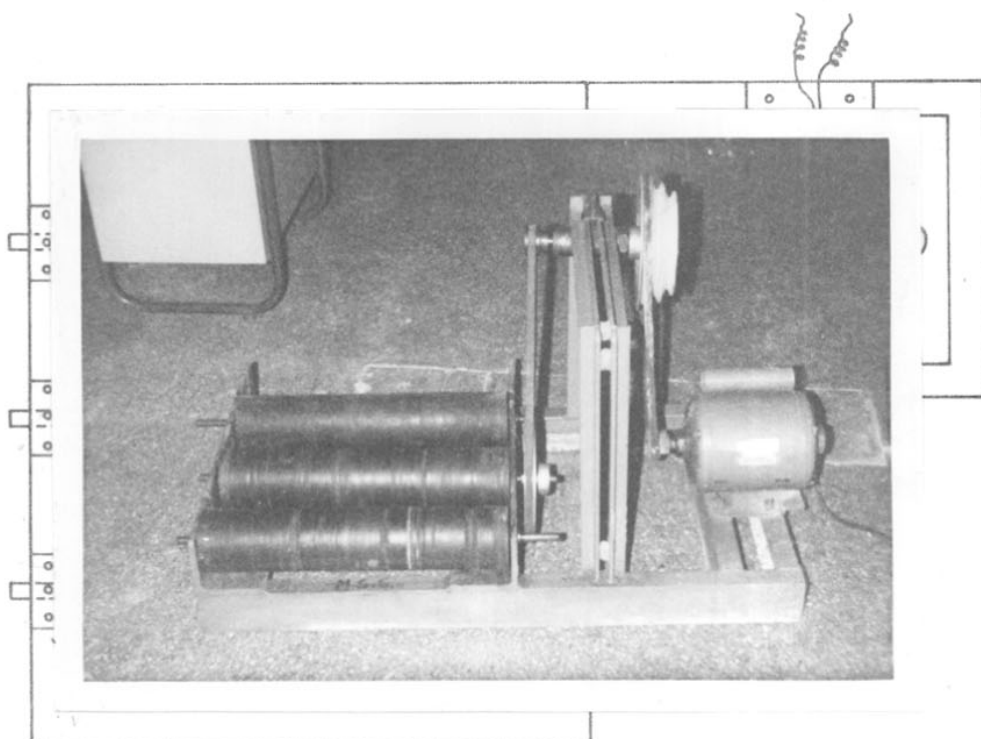


FIG. 2-3: BALL MILLING UNIT

distilled water. This is called FRITTING. The glass lumps and frits were pounded in a stainless steel mortar-pestle to about 40-60 mesh particle size.

The coarse powder was ball-milled in stainless steel jar with s.s. balls under distilled water for 50 hours. The glass slurry was dried. The particle size was measured from the SEM photomicrograph and was found to be ^{B-10}~~2.3~~ μ m on average, figure (2.4).

2.2.2 ORGANIC BINDER PREPARATION

Generally, 8% ethyl cellulose in an organic solvent mixture is used as a binder. The solvent mixture depends on the type of the material (amorphous, crystalline, coarse, fine etc) under study which is to be formulated in the form of a paste. Moreover, screen clogging and quick drying of solvents are detrimental to obtain first class prints. The volatile nature of the solvent system plays a decisive role in the screen printing. Excessively volatile solvent tends to dry out during printing and a solvent of very low volatility does not provide good wetting of the solid particles. Hence, it is always the practice in the thick film processing to use a right combination of several solvents having different volatility values.

Fluidity of the paste depends on the extent of the organic part which goes in its formulation. Paste materials must exhibit certain amount of yield such that easy flow occurs under squeegee pressure. It should stiffen and regain its viscosity and remain in that state after deposition. Too much of flow gives rise to smearing and poor definition of the prints; too little flow results in the retention of the screen pattern on the prints. Extreme case would be patchy prints.⁹²

The ratio of organic binder to the inorganic solids depends largely on the nature and physical structure of the active material.

Several formulations were studied. The results are presented in table (2.2).

From the above results, we fixed the inorganic to organic ratio at 80:20. Moreover, this paste was thixotropic in nature. This ratio was maintained in all our further formulations.

Thus, 8% of the 20 parts of organic content was ethyl cellulose. The solvent mixture consisted of butyl cellosolve, butyl carbitol acetate and terpineol in the ratio 25:25:50 (v/v).

Table 2.2 - Effect of the organic binder to Cd_2SnO_4 glass ratio on the quality of the prints

Cd_2SnO_4 + glass (%)	Ethyl cellulose (%)	Solvent mixture (%)	Result
85	1.2	13.80	Paste was thick screen clogging
80	1.6	18.40	Paste was paint-like in consistency easy to print, good line definition, wetted the substrate.
70	2.4	27.60	Fluidity increased films were thin.
65	3.0	32.00	Prints were patchy, no line definition, island formation present

The cellulose was well massicated in the solvent mixture in an agate mortar to get a clear sticky mass. The Cd_2SnO_4 glass powders in the ratio (95:5) were mixed separately. This was added to the binder and processed to get a smooth yellow paste. This is referred to as cadmium stannate paste in the following pages unless otherwise stated.

Table (2.3) shows the components of the paste, and their functions for a typical formulation.

The five thick film paste formulations based on the glass content (reasons are given in the later section) are presented in table (2.4).

2.3 SCREEN PRINTING TECHNIQUE

2.3.1 PREPARATION OF THE STENCIL

The screen frames are usually made of either wood or metal. We selected smooth, soft and seasoned wood for our purpose. The frame (8" x 10" size) had rigid corners. The rim was 1" wide and a depth of 0.5".

Silk bolting cloth (gauze) of 160 mesh number was degreased and cleaned. It was stretched in wet condition over the screen frame. Care was taken to have even tension in the fabric. 'Stick fast', a thermosetting resin, which cured at room temperature, was applied on

Table 2.3

Sl.No.	Component	Function	Wt.(%)
1.	Cd_2SnO_4	Electrically active material under study	75.0
2.	Lead borosilicate glass	Permanent binder	5.0
3.	Ethyl cellulose	Organic filler controls viscosity	1.6
4.	Solvent mixture (BC + BCA + TPL)	Vehicle facilitates easy printing	16.4
5.	Butyl lactate, Hyoxyd-X-45	Flow control surfactant, wetting agents	2.0

Table 2.4 - Compositions of the formulations

Sl.No.	Cd_2SnO_4 (%)	Glass (%)	PbO content (%)	Organic part (%)
1.	75.0	5.0	3.3	20
2.	78.0	2.0	1.32	20
3.	79.0	1.0	0.66	20
4.	79.5	0.5	0.33	20
5.	79.9	0.1	0.066	20

the rim of the frame. Immediately, the cloth was pressed down on the resin and evened out. The fabric was held stretched till the setting of the resin was complete. The excess cloth was cut out. The frame was painted with a lacquer to make it water-proof. The screen was then washed with warm water.

2.3.2 PREPARATION OF PHOTOSENSITIVE EMULSION

Polyvinyl alcohol and ammonium dichromate solutions (both 10% w/v) were prepared. 10 ml of ammonium dichromate (sensitiser) were added to 100 ml of PVA solution and mixed well. The sensitised solution was stored in amber coloured bottle in dark.

2.3.3 COATING OF THE SILK SCREEN FABRIC

The screen was coated in day light (sunlight was avoided). The solution was poured on the underside of the screen along one of the edges. A wooden scraper was applied on the screen and pushed the solution back and forth 2-3 times to get a uniform coat. The solution on the bottom side was evened out.

The screen was kept in dust-free dark room. An electric fan was switched on and directed towards the screen. This facilitated to dry the coat in about 15-20 minutes. A second coat if necessary, was given on this dried coat to get a tough screen. The dried screen was examined in orange safe light.

2.3.4 TRANSFERRING OF DESIGN TO THE SCREEN

A soft foam rubber base was placed below the screen. The photographic positive of the design (5 mm x 20 mm) was laid flat on the sensitised screen and was secured with a adhesive tape. A clean glass plate was positioned on the film and was securely clamped to the screen frame. Perfect contact between the film and the screen was ensured by the soft foam rubber pieces. The positive was exposed to light.

Different light sources are used in practice. Distance of the light source and time of exposure are the factors to be reckoned, table (2.5). Exposure step is the most important processing step.¹²⁵

It was essential to control the temperature at the face of the glass at 30°C. After exposing the screen to the sunlight, it was brought into the dark room. The positive and the glass plate were removed and the silk screen was immersed in cold water for 2 minutes. This was followed by a second treatment in a fresh bath of water at 35 - 40°C. All the soluble PVA was removed. A light spray of water cleared the pattern. The screen was kept on a filter paper to blot out the moisture. The stencil was dried and examined for any flaws. Any 'pin holes' outside the design were blocked by applying

Table 2.5 - Factors governing exposure

Light source	Distance from light source	Time of exposure required
Strong sunlight	-	5 min.
Bright daylight	-	10 min.
Dull daylight	-	upto 2 h.
Mercury vapour lamp	450 mm	15 min.
150 W lamp	450 mm	3 h.
300 W lamp	600 mm	upto 2 h.

the same emulsion and following the rest of the procedure. The stencil was then ready for screen printing. Figure (2.5) depicts the stencil.

2.3.5 PRINTING BOARD

A formica top wooden board was taken. A hard rectangular wooden bar (teak wood) was fixed at one end of the board with hinges. The stencil frame was fixed to the bar with a 'c' lamp. Using some packing, the stencil was adjusted to fall exactly on the substrate kept in a recess curved out on the board. It could be replaced by a fresh one for printing a large number of samples. The hinge arrangement provided easy operation of lifting and exact positioning of the stencil frame.

The printing board is shown in the figure (2.6).

Figure (2.7) shows the semi-automatic screen printing machine (Accu-Coat, Model 3100) of M/s. Aremeo, U.S.A. This was used to screen print some of the samples.

2.3.6 SQUEEGEE

Polyurethane squeegee was used. The squeegee material was resistant to abrasion, distortion and swelling in the solvents during the printing operation. The hardness was 50-95 on durometer.

Suitable size (5 cm^2 square of 0.8 cm thick) was cut and fixed to a wooden handle. Figure (2.8) depicts the squeegee.

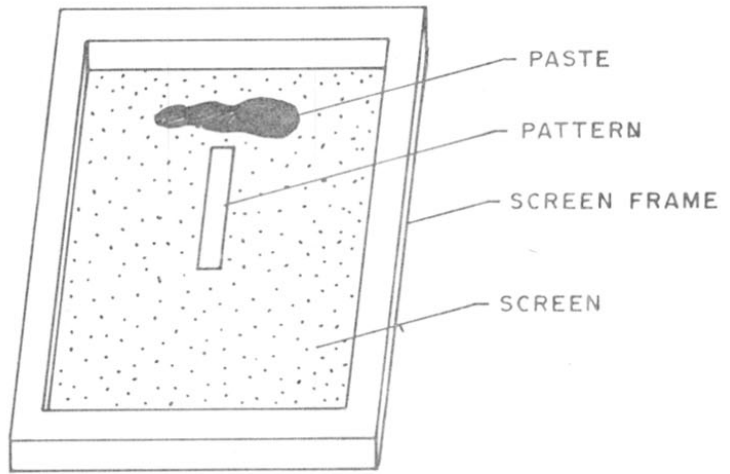


FIG. 2·5: SCREEN STENCIL

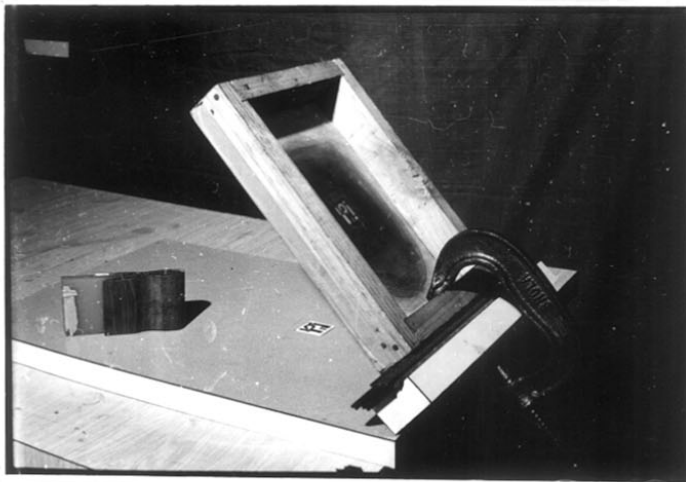


FIG. 2·6: SCREEN PRINTING BOARD

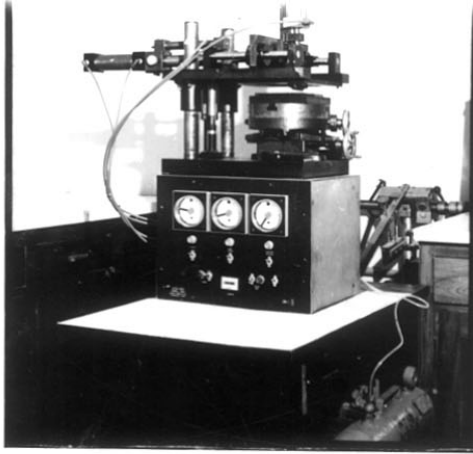


FIG. 2·7: AREMCO SCREEN PRINTING MACHINE (MODEL 3100)

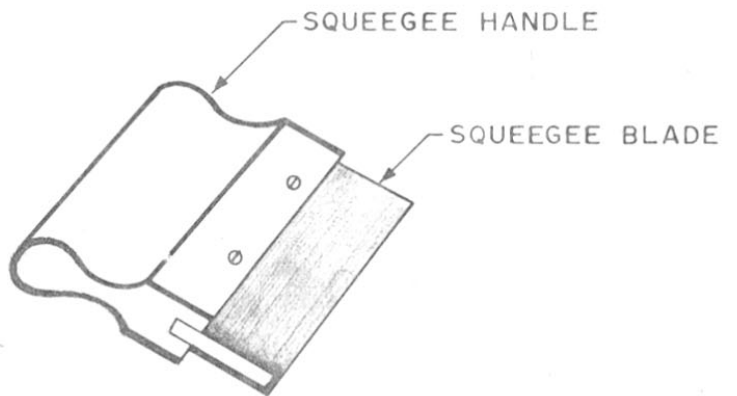


FIG. 2·8: SQUEEGEE

2.3.7 SUBSTRATE

Since our study involved firing of the sample films at 500-900°C, we used 96% alumina substrates. They were supplied by M/s. Technical Ceramics Products Division, U.S.A. Substrate material has direct bearing on the properties of thick films.

Typical values of 96% Al₂O₃ substrates

Dielectric constant (1 MHz) 25°	..	9.2
Volume resistivity (Ω-cm), 25°C	..	10 ⁴
Dielectric strength, V/mil, 60 Hz	..	225
Loss tangent/dissipation factor	..	0.001
Loss factor	..	0.009
Density (g/cm ³)	..	3.75
Maximum temperature (°C)	..	1700
Thermal conductivity (cal/cm/sec/cm ² /°C)	..	0.063
Thermal coefficient of expansion, 25-200°C	..	5.9x10 ⁻⁶
Hardness (Rockwell)	..	79

2.3.8 CUTTING OF SUBSTRATES

Substrate scriber of M/s. Mechanization Associates, U.S.A. (Model 1300C), was used for the purpose. The top

plate of the scriber is provided with a vacuum chuck for holding the substrate. The diamond cutter fixed to the carriage assembly cuts the substrate while moving back and forth. One revolution of index wheel advances the chuck assembly by 50 mils. One can advance it by as small a distance as 5 mils. The depth of the cut is adjusted by the height adjustment knob. Several such strokes result in a deep scribe. The substrate is then fractured by holding it with one hand at the edge and pulling it while bending. Figure (2.9) shows the scriber.

2.3.9 CLEANING OF THE SUBSTRATES

The substrates were soaked in a liquid detergent for one hour. They were then washed thoroughly, first with tap water and then with distilled water. Next, they were rinsed with deionised water. Finally, the substrates were given a wash with distilled acetone. After draining, the pieces were dried in an electric oven at $110^{\circ}\text{C}/2$ hours. The dried substrates were cooled in a desiccator. Required number were taken out at a time for screen printing.

2.3.10 SCREEN PRINTING OF Cd_2SnO_4 PASTE

a) WITH PRINTING BOARD

The Al_2O_3 substrate was seated in the recess on the printing board (Fig.2.6). It was held by the adhesive

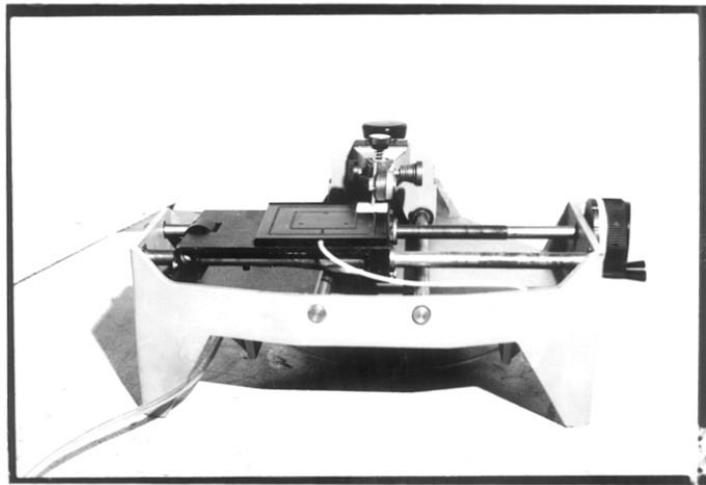


FIG. 2.9. SUBSTRATE SCRIBER

tape at the corners. This arrangement prevented the substrate from sticking to the stencil and coming along with it after the printing operation was over. The stencil (5 mm x 20 mm) was fixed to the board and was lowered on to the substrate. The distance between the stencil and the board was adjusted. Paste was deposited at one end of the pattern. The squeegee was brought at an approach angle of 45° into physical contact with the stencil. As the squeegee advanced, the screen got lowered and stress was induced into the paste. This resulted in lowering the viscosity of the paste which then passed through the stencil easily and got deposited on the substrate. By this time, the squeegee had already advanced further. The screen was then snapped back because of its tension and got separated from the substrate. This continuous process resulted in the desired print of 5 mm x 20 mm. Required number of such prints were made. Sequence of operation is shown in the figure (2.10).

b) WITH SCREEN PRINTING MACHINE

Aremco Accu-Coat, model 3100 screen printing machine was also used (Fig.2.7). The substrate was fixed stationary on the vacuum manifold assembly fastened to the X-Y rotational table. The position

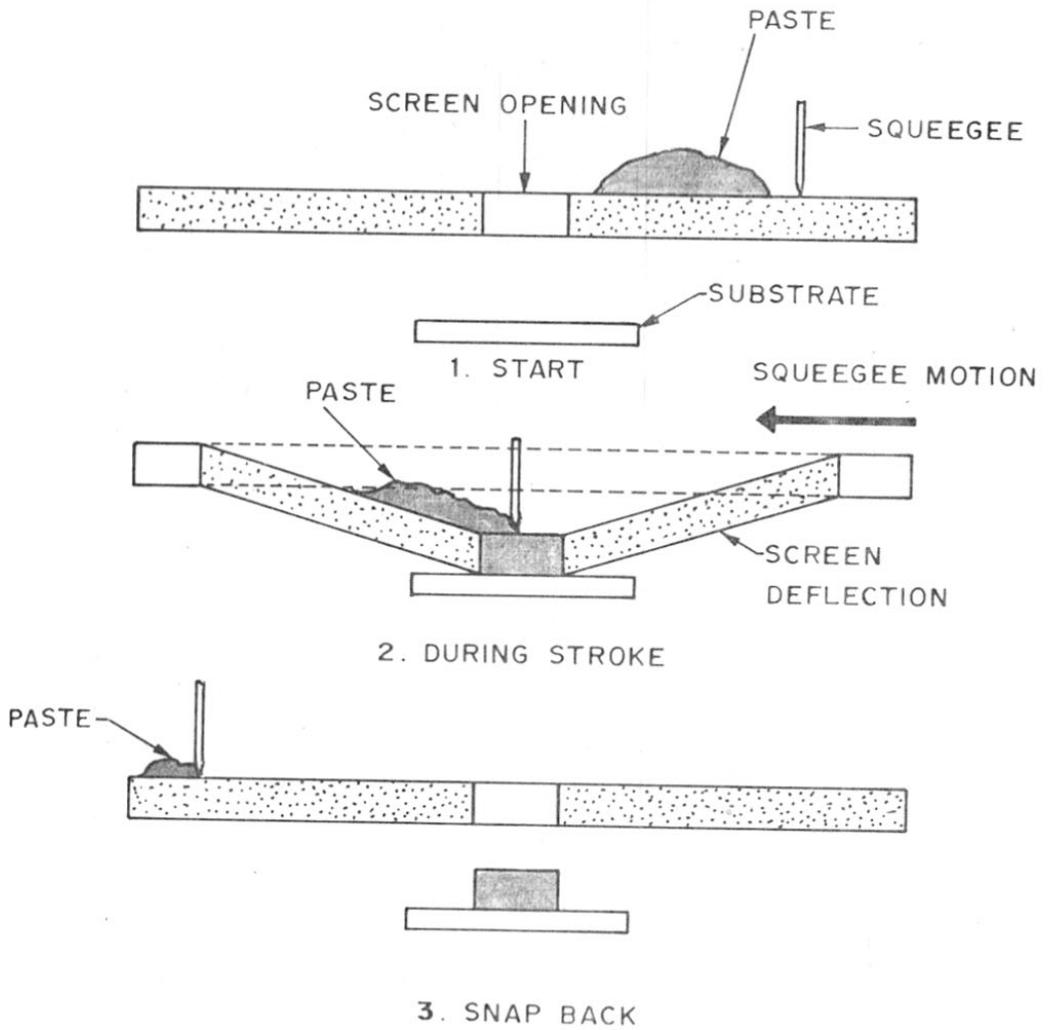


FIG. 2·10: SCREEN PRINTING CYCLE ⁽¹²²⁾

of the substrate could be precisely adjusted in the x-, y- and θ directions. The stencil was fixed to the upper platen which moved vertically down the ground pillars. This provided close alignment and reproducibility. The snap-off distance (down to 0.002") was adjusted by the micrometer. The squeegee holder assembly moved horizontally along the shafts. The squeegee height was suitably adjusted.

The paste was put on the stencil. The platen, print-stroke and squeegee switches were operated in sequence to get a print. The movements were solenoid controlled through timers. The machine operated on 'hydro-check' system.

2.3.11 DRYING OF THE PRINTS

The wet prints were allowed to remain on a clean stainless steel plate for 10 minutes. They were then transferred to a s.s. cubicle in which an IR lamp was fixed at the top. The distance between the prints and the lamp was adjusted such that the samples could dry at 150°C. The drying was completed in 15 minutes.

2.3.12 FIRING OF THE PRINTS

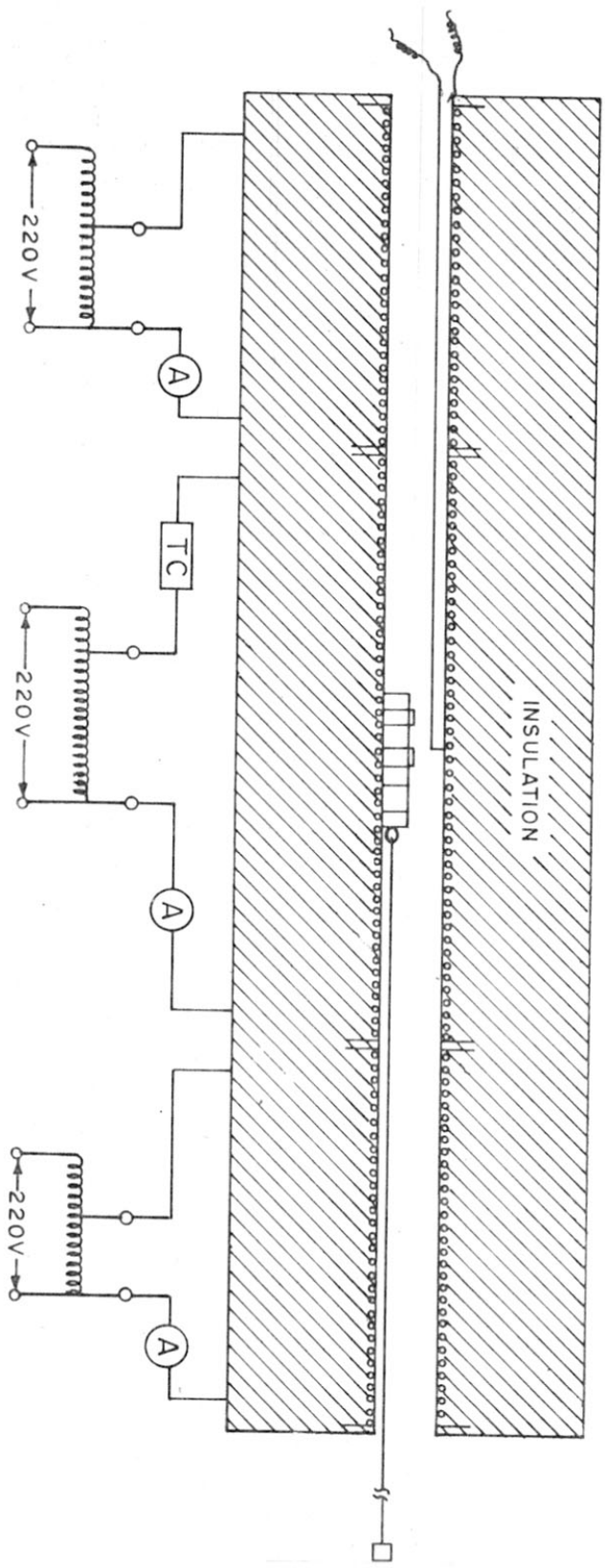
A. DETAILS OF THE FURNACE ASSEMBLY

A three-zone tubular furnace was specially fabricated. It was a fused quartz tube (2" dia x 60" long),

wound with kanthal resistance wire (20 SWG). The current through the three circuits was independently controlled through dimmerstats and ammeters. The length of the middle circuit (70[~]) was double the length of either of the end circuits (20[~] each). Chromel-alumel thermocouple measured the temperature. Temperature controller (Aplab Type No. PTC-372) maintained the desired value. The furnace was tilted up towards the outlet end. This provided a natural draught for the products of pyrolysis. Figure (2.11) gives the details of the furnace.

B. CALIBRATION OF THE FURNACE

The power was supplied to the three circuits through the voltage stabiliser. The peak firing temperature was fixed at a particular value, say 500, 600, 700, 800 or 900°C by the temperature controller. A second thermocouple (5 ft long) in a silica tube was introduced in the furnace. The free ends were connected to the D.C. microvoltmeter (Philips, PP9004). The thermocouple was pulled out inch by inch, every time noting the microvoltmeter reading. The temperature was plotted against the position in the furnace. The temperature profile is shown in the figure (2.12). Such profiles were drawn for each peak temperature. The same BELL shape was obtained for all the peak temperatures.



A — AMMETER
 TC — TEMPERATURE CONTROLLER

FIG. 2-11: THICK FILM FURNACE

C. SILICA TROLLEY

The silica trolley shown in figure (2.13) was fabricated for carrying the samples in the furnace from end to end. A stainless steel rod (2 mm dia) was hooked to the ring of the trolley. The other end of the rod was connected to the copper wire which in turn was wound on a wheel. The wheel was coupled to a synchronous motor through a gear system. The speed of the wheel could be varied by adjusting the gear system. Complete assembly is depicted in figure (2.14).

D. LOADING AND FIRING OF THE SAMPLE FILMS

The peak firing temperature was fixed at a desired value. The silica trolley loaded with samples was introduced at the front end. The trolley was hooked to the steel rod. The synchronous motor was switched on. The copper wire got wound on the wheel pulling the trolley at the constant speed (~ 2" per minute).

In the pre-peak firing temperature zone, the organic matter (both ethyl cellulose and the remaining vehicle) was completely burnt out when the sample reached 300°C .¹⁰⁴ The glass started softening and melted as the peak firing zone was approached. The synchronous motor was switched off. The samples were soaked at peak temperature for 20 minutes. The synchronous motor was then switched on.

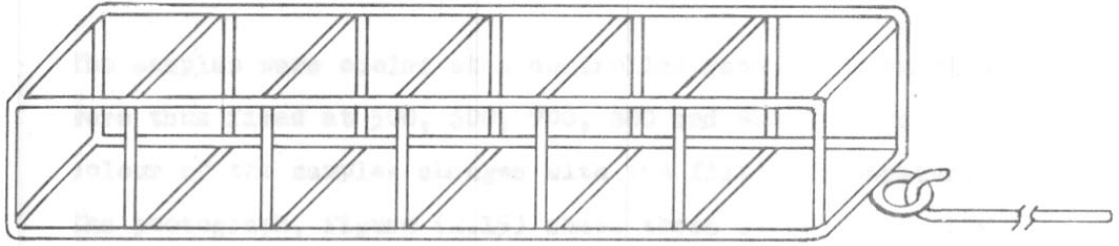


FIG. 2-13: SILICA TROLLEY



FIG. 2-14: THICK FILM FURNACE ASSEMBLY

The samples were cooled at a controlled rate. The samples were thus fired at 500, 600, 700, 800 and 900°C. The colour of the samples changed with the firing temperature. The photograph, figure (2.15) shows these changes.

2.4 DEPOSITION OF ELECTRODES

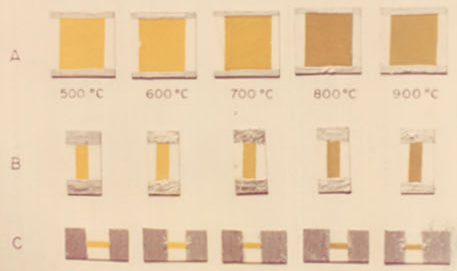
Air drying silver paste and vacuum evaporated silver were tried for electrodes.

A stencil was made to give 2 mm prints at intervals of 2 mm across the fired Cd_2SnO_4 thick film. Silver paste was screen printed on the sample. Likewise, silver was deposited by vacuum evaporation.

The resistance of each portion of the sample was measured in both the cases. The sum of the resistance values of the segments, after correcting for the lengths of the sample covered by the middle electrodes, was nearly equal to the total resistance (end to end) of the sample. This proved that the contact resistance was negligibly small.

2.5 THERMOGRAVIMETRIC ANALYSIS

Thermal analysis is a good analytical technique for the systematic studies of materials under thermal treatment. The physical and chemical changes are recorded with respect to the sample temperature.



A: SAMPLES FOR XRD AND DR SPECTRA
B: SAMPLES FOR ELEC. CONDUCTIVITY
C: SAMPLES FOR THERMO EMF

FIG 2-15

Thermal Analyser (Simultaneous Thermal Analysis Apparatus, NETZSCH-Gerätbau, GmbH, F.R. Germany) was used for studying the thermal effects on the Cd_2SnO_4 samples.

The unit is capable of recording thermal gravity (TG), differential thermal analysis (DTA), derivative thermogravimetry (DTG, first derivative TG, w.r.t. time), and derivative differential thermal analysis (DDTA, first derivative of DTA, w.r.t. time).

It consists of (a) a measuring part with a high temperature furnace (upto $1600^{\circ}C$), which is well insulated to maintain the desired rate of heating, (b) recording and controlling cabinet, and (c) vacuum system. Highly sensitive balance is installed. The furnace can be swung out with a hoisting device. The sample is mounted on to a plug, connected to the balance beam.

The recording of the values is based on the plug-in system. The multiple recording unit registers 6 measuring values with different colours. The printing sequence is at 1 second intervals. There are 8 chart speeds available for selection. The input voltage is 0-25 mv and the recording width is 250 mm.

A matrix selector is provided to facilitate the easy selection of the channels of the compensation point printer.

A constant ambient temperature is maintained for the unit.

SAMPLE MOUNTING

The furnace was moved upwards and swung to the right side. A known weight of (20-50 mg) of the sample was taken in a tared platinum crucible specially designed for it. It was carefully mounted on a ceramic capillary at the centre of the furnace. Pt - 10% Rh - Pt thermocouple measured the temperature.

The furnace was brought down and properly aligned. The furnace was switched on after setting the desired heating rate. The plugs selected for temperature, TG, DTA and DTG were inserted in the matrix selector. Proper programming was done for the sequential operation of the pointers.

2.6 X-RAY ANALYSIS OF PbO-DOPED Cd₂SnO₄ THICK FILMS

SAMPLE PREPARATION

The cadmium stannate paste (page 77) was screen printed on clean, dry 96% Al₂O₃ substrates using a stencil to deposit 20 mm x 22 mm, following the technique described earlier (2.3.10). A number of samples thus printed were dried, and then fired at 500, 600, 700, 800 and 900°C in the thick film furnace.

The X-ray Diffractometer (Philips, Model PW1730) was used for our structural studies. The thick film sample was directly fixed on the sample holder.

The diffracted X-ray reflections were recorded on chart paper with their intensities against ' 2θ ' values. Cu K α ($\lambda = 1.5404 \text{ \AA}$) X-ray radiation was used with Ni filter.

2.7 SCANNING ELECTRON MICROSCOPE ANALYSIS

The doped Cd₂SnO₄ thick film samples (5 mm x 10 mm), fired at 500, 600, 700, 800 and 900°C were scanned for studying the sintering effects.

SEM technique is a valuable tool. It has a greater depth of field and resolution compared to conventional light section microscope and transmission electron microscope.

SEM is equipped with X-ray analytical capabilities. One can obtain topographic, crystallographic and compositional information rapidly and efficiently. Spot analysis is also possible.

The basic function of the instrument is to produce an image of three dimensional picture on a cathode ray tube. When a finely focussed electron beam impinges on a specimen surface, different types of signals are produced.

These are used to measure various characteristics of the sample surface.

Cambridge stereo scan 150-SEM was used. This has three-lens system with specimen detail resolution achievable to better than 70 \AA .

The magnification ranges from $\times 20$ to $\times 100,000$ which represents a scanned area on the specimen from $6 \text{ mm} \times 5 \text{ mm}$ to $1.2 \mu\text{m} \times 1 \mu\text{m}$ at 10 mm working distance. Additional variable magnification can be obtained using a zoom facility. The true size of the particle is indicated by the micron (μm) mark on the display. The image displayed on the CRT is photographed by a 35 mm camera. The photomicrographs of the samples were taken for evaluation.

2.8 ELECTRICAL CONDUCTIVITY (D.C.)

Two probe D.C. method was used for measurements. Both two-probe^{10,23,61} and four-probe^{23,57,61,75} are reported in literature.

EXPERIMENTAL SET UP

The thick film sample was mounted on a teflon block using phosphor bronze spring clips suitably fixed. A chromel-alumel thermocouple was attached to the substrate. Resin coated copper wires were fixed with the clips. The teflon block was then introduced into a glass container.

The leads and thermocouple wires were taken out through the araldite seal in the holes of the glass cap.

The cold junction of the thermocouple was immersed in kerosene oil cooled by ice made from distilled water. Measurements were carried out under vacuum (10^{-2} torr).

The glass assembly was introduced into a wire-wound tubular furnace. All the wires were connected to the terminals provided on a panel board appropriately. The current to the furnace was controlled through a dimmerstat. A second thermocouple (Cr-Al) was introduced in the annular space of the glass assembly and the furnace such that its hot junction was at the middle of the furnace. The furnace temperature was maintained at a desired value by the temperature controller (Aplab Model 9601).

Sample temperature was measured by the Philips DC Microvoltmeter (Type PP9004). The resistance of the sample was measured by VTVM (Ruthonsha-Simpson, Type 221-I).

The experimental set up is shown in the figure (2.16).

2.9 THERMOEMF MEASUREMENTS

A. SAMPLE PREPARATION

A simple method of making the stencil was devised since the number of samples required was small.

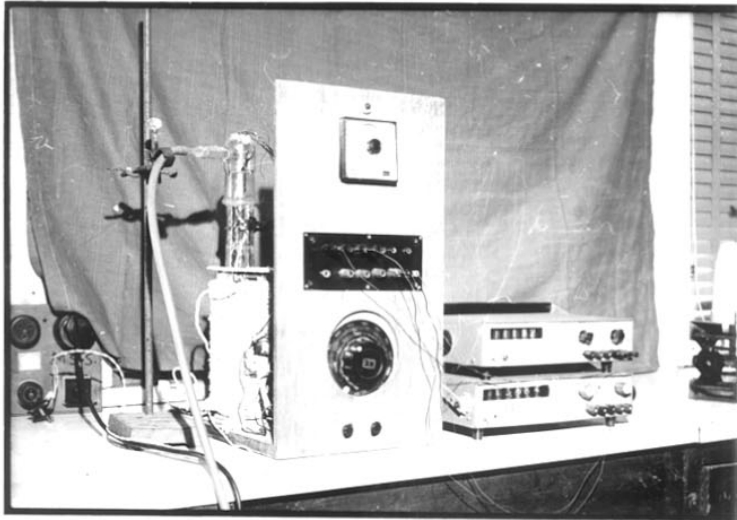


FIG. 2.16. EXPERIMENTAL SETUP FOR
CONDUCTIVITY MEASUREMENTS

Adhesive film was fixed on a microslide. A portion of the film (2 mm x 10 mm) was cut out from its centre with a sharp blade. The rest of the film was carefully peeled off from the microslide and was transferred on to a clean screen (160 mesh). The screen was placed on a level place and the film was rubbed from inside to adhere perfectly to the screen.

Cadmium stannate paste was screen printed on Al_2O_3 substrates using the above stencil. The prints were dried ($150^{\circ}C/15$ min.) and fired at different temperatures. Silver electrodes were deposited by vacuum evaporation on the ends of the samples leaving an interelectrode distance of 6 mm (figure 2.17a).

B. DESCRIPTION OF THE SAMPLE HOLDER

Two mica pieces (15 mm x 20 mm) were fixed in the grooves of the two teflon pieces with a 3 mm gap between them. Heat conduction through mica was thus avoided. The sample was placed on the mica pieces, one end on each of them. A microheater (SnO_2 coated glass plate, 50 μ) was seated on one end by cutting out small portions in the teflon pieces. Air drying silver paste was applied to the microheater for the electrodes. Two phosphor bronze clips fastened to the teflon blocks held the microheater and also provided electrical contacts (figure 2.17b). Two copper-constantan thermocouples were

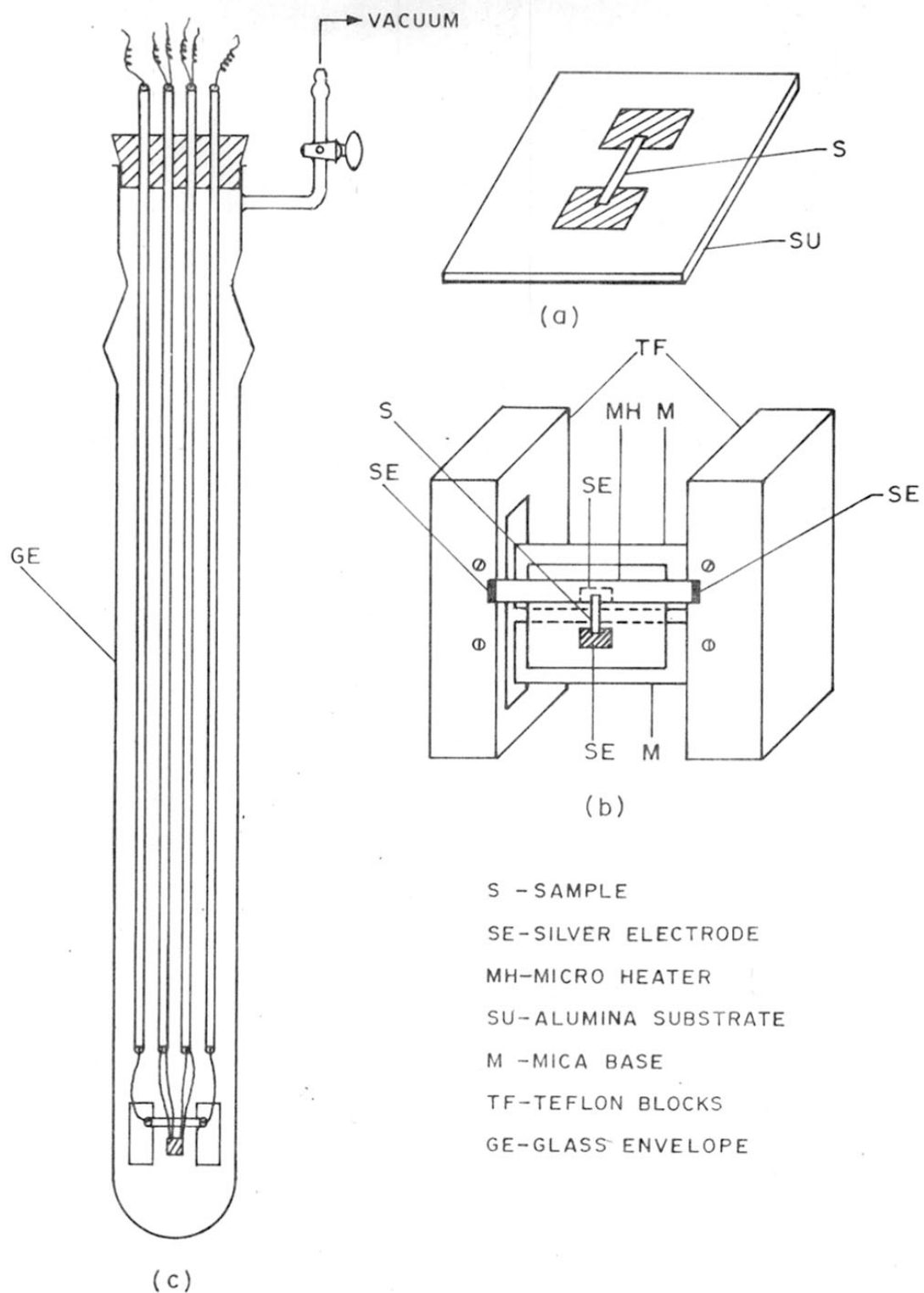


FIG. 2-17: SAMPLE HOLDER FOR THERMO EMF MEASUREMENTS

soldered on to the silver electrodes with the junction tips just touching the sample ends for temperature measurement. Thermoemf was measured with the copper wires of the thermocouples.

The measurement circuitry was shielded using a copper enclosure to avoid any electrostatic pick up. Shielded wires were used for all external connections and were properly earthed.

All the wires coming out from the sample passed through 2 mm copper tubes. The annular space at the ends was sealed with araldite. The sample holder was introduced into a glass envelope which was fitted into a copper cap (figure 2.17c).

The assembly was fixed in a thermostat (VEB, MLW, Prifgerate Werk Medingen, DDR, Model u-10). This can control the temperature of the bath from -60 to $+300^{\circ}\text{C}$ with a regulating accuracy of $\pm 0.02^{\circ}\text{C}$. The unit has a well insulated chamber with contact and control thermometers, stirring system, heaters and pump. The medium is changed depending on the temperature required. The cooling receiver has a copper coil seated at the bottom. Cooling agents like ice, ice + salt mixture and solid CO_2 are used as the case demands. The valve relay is connected to the cooling receiver and the thermostat by the rubber tubing.

The electrically connected valves of the valve relay (connected to the thermostat relay) direct the cooling medium either to the cooling receiver or to the thermostat chamber. It controls the temperature of the thermostat bath by supplying the cooled liquid at intervals. Figure (2.18) shows the set up.

A regulated D.C. power supply was connected to the microheater. D.C. Microvoltmeter was used to measure the emf and the temperatures at the two ends of the sample.

The cold junctions of the thermocouples were kept in kerosene oil in test tubes kept in ice made from distilled water packed in a thermos flask.

2.10 DIFFUSE REFLECTANCE SPECTRA

The same samples used for X-ray diffraction were used for taking diffuse reflectance spectra also. Pye Unicam SP8-100, UV-Vis spectrophotometer was used for the purpose.

The diffuse reflectance of the flat surfaces was measured in conjunction with wavelength programmer in the range 800 nm to 300 nm. The black reference plaque consisted of a disk of unpolished black perspex which typically had a diffuse reflectance of 0.3%.

2.11 X-RAY PHOTOELECTRON SPECTROSCOPIC ANALYSIS

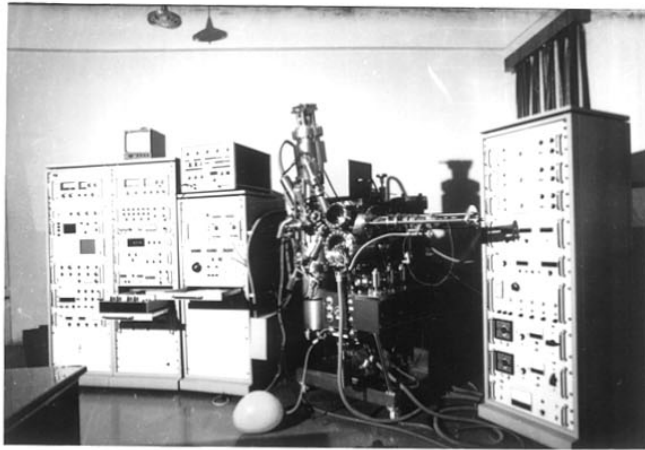
XPS is a very good analytical tool which provides detailed information about the electronic structure of materials. The electronic energy levels are sensitive to their chemical environment and therefore it is the best technique for the determination of different oxidation states of atoms in molecules. It is essentially a surface analysis technique.

ESCA-3, Mark II, spectrometer of M/s. VG Scientific Ltd., U.K., was used. The unit is fitted with a sample preparation chamber in which an argon ion gun is provided. The base pressure is of the order of 10^{-8} - 10^{-9} torr. MgK α (E = 1253.6 eV) and AlK α (E = 1486.6 eV) anodes are used for X-ray generation.

All spectra were taken with pass energy at 50 eV, entry and exit slit at 4 mm, time constant of 0.1 second and sweep time of 300 seconds.

The sample was prepared by screen printing Cd₂SnO₄ paste using the stencil (5 mm x 10 mm, adhesive tape method). The drying and firing of the samples were done in the same way as before.

The thick film sample was mounted on a standard ESCA sample holder, (figure 2.19) using metal clips. Silver



ESCA UNIT

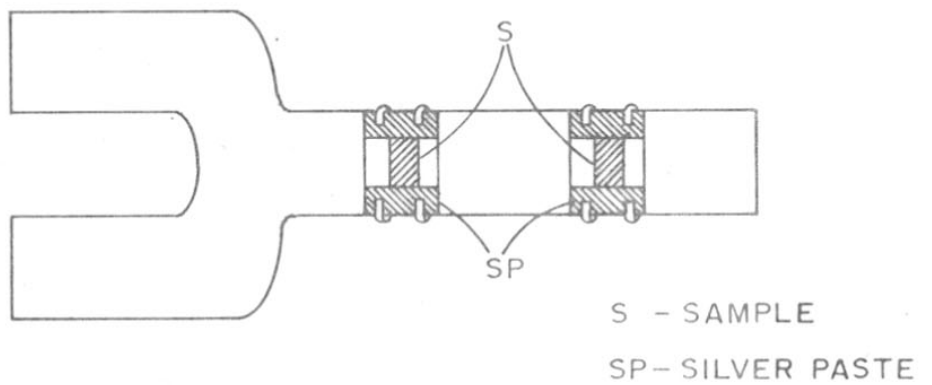


FIG. 2-19: ESCA SAMPLE HOLDER

paste¹⁰⁵ was brushed to the sample edge connecting it to the substrate and the metal plate. This was necessary to avoid charging effect.

Spectra were recorded for the thick film samples fired at (a) 600, (b) 700, (c) 800, (d) 900°C and one parent material with and without glass on the basis "as received".

2.12 MOSSBAUER SPECTROSCOPIC RESULTS

Mossbauer spectroscopy is an analytical technique based on the phenomenon of recoilless emission and absorption of Gamma rays emitted by the nuclei bound in solids. The absorption of Gamma rays induces transitions between the quantum states of the absorbing system. Because of the high resolution, it is possible to obtain fractional line widths of the order of 10^{-13} . The perturbations of the nuclear energy levels through the hyperfine interactions can be possible to measure in the range of 10^{-6} to 10^{-10} eV.

The Mossbauer spectra were taken using a MBS-35 spectrometer (Electronic Corporation of India) operated in the constant acceleration mode coupled to a ND100 multi-channel analyser. The spectrometer was calibrated with a 1 mil natural iron foil using a 4m Ci ⁵⁷Co in Pd matrix. All the spectra were recorded with 2 mCi Ba ¹¹⁹SnO₃

matrix (New England Nuclear Corporation). The absorbers were prepared by spreading well ground powder of each sample between two Al foils of 1 inch radius, sandwiched between two brass rings. The thickness of the absorber was so adjusted that it contained 40 mg/cm^2 of natural tin. In all the cases 10^6 counts were collected in each channel.

CHAPTER - III : RESULTS AND DISCUSSION

3.1 THERMOGRAVIMETRIC ANALYSIS

The differential thermal analysis (DTA), thermogravimetric (TG) and differential thermogravimetric (DTG) graphs obtained for the samples of (i) $2 \text{ CdO} + \text{ SnO}_2$, (ii) $\text{ Cd}_2\text{ SnO}_4$ and (iii) 95 parts $\text{ Cd}_2\text{ SnO}_4$ + 5 parts glass in oxygen atmosphere are presented in figures 3.1, 3.2 and 3.3 for the temperature range $25\text{-}1000^\circ\text{C}$. The rate of heating was adjusted at $10^\circ\text{C}/\text{minute}$ in all the cases.

(1) $2 \text{ CdO} + \text{ SnO}_2$

 CdO and SnO_2 were mixed in the mole ratio of 2:1 and the physical mixture weighing 22 mg was run through the thermal analyser. This was carried out to fix the reaction temperature and also to know any other changes occurring during heating.

DTA thermogram shows that the sample undergoes two clear endothermic changes followed by an exothermic change on heating it upto 1000°C . The first endothermic peak is at 221°C , the second at 300°C , a small hump at 368°C and the exothermic peak is at 583°C (between 370 and 950°C).

The DTG curve shows three distinct peaks corresponding to the above first three temperatures.

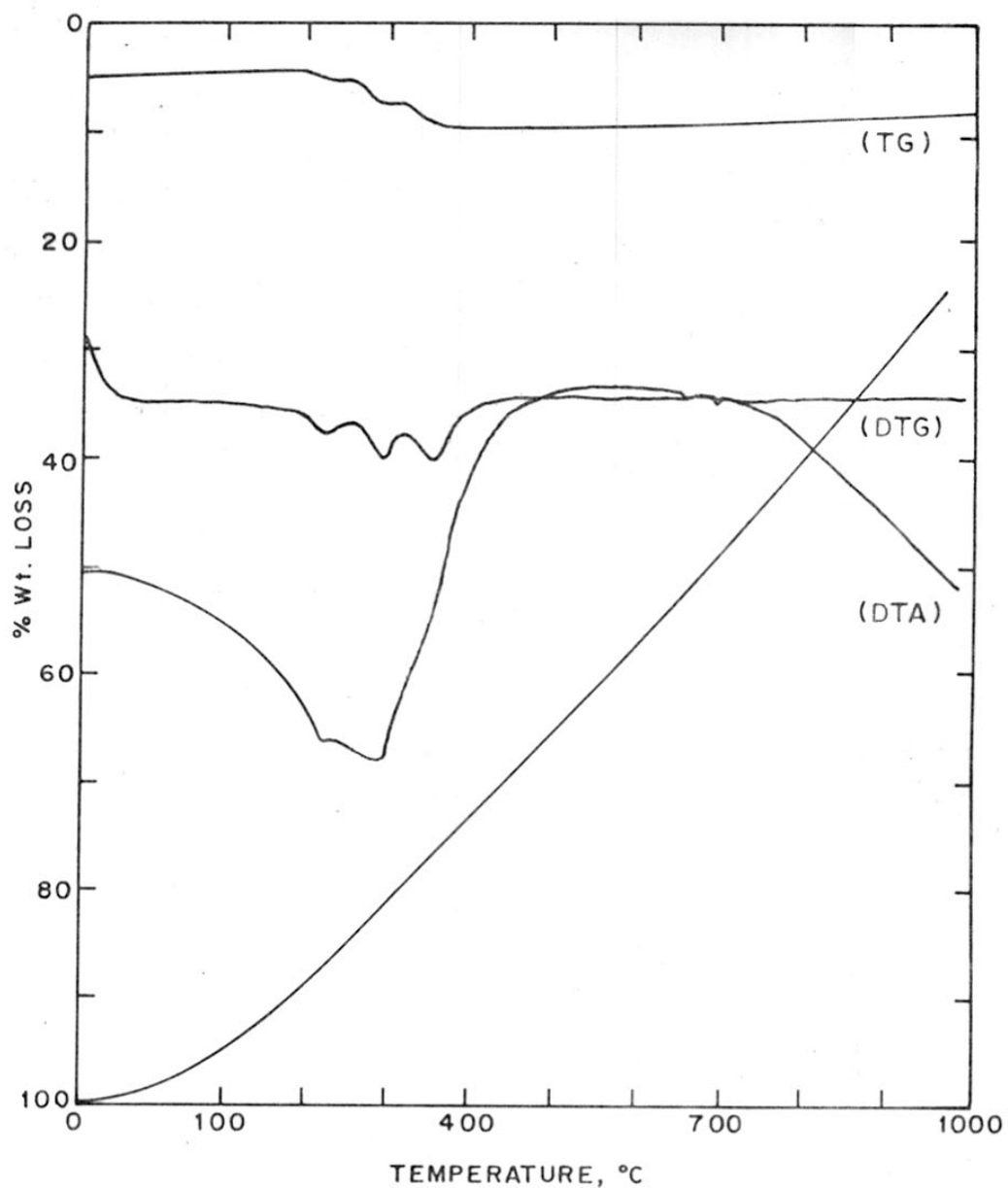


FIG.3-1: TG, DTG AND DTA CURVES FOR THE
SAMPLE (i) $2\text{CdO} + \text{SnO}_2$ PHYSICAL MIXTURE

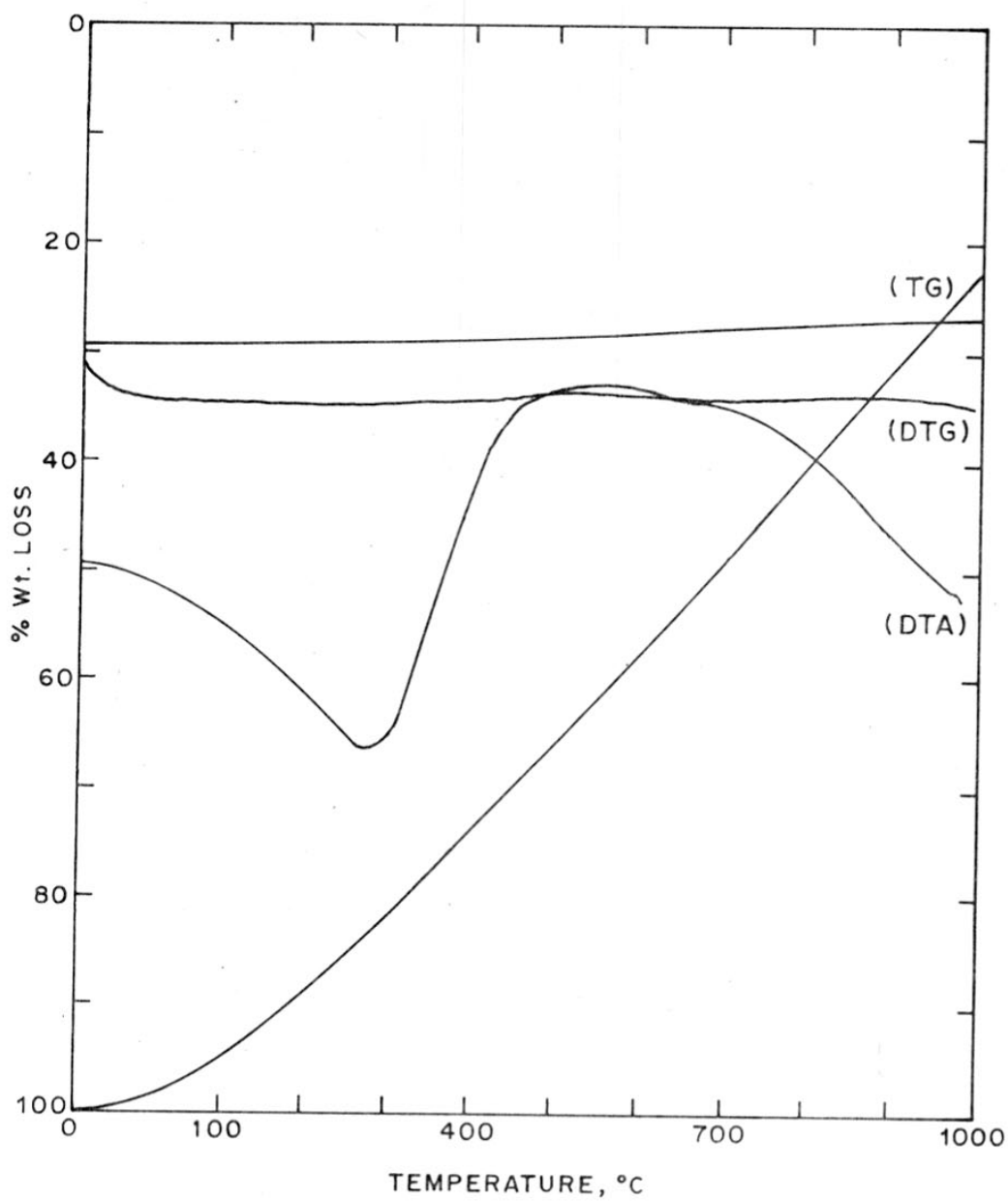


FIG. 3.2: TG, DTG AND DTA CURVES FOR
THE SAMPLE (ii) Cd_2SnO_4

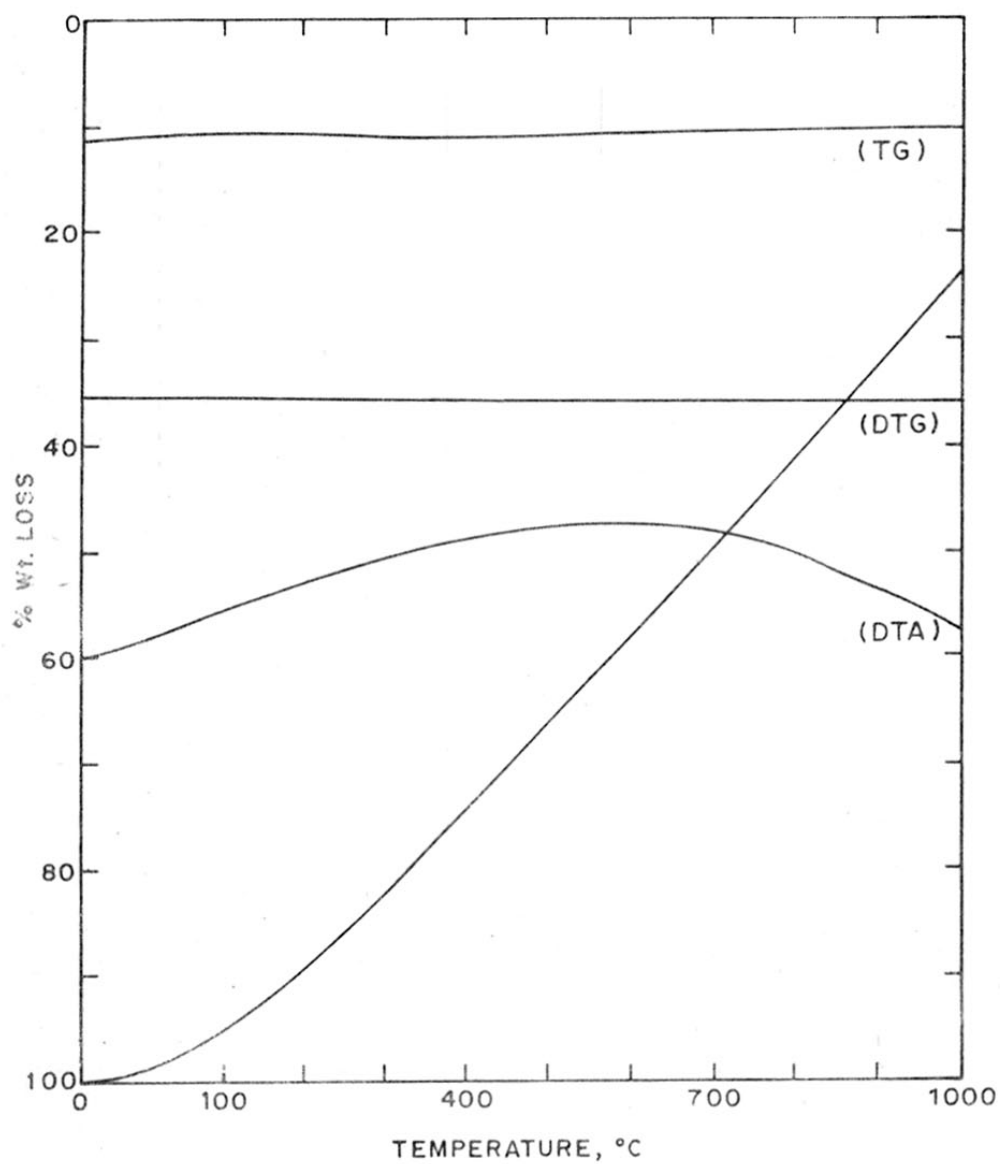


FIG. 3-3: TG, DTG AND DTA CURVES FOR
THE SAMPLE (iii) 95 Cd_2SnO_2 + 5 GLASS

The TG curve indicates that the three endothermal changes are accompanied by the loss of weight of $0.6 \pm 0.2\%$ at 221°C , $2.2 \pm 0.2\%$ at 300°C and $2.2 \pm 0.2\%$ at 368°C .

The first endothermic peak at 221°C in the DTA curve may be due to the loss of moisture from the sample. The TG curve showed a weight loss of $0.6 \pm 0.2\%$. The second endothermic peak may be attributed to the decomposition of $\text{Cd}(\text{OH})_2$ present in CdO reactant itself. Such a possibility is reasoned from the M. Wada and Y. Iida's¹⁰⁶ thermal analysis studies on CdO . They observed two endothermic peaks at 290 and 420°C . They attributed them to the decomposition of $\text{Cd}(\text{OH})_2$ and CdCO_3 which they presumed to have formed during grinding. They independently carried out thermal analysis of a mixture of $\text{Cd}(\text{OH})_2$ and CdCO_3 which confirmed their earlier results.

We also carried out X-ray studies on CdO samples heat-treated at different temperatures in order to verify the above results. The diffractograms for the samples (i) at R.T. and (ii) dried at 160°C and quenched contained $d = 3.206 \text{ \AA}$, 2.928 \AA , 2.878 \AA and 2.409 \AA lines extra. These were absent in the diffractogram for the third sample heated at 325°C and quenched. Incidentally, all the lines of the third sample matched well with those reported in the ASTM card¹⁰⁷ for CdO . This study indicated

that the extra lines present in the X-ray patterns for (i) and (ii) might be due to $\text{Cd}(\text{OH})_2$. These disappeared when the sample was heated at 325°C .

The third loss may be assigned to the dissociation of CdO . Decomposition of $\text{Cd}(\text{OH})_2$ and dissociation of CdO are endothermic processes.

The broad exothermic peak on DTA may be attributed to the reaction of $2\text{CdO} + \text{SnO}_2$. There is a gradual reaction taking place. The compound formation is not a sudden transition which would have given a sharp exothermic peak. This lends support to the fact that the reaction between 2CdO and SnO_2 requires prolonged heating and is completed at around 950°C .

The oxide mixture was, therefore, heated at 1050°C for 6 hours to complete the compound formation. During this reaction, after the initial loss, there is subsequent gain in oxygen ($\sim 2\%$), leading to a net loss of 2.4% . This means either the formula is $\text{Cd}_2\text{SnO}_{4-x}$ or some free Cd is present as an outside phase.

X-ray analysis of the Cd_2SnO_4 sample revealed the presence of Cd peaks ($d = 2.34 \text{ \AA}$ and 1.416 \AA) in the diffractogram.

(11) Cd₂SnO₄

The basic material, Cd₂SnO₄, was thermally analysed to know whether any phase changes were occurring in it during the heating process.

The weight of the sample taken was 21.75 mg. The TG curve (figure 3.2) indicates no mass loss upto 369°C. Thereafter, there is a continuous gain of 2.3% by 1000°C.

DTG curve shows a broad but very narrow hump between 470 and 605°C.

However, the DTA curve shows an endothermic peak at 270°C. A similar broad exothermic peak at 592°C (between 369 and 1000°C) similar to that in the figure 3.1. The peak point here is slightly at a higher temperature.

The compound, Cd₂SnO₄ was formed at 1050°C/6 hours in a muffle furnace. During this process, the extent of the overall loss of oxygen occurring could be seen from the TG curve (Fig. 3.1).

In the present case, TG curve (Fig. 3.2) indicated no change in mass till 369°C. Vieltange¹⁰⁸ also has reported that oxidation of cadmium in air was negligible upto 400°C.

The increase in mass after 369°C may be due to the oxidation of cadmium. This indicated that annealing of

the sample in air between 400 to 1000°C was required to regain the small amount of oxygen loss occurred during the compound formation.

(iii) 95 Cd₂SnO₄ + 5 glass

Thermal analysis of the sample was carried out in oxygen atmosphere. Figure 3.3 depicts the thermal changes. The sample weight was 46.5 mg.

In this case, the TG curve shows a gradual but a small increase in mass from room temperature upto 963°C, unlike in the case of Cd₂SnO₄ where the gain starts at a higher temperature (369°C). It is about 1.3% only. But there is no perceptible change in the DTG curve.

DTA curve shows a broad, single exothermic peak starting almost from the room temperature to 1020°C, the peak being at 582°C. It is significant to note that there is no endothermic peak present in the DTA curve.

The exothermic peak on DTA may reflect the thermal changes taking place with the incorporation of PbO into Cd₂SnO₄ matrix.

3.2 X-RAY DIFFRACTION

Crystallographic data provides evidence for the completion of the compound formation, for the structural

transformations and also indicate whether the dopant has gone into the host matrix.

X-ray diffractograms for the host material, Cd_2SnO_4 , and for the doped (3.3% PbO) thick film samples fired at different temperatures (500-900°C) are presented in the figures 2.1 and 3.4 to 3.8. The 'd' values were calculated from the ' 2θ ' values based the Braag's Law, $n\lambda = 2d\sin\theta$, where n = an integer (the order of the diffracted rays), λ = wavelength, d = interplanar distance of the atoms, 2θ = angle between the diffracted and emergent rays. The relative intensity values were estimated. A value of 100 was assigned to the maximum peak height. For the rest of the reflections, the values were given as ratios of their respective peak heights to the maximum peak height.

The structural data for all the samples are shown in the tables 3.1 to 3.5.

It can be seen that the host material is almost pure Cd_2SnO_4 with very faint lines for CdO and CdSnO_3 phases (< 5%). However, when this material is mixed with lead glass and fired at 500°C, then the prominent lines of CdO and CdSnO_3 appear indicating the decomposition of the type $\text{Cd}_2\text{SnO}_4 \rightarrow \text{CdO} + \text{CdSnO}_3$ (see diffractograms 2.1 and 3.4 - 3.8 and tables 2.1 and 3.1 to 3.5). At

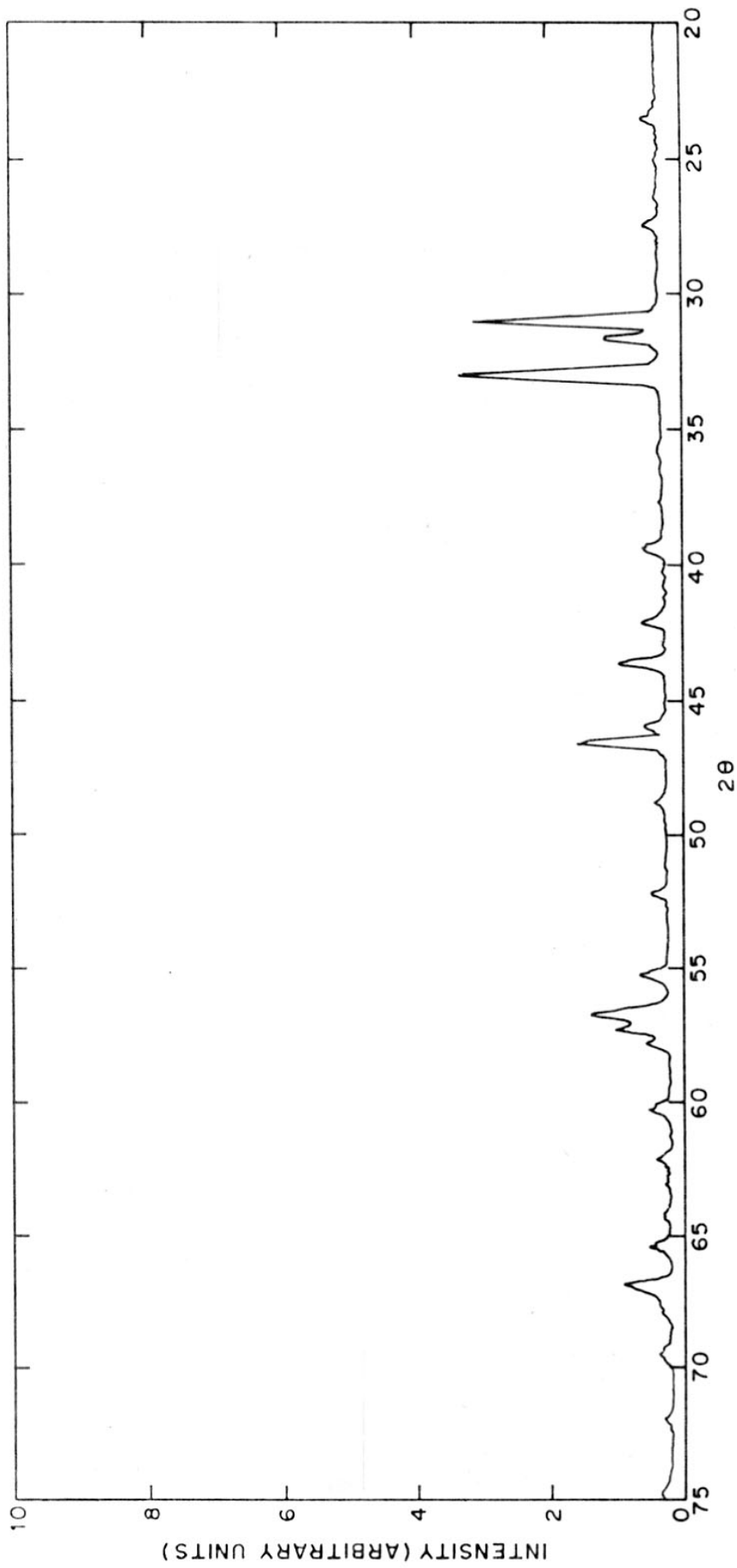


FIG. 3·4: X-RAY DIFFRACTOGRAM OF $(\text{Cd}_{1.90}\text{Pb}_{0.10}\text{SnO}_4)$
THICK FILM FIRED AT 500 °C.

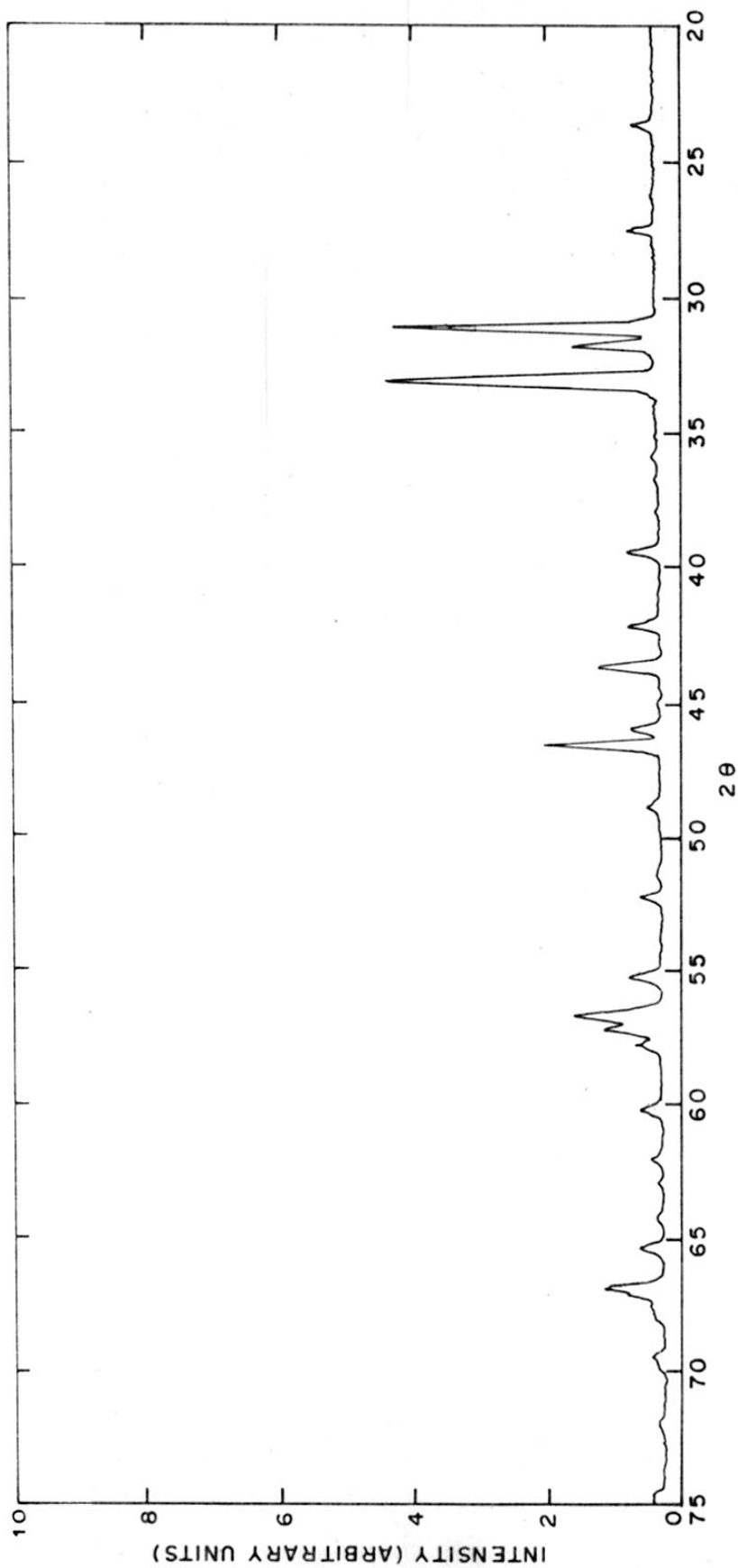


FIG. 3-5: X-RAY DIFFRACTOGRAM OF $(\text{Cd}_{1.90}\text{Pb}_{0.10}\text{SnO}_4)$
THICK FILM FIRED AT 600 °C

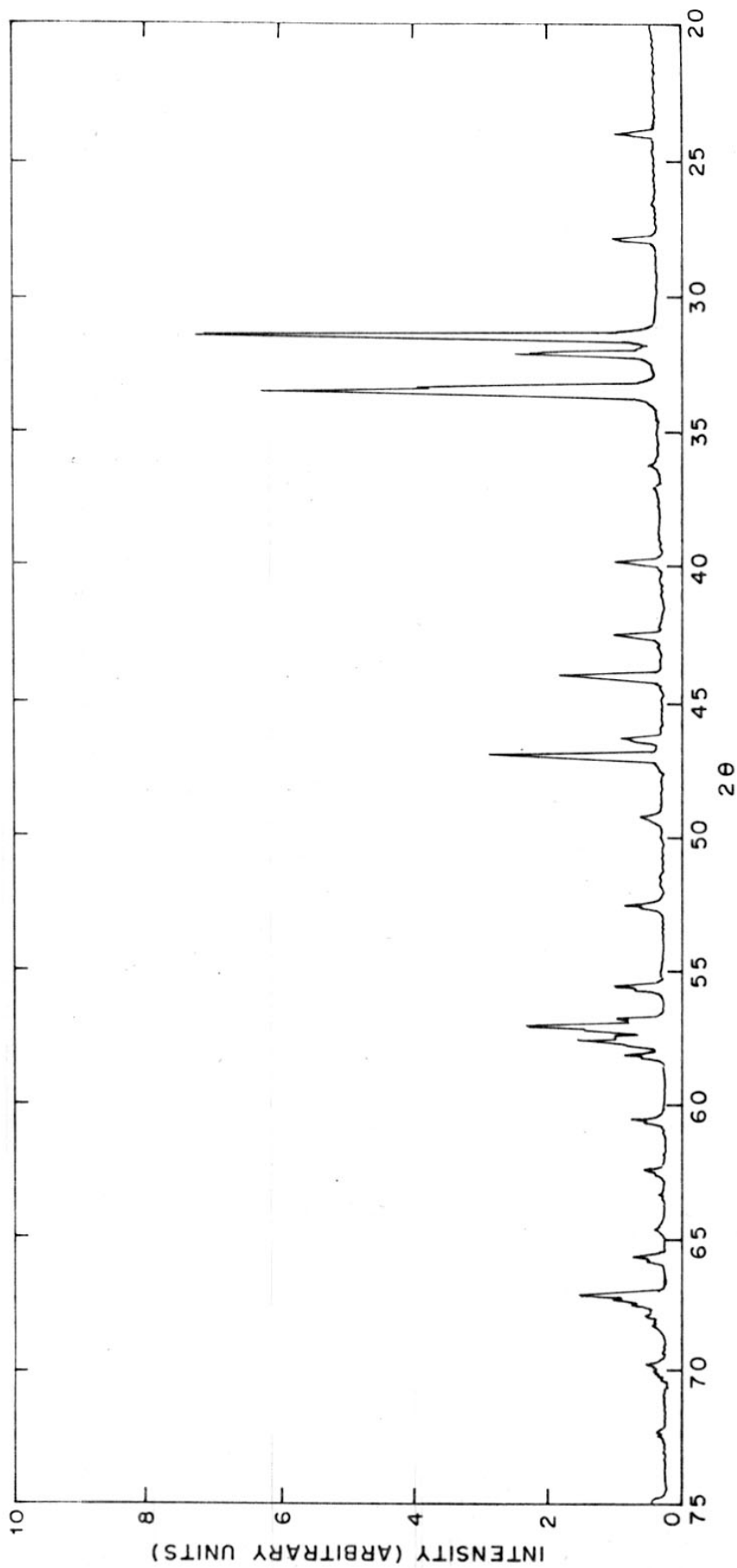


FIG. 3-6: X-RAY DIFFRACTOGRAM OF $(\text{Cd}_{1.90}\text{Pb}_{0.10}\text{SnO}_4)$
THICK FILM FIRED AT 700 °C

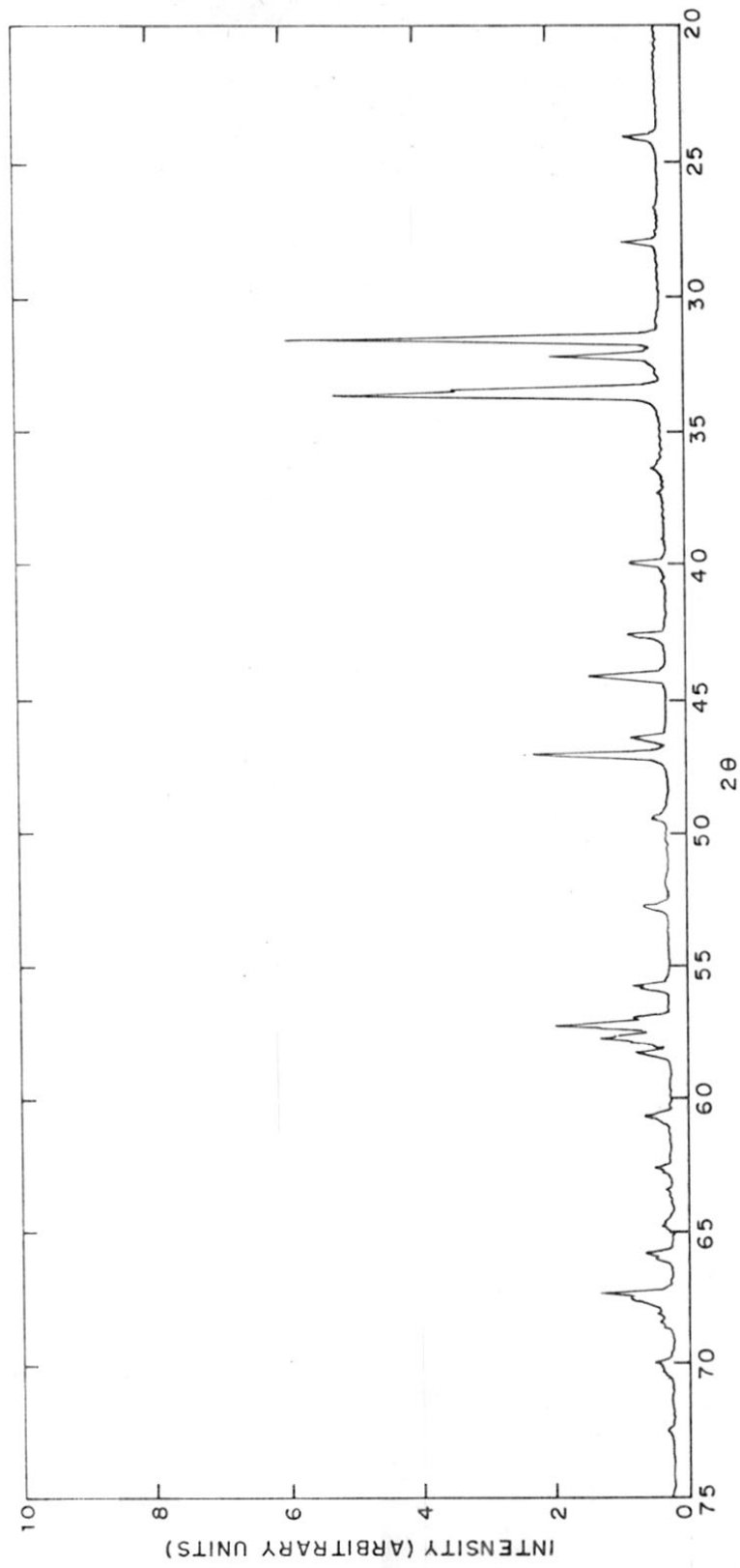


FIG. 3.7: X-RAY DIFFRACTOGRAM OF $(\text{Cd}_{1.90}\text{Pb}_{0.10}\text{SnO}_4)$

THICK FILM FIRED AT 800 °C.

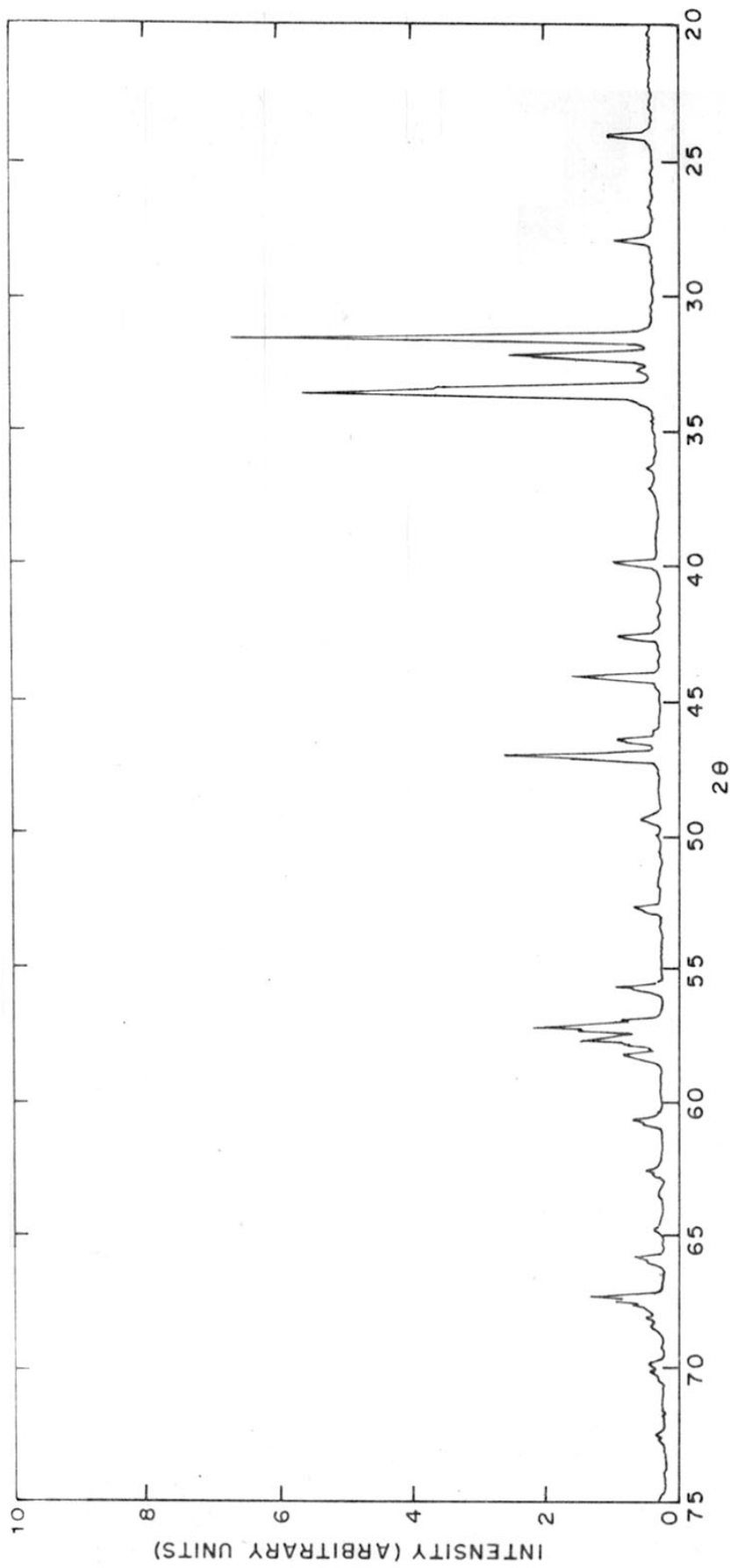


FIG. 3-8: X-RAY DIFFRACTOGRAM OF $(\text{Cd}_{1.90}\text{Pb}_{0.10})\text{SnO}_4$
THICK FILM FIRED AT 900 °C

Table 3.1 - Diffraction data for $\text{Cd}_{1.9}\text{Pb}_{0.1}\text{SnO}_4$
thick film fired at 500°C .

No.	2θ	d	I/I ₀	hkl
1	23.50	3.7824	9	-
2	27.40	3.2522	9	-
3	31.00	2.8823	90	310
4	31.65	2.8245	27	020
5	33.00	2.7120	100	011,120
6	39.35	2.2877	10	410
7	41.10	2.1943	10	-
8	42.65	2.0718	23	021
9	45.90	1.9754	10	CdSnO_3
10	46.55	1.9493	45	401
11	48.85	1.8628	5	030
12	52.15	1.7524	9	321
13	55.20	1.6625	12	CdO
14	56.70	1.6121	38	330
15	57.20	1.6091	26	511
16	57.80	1.5938	11	421
17	60.20	1.5359	10	002
18	62.12	1.4929	7	430
19	64.20	1.4495	3	521
20	65.38	1.4261	10	611,212
21	66.80	1.3992	23	302

Table 3.1 (contd.)

22	69.42	1.3527	5	022
23	72.00	1.3104	3	402
24	74.80	1.2682	7	711
25	76.00	1.2511	4	322
26	76.84	1.2395	4	630
27	81.70	1.776	6	721,132
28	83.40	1.1579	7	-
29	84.00	1.1511	7	631,232
30	85.00	1.1401	8	811

Table 3.2 - Diffraction data for $\text{Cd}_{1.9}\text{Pb}_{0.1}\text{SnO}_4$
thick film fired at 600°C

No.	2θ	d	I/I_0	hkl
1	23.65	3.6085	9	
2	26.50	3.3606	9	
3	31.10	2.8732	99	310
4	31.70	2.8202	31	020
5	33.10	2.7040	100	001,120
6	39.45	2.2821	11	410
7	42.15	2.1420	12	320
8	43.70	2.0696	22	021
9	45.95	1.9733	10	CdSnO_3
10	46.60	1.9473	43	401
11	48.95	1.8591	5	030
12	52.30	1.7477	8	321
13	55.35	1.6584	11	CdO
14	56.80	1.6195	34	330
15	57.30	1.6065	21	511
16	57.85	1.5925	9	421
17	60.25	1.5347	8	002
18	62.10	1.4933	4	430
19	65.50	1.4238	8	611,212
20	66.90	1.3974	20	302
21	67.20	1.3919	14	

Table 3.2 (contd.)

22	69.50	1.3513	5	022
23	74.70	1.2696	5	711
24	75.00	1.2653	5	041
25	76.00	1.2511	4	322
26	76.85	1.2393	3	630
27	81.48	1.1802	5	
28	83.50	1.1567	5	
29	84.10	1.1500	6	631,232
30	85.10	1.1390	6	811

Table 3.3 - Diffraction data for $\text{Cd}_{1.9}\text{Pb}_{0.1}\text{SnO}_4$
thick film fired at 700°C

No.	2θ	d	I/I ₀	hkl
1	24.00	3.7047	9	120
2	27.90	3.1951	10	001
3	31.50	2.8376	100	130
4	32.10	2.7775	30	200
5	33.40	2.6804	52	210
6	33.55	2.6688	86	111
7	36.22	2.4779	2	040
8	37.12	2.4199	1	121
9	39.85	2.2602	10	140
10	42.56	2.1223	10	131
11	44.04	2.0544	22	211
12	46.40	1.9552	9	041
13	47.00	1.9317	38	221
14	49.34	1.8461	4	141
15	52.60	1.7384	7	320
16	55.65	1.6501	10	060
17	55.80	1.6461	4	-
18	56.88	1.6174	10	330
19	57.14	1.6111	30	151
20	57.30	1.6065	18	-
21	57.50	1.6014	11	241

Table 3.3 (contd.)

22	57.70	1.5963	19	002
23	57.85	1.5926	10	-
24	58.20	1.5838	8	311
25	58.30	1.5813	4	
26	60.60	1.5267	7	321
27	60.75	1.5232	4	
28	62.50	1.4847	4	340
29	64.70	1.4395	2	251
30	65.72	1.4196	7	260
31	65.90	1.4161	4	
32	67.35	1.3891	11	132
33	67.55	1.3855	12	202
34	67.90	1.3792	4	-
35	68.30	1.3721	3	410
36	69.80	1.3462	4	212
37	72.35	1.3049	2	341

Table 3.4 - Diffraction data for $\text{Cd}_{1.9}\text{Pb}_{0.1}\text{SnO}_4$
thick film fired at 300°C

No.	2θ	d	I/I_0	hkl
1	24.10	3.6896	9	120
2	28.00	3.1839	9	001
3	31.55	2.8332	100	130
4	32.20	2.7775	30	200
5	33.45	2.6766	56	210
6	33.65	2.6611	88	111
7	36.35	2.4694	3	040
8	39.90	2.2575	10	140
9	42.65	2.1181	10	131
10	44.15	2.0495	21	211
11	46.50	1.9513	10	041
12	47.05	1.9297	38	221
13	49.40	1.8433	5	141
14	52.70	1.7354	7	320
15	55.75	1.6475	9	060
16	56.98	1.6148	10	330
17	57.20	1.6091	31	151
18	57.10	1.5988	13	241
19	57.70	1.5963	19	002
20	58.25	1.5825	9	311

Table 3.4 (contd)

21	60.25	1.5255	6	321
22	62.54	1.4839	4	340
23	64.72	1.4391	3	251
24	65.80	1.4180	7	260
25	66.00	1.4142	4	-
26	67.30	1.3900	19	132
27	67.50	1.3864	11	202
28	68.00	1.3774	4	410
29	68.40	1.3703	4	212
30	69.85	1.3454	5	341
31	72.45	1.3033	2	102
32	75.00	1.2653	4	-
33	76.40	1.2455	5	-
34	76.60	1.2428	2	-
35	77.15	1.2352	2	-

Table 3.5 - Diffraction data for $\text{Cd}_{1.9}\text{Pb}_{0.1}\text{SnO}_4$
thick film fired at 900°C

No.	2θ	d	I/I ₀	hkl
1	24.10	3.6896	10	120
2	28.00	3.1839	9	001
3	31.55	2.8332	100	130
4	32.20	2.7775	34	200
5	32.80	2.7281	3	
6	33.40	2.6804	52	210
7	33.45	2.6611	82	111
8	36.32	2.4713	2	040
9	39.90	2.2575	16	140
10	42.60	2.1180	15	131
11	44.15	2.0495	21	211
12	46.50	1.9513	10	041
13	47.08	1.9286	37	221
14	49.40	1.8433	5	141
15	52.72	1.7348	6	320
16	55.75	1.6474	10	060
17	55.90	1.6434	6	
18	56.95	1.6155	10	330
19	57.20	1.6091	29	151
20	57.35	1.6052	19	241
21	57.72	1.5958	19	002

Table 3.5 (Contd.)

22	58.28	1.5818	9	311
23	60.70	1.5244	9	321
24	62.70	1.4826	7	340
25	62.80	1.4784	2	
26	64.72	1.4391	2	251
27	65.80	1.4180	7	260
28	66.00	1.4142	4	
29	67.30	1.3900	15	132
30	67.50	1.3864	11	202
31	67.65	1.3837	7	410
32	68.00	1.3774	4	
33	68.34	1.3703	3	212
34	69.90	1.3446	4	
35	70.10	1.3412	3	420
36	72.45	1.3033	2	142

higher temperatures, 700-900°C, these extra phases gradually disappear suggesting a reformation of Cd_2SnO_4 . During this process of recombination, it is likely that PbO from the glass phase competes with CdO and gets incorporated in the Cd_2SnO_4 phase. It is also likely that metal:oxygen ratio is more than 3:4 leading to the donor centres which have been responsible for the enhanced conductivity.

The diffraction lines belonging to Cd_2SnO_4 phase (table 2.1) are separated out to determine its lattice constants. Since the crystal structure of Cd_2SnO_4 is known to be orthorhombic, we have indexed the peaks on the basis of orthorhombic unit cell and the (hkl) values of Shannon.⁵⁷

It is interesting to compare the X-ray data for our sample with those reported by the two groups of workers represented by Smith¹⁴ and Tromel.³⁶ Both these groups say that the Cd_2SnO_4 has orthorhombic crystal structure and belongs to Sr_2PbO_4 family with somewhat different cell dimensions. The space group is stated to be Pbam . It contains octahedrally coordinated Sn^{4+} .

The difference between these two groups is in the values of lattice parameters. The values for a and b are

interchanged and the c value has increased slightly. These values are shown in the table 3.6.

The diffractograms show some weak lines due to the presence of CdO and a little metastannate phase ($d = 2.34 \text{ \AA}$ and 1.416 \AA for CdO and $d = 1.6625 \text{ \AA}$ for CdSnO_3). In the case of the samples, C, D and E both the lines $d = 2.788 \text{ \AA}$ and $d = 1.610 \text{ \AA}$ correspond to CdSnO_3 and Cd_2SnO_4 phases. Both these lines are comparatively strong.

In the case of thick film samples, the peaks due to Cd_2SnO_4 were indexed on the basis of orthorhombic unit cell and the indexing given by Smith¹⁴ and Shannon⁵⁷. The cell dimensions calculated from X-ray data obtained for various samples are presented in the table (3.7).

We can see from the table (3.7) that the cell dimensions a and b increase and c decreases for the sample A (500°C), compared to those of the host material. $\frac{a}{c}$, $\frac{b}{c}$ ratios increase and the unit cell volume decreases. These values register further increase for the sample B over those of A. This situation indicates the beginning of the incorporation of Pb^{2+} into the Cd_2SnO_4 host matrix.

Table 3.6 - Lattice parameter values for Cd_2SnO_4
from different sources

Source	Lattice parameters (\AA)			Unit cell volume (\AA) ³
	a	b	c	
Smith ¹⁴	10.01	5.55	3.07	170.6
Tromel ³⁶	5.546	9.888	3.193	175.1
Shannon ⁵⁷	5.5684	9.8871	3.1923	175.8
Present work	5.5458	9.8686	3.189	174.5

Table 3.2 - Cell dimension values for the samples Cd_2SnO_4

A, B, C, D and E.

No.	Sample	Firing temperature ($^{\circ}C$)	Cell dimensions (\AA)			a/c	b/c	Unit cell volume (\AA^3)
			a	b	c			
1	Cd_2SnO_4	-	5.5458	9.8686	3.189	1.739	3.095	174.5
2	A	500	5.5773	10.0363	3.0694	1.817	3.270	172.2
3	B	600	5.5884	10.0733	3.0718	1.819	3.279	172.9
4	C	700	5.5550	9.9023	3.1951	1.739	3.099	175.8
5	D	800	5.5477	9.9850	3.1839	1.742	3.136	176.4
6	E	900	5.5550	9.9844	3.1839	1.745	3.136	176.6

When we come to the samples C and D, c value increases and a, b values decrease. $\frac{a}{c}$ and $\frac{b}{c}$ ratios also decrease. But the unit cell volume increases. These variations can be attributed to the conversion of $Pb^{2+} \rightarrow Pb^{4+}$ taking place at the higher temperatures. The system appears to have stabilized by $900^{\circ}C$ (sample E) as indicated by the almost non-variant values of the lattice parameters and the unit cell volume. These conclusions are consistent with the conductivity data.

From the ionic radii data, Pb^{2+} (1.20 \AA) is greater than Cd^{2+} (0.97 \AA). This causes the increase in a and b values. The unit cell volume also increases. With the oxidation of $Pb^{2+} \rightarrow Pb^{4+}$, the ionic radius of Pb^{4+} being small (0.84 \AA), there is decrease in the a and b values.

The addition of PbO dopant can also be observed visually by the distinct colour changes occurring in the samples at different firing temperatures. From bright yellow (basic material), it changes to green ($900^{\circ}C$) through yellow ochre ($700^{\circ}C$).

In the case of CdO , Haul and Just¹⁰⁹ proposed a transport mechanism involving vacancies in the anion sublattice from their lattice diffusion studies. They doped CdO with lithium and indium. Li^{+} created additional oxygen vacancies and In^{3+} decreased their concentration.

They, therefore, preferred the scheme of oxygen vacancies instead of cadmium excesses for explaining the non-stoichiometry.

Smith¹⁴ observed that complete volatilization of CdO occurred from Cd_2SnO_4 when it was heated at $1240^\circ\text{C}/1$ hr. The melting temperatures of CdO and PbO are >1500 and 886°C respectively.¹¹⁰

The presence of CdSnO_3 phase indicates the existence of free CdO in our sample which is observed by the CdO lines (weak) in the diffractograms.

The gradual disappearance of CdO line, $d = 1.616 \text{ \AA}$ from A to E is noteworthy. The conductivity values also increase correspondingly. Such a result was also reported by Haacke et al.⁶¹ They further mentioned that the disappearance of CdO was interpreted as follows: CdO was dissociated and cadmium was diffused into Cd_2SnO_4 lattice to form interstitial donors. This was revealed in the increase in the lattice constant. It was cubic structure in their case. This type of situation was observed in our samples also, although our samples had orthorhombic structure. The increase in the lattice parameter values due to Cd interstitials possibly enhanced by the dopant induction.

In the case of chemical doping, the sheet resistivity is relatively unaffected by heating or other ambient conditions. It is an irreversible process. Nozik²³ reported that $\text{Cd}_2\text{SnO}_{4-x}$ was conducting.

Shannon et al⁵⁷ opined that chemical doping might also result in some oxygen deficiency. This, of course, depended on the nature of the dopant.

Possibly, the similar situation exists in our samples.

3.3 SCANNING ELECTRON MICROSCOPIC RESULTS

The photomicrographs for the samples A, B, C, D, E and F are shown in the figures (3.9 - 3.14). The magnification is 5Kx.

Clusters of particles are the common features in all the cases. The individual particles are of $1 \mu\text{m}$ in size.

The sample F, being a physical mixture of Cd_2SnO_4 and glass, some glass frit particles ($5-10 \mu\text{m}$) are visible. The Cd_2SnO_4 particles also are loosely bound agglomerates. Many individual particles are seen in the photomicrograph (Fig. 3.9).

The glass frit particles are smoothed out in the sample A, fired at 500°C . Some surface softening



FIG. 3.9.

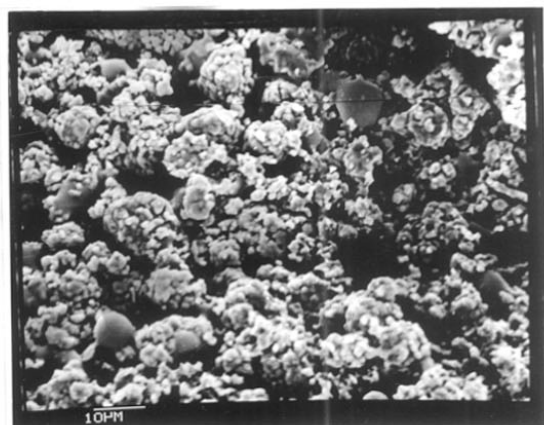


FIG. 3.10.

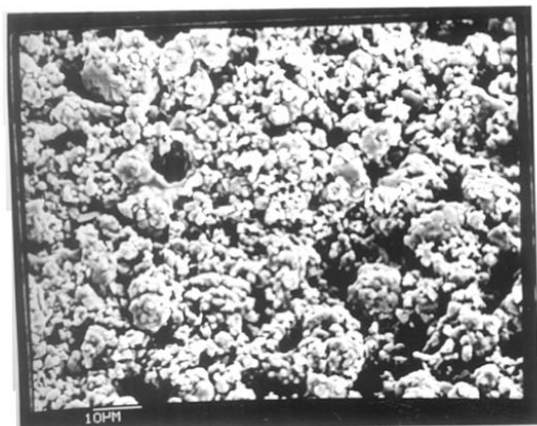


FIG. 3.11.

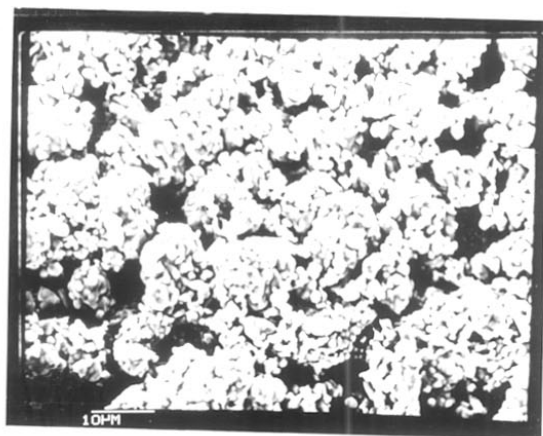


FIG. 3.12.

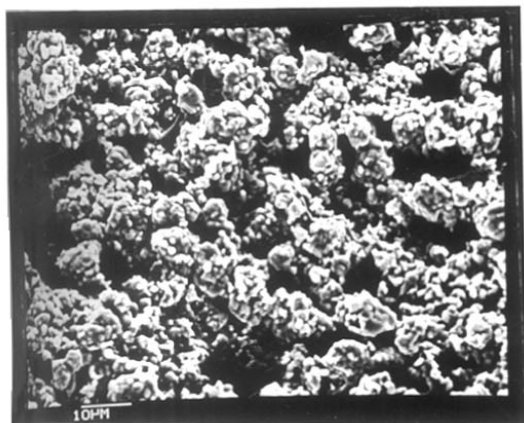


FIG. 3.13.

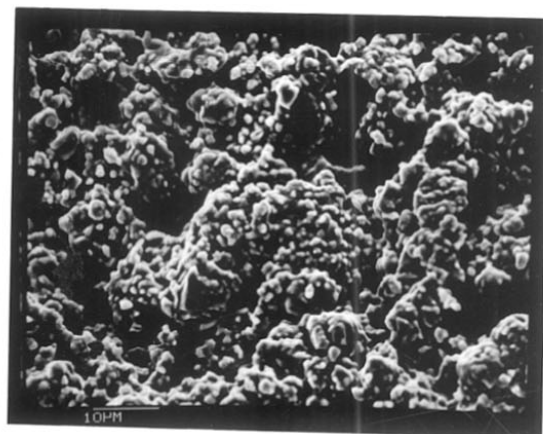


FIG. 3.14.

has taken place. The softening point of glass is around 520°C . The glass particles are smaller in size (Figure 3.10).

In the case of the sample 'B', fired at 600°C , the glass frit particles have completely melted out. The Cd_2SnO_4 particles have coalesced into bigger agglomerates (Figure 3.11).

The clusters have grown in size for the sample 'C', fired at 700°C , (Figure 3.12).

Sintering of the clusters has set in when the sample D is fired at 800°C . The smaller size of the clusters is indicative of this physical transformation, (Figure 3.13).

For the sample E, fired at 900°C , both coalescing and sintering have taken place. It gives an appearance of one large cluster of particles (Figure 3.14).

It is clear from the above photomicrographs that the coalescing and sintering of particles has occurred with the increase in firing temperature. The glass softening and homogenising with Cd_2SnO_4 is also indicated providing credence to the fact that Cd_2SnO_4 has been doped with PbO .

3.4 ELECTRICAL CONDUCTIVITY (D.C.)

During our experiments, it was observed that when the thick films made from Cd_2SnO_4 with and without glass, but fired at the same temperatures, had different properties. The colour of the films as well as the electrical conductivity values were different. It was, therefore, concluded that it would be worthwhile first to investigate the reaction, if any, between the glass composition and Cd_2SnO_4 .

A homogeneous mixture of Cd_2SnO_4 and glass was placed on alumina substrates in small HEAPS and fired at various temperatures (500-900°C) in the thick film furnace. Visually, the powder heaps appeared to have the same shades of colour as we had in the case of thick films fired at the corresponding temperatures.

The percentage of the glass in the paste was then varied and the electrical properties were measured. The glass constituent was changed from 5.0% to 2.0, 1.0, 0.5 and 0.1% of Cd_2SnO_4 -glass mixture. Further processing conditions were kept the same to get the thick films.

The results showed that for a given firing temperature, the electrical resistance increased with the decreasing percentage of glass. And for a given

composition, increasing firing temperature decreased the resistance. The colour of the thick film and its electrical conductivity were also seen to be related. The higher resistance films were bright yellow in colour and the resistance decreased as the colour of the films moved towards green.

It turned out that the lead oxide (PbO) constituent of the glass was responsible in effecting the above changes. This became clear when we added the oxides, which were used for glass formation, individually to Cd_2SnO_4 and fired. The quantities of the oxides were based on the glass composition and its proportion to Cd_2SnO_4 . The Cd_2SnO_4 and the individual oxide were mixed well and the paste was formulated in each case. The paste was screen printed and fired at the same temperatures (500-900°C). This was repeated for all the glass percentages mentioned above. It was found from this study that lead oxide alone gave different shades of colour to the films and not the other component oxides of the glass.

This established the fact that, in our case, the glass reacts with Cd_2SnO_4 and it does not remain merely as an inert, passive material. It performs a dual role:

(i) to form the usual vitreous bond for the thick films and (ii) to provide an "impurity", a new role, to Cd_2SnO_4 , thereby influencing its electrical, structural and optical properties.

Shannon et al⁵⁷ mentioned two methods of introducing carriers for high conductivity in Cd_2SnO_4 : (a) by creating oxygen vacancies and (b) by chemical doping. The former process was reversible and the latter one was stable. They studied both the methods. Antimony was used as the dopant for Cd_2SnO_4 (e.g. $\text{Cd}_2\text{Sn}_{1-x}\text{Sb}_x\text{O}_4$).

Haacke et al⁵³ reported the influence of the additives on the properties of Cd_2SnO_4 thin films. They mentioned that the inclusion of In or Pb improved the clarity of the sputtered films.

Haacke et al⁶¹ also reported the increase in mobility with Ta doping ($\text{Cd}_2\text{Sn}_{0.98}\text{Ta}_{0.02}\text{O}_4$) in Cd_2SnO_4 . They found indium to be the donor when it substituted Cd, for e.g. $\text{Cd}_{1.98}\text{In}_{0.02}\text{SnO}_4$ and Sb or Ta when substituted on Sn sites. However, they could not ascertain the effect with Ti, Zr, V, Nb, Mo, W, Rh, Cu, Ag, P, Bi and Tl when used as dopants.

Miyata et al⁶⁶ also studied the effect of indium doping on the electrical properties of Cd_2SnO_4 .

In our method, chemical doping of Cd_2SnO_4 with PbO has the advantage of being unaffected by the atmosphere. This did not require any inert or reducing atmosphere as has been the case with the sputtered thin films.

If the entire PbO in the glass gets transferred into the Cd_2SnO_4 matrix, which seems to be happening, then the compositions corresponding to the different glass percentages mentioned above would be as follows.

Table 3.8 - Dopant percentages and compositions of the samples

No.	Glass (%)	PbO (wt. %)	Composition (Cd_2SnO_4 -PbO nominal formula)
1	0.1	0.066	$\text{Cd}_{1.998}\text{Pb}_{0.002}\text{SnO}_4$
2	0.5	0.33	$\text{Cd}_{1.99}\text{Pb}_{0.01}\text{SnO}_4$
3	1.0	0.66	$\text{Cd}_{1.98}\text{Pb}_{0.02}\text{SnO}_4$
4	2.0	1.32	$\text{Cd}_{1.96}\text{Pb}_{0.04}\text{SnO}_4$
5	5.0	3.30	$\text{Cd}_{1.9}\text{Pb}_{0.1}\text{SnO}_4$

Nozik²³ had measured the conductivity of Cd_2SnO_4 thin films between 77° and 300°K . Shannon et al⁵⁷ presented the results of ρ vs T for the single crystals upto 300°K . Miyata et al⁷² carried out the measurements upto 333°K .

We carried out the measurements in the temperature range of $300\text{--}460^\circ\text{K}$ for a large number of samples. Representative results are presented in the following pages. The graphs indicate the $\log R - 1000/T$ relation in all the cases.

The activation energy was calculated from the equation

$$\Delta E = 0.1986 \frac{\log R_1 - \log R_2}{\frac{1000}{T_2} - \frac{1000}{T_1}} \quad 3.1$$

$$\text{derived from } R = R_0 \exp \frac{-\Delta E}{KT} \quad 3.2$$

For each composition (table 3.8), the sample thick films were fired at $600, 700, 800$ and 900°C in the thick film furnace. The thick films were kept at peak temperature for 20 minutes. They were then annealed at 180°C under vacuum before the conductivity measurements were carried out.

Contacts are provided to the samples to study the electrical characteristics. But then, these should not impede the flow of charge carriers.

The conditions for an ideal contact are: (a) the electrodes should not introduce resistance to the flow of current (contact resistance), (b) variations in the applied voltage and the temperature should not have any deleterious effect on the electrode material and (c) there should be compatibility between the contact and the sample materials.

An ohmic contact ($\frac{dI}{dV} = \text{constant}$) is always a prerequisite for the electrical conductivity measurements. The difference in the work functions (ϕ_c, ϕ_s) between the contact material and the semiconductor material results in non-ohmic contacts. This difference is generally referred to as the energy barrier. Problems associated with the barrier layers can be surmounted by having pressure contacts and proper choice and selection of the electrode material.

Different materials have been used as contacts for cadmium stannates. In literature, it is mentioned that Coffeen¹¹ used silvering of stannate samples for the dielectric measurements. Silver loaded epoxy

contacts were used by Nozik.²³ Haacke et al⁶¹ used indium soldered contacts for the standard two probe method for the conductivity measurements of the Cd_2SnO_4 sputtered films.

We tried vacuum evaporated gold, silver, aluminium and air drying silver paste.¹⁰⁵ The last one was found to be convenient and satisfactory and gave ohmic contact.

The measured V-I curves for both the polarities had slopes practically constant, thus establishing the good contact quality.

The voltage across a standard resistor was used to calculate the circuit current. Using this value of current and the potential drop across the sample, the sample resistance was calculated from the Ohm's law, $I = \frac{V}{R}$, where I = current, V = potential drop across the sample and R = sample resistance. Resistance values were calculated at different temperatures ranging from 300-460°K.

Table (3.9) gives the resistance values (in K^{-1}) of the samples measured at 323°K.

For a given dopant concentration, the resistance decreases with the increase in the firing temperature. For a given firing temperature, it appears that the resistance value generally decreases with the dopant

Table 3.9 - Effect of the dopant concentration and sample firing temperature on the resistance values

Firing temperature (°C)	Colour of the sample	Dopant (PbO) concentration (%)				
		0.006	0.33	0.66	1.32	3.30
600	Bright yellow	15 850	588	60.3	234.5	505.8
700	Yellow ochre	118.0	48.8	18.9	10.7	33.9
800	Green	8.5	9.7	2.1	5.7	6.2
900	Green	0.50	0.52	0.09	0.22	0.64

concentration upto 0.66% level. It then increases with further increase of the dopant. PbO of 0.66% seems to be an optimum level to get very high conductivity value in the doped Cd_2SnO_4 .

The resistance-temperature relation for the samples fired at 600, 700, 800 and 900°C is plotted in the figures (3.15-3.34). The curves have generally 2-3 slopes. Table (3.10) shows the temperatures at which the low slope changes to high slope.

For the thick films of composition $\text{Cd}_{1.998}\text{Pb}_{0.002}\text{SnO}_4$ fired at 600-900°C, the change of slope occurs at 84°C. It is also the same for all the compositions (except 0.01%) fired at 600°C. With the increase in the dopant concentration, this temperature increases systematically from 97 to 127 and 144°C for the films fired at 700, 800 and 900°C.

The activation energies corresponding to the different slopes of the curves (figures 3.15-3.34) are calculated. The values are presented in the tables (3.11) and (3.12).

From the tables (3.10) to (3.12), it is observed that the low activation energy values are indicated in the temperature ranges 300-384°K, 300-397°K and 300-427°K. The ΔE value reduces with the increase in firing

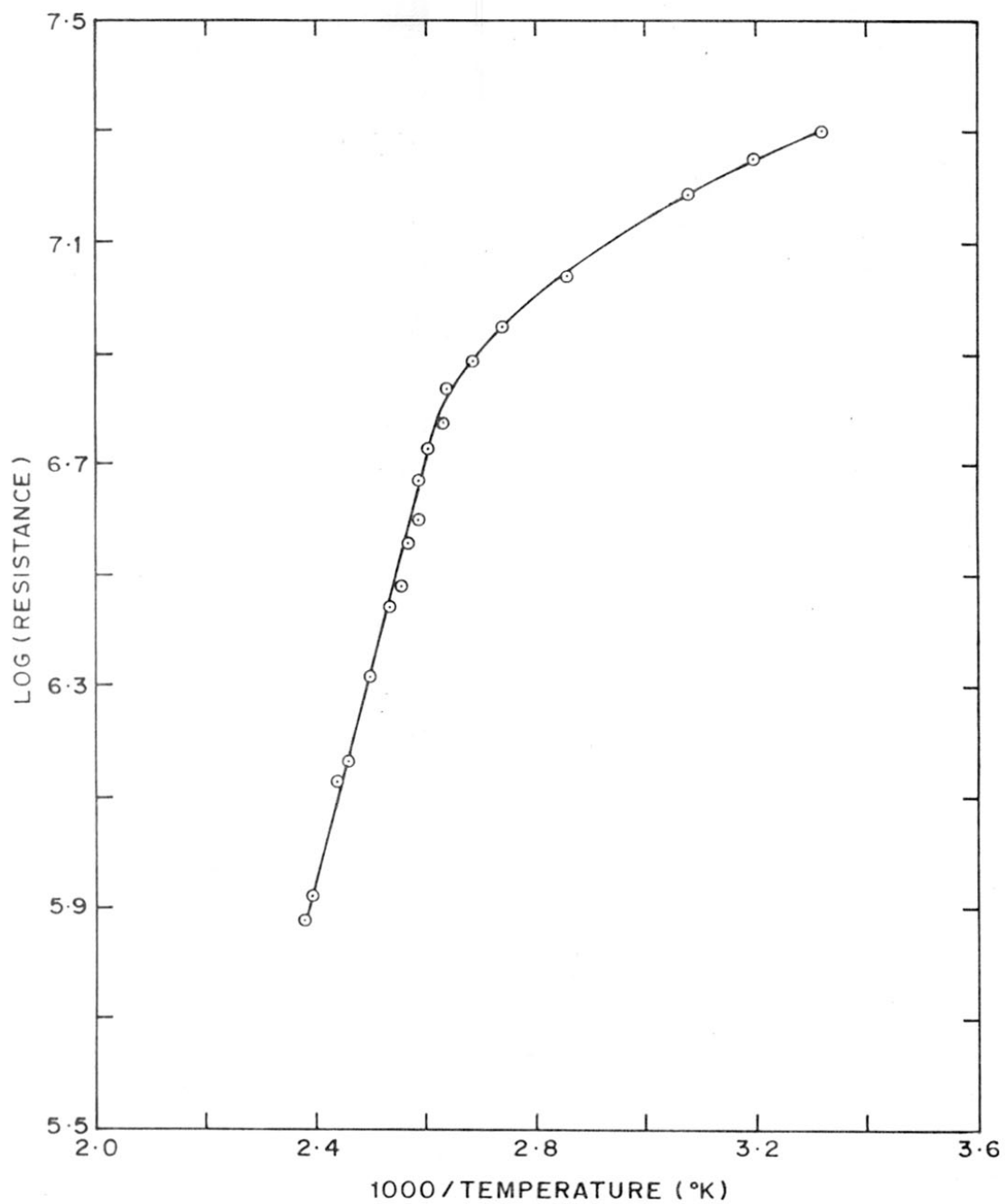


FIG. 3-15: LOG (RESISTANCE) Vs 1000/T FOR $(\text{Cd}_{1.998} \text{Pb}_{0.002} \text{SnO}_4)$
THICK FILM FIRED AT 600 °C

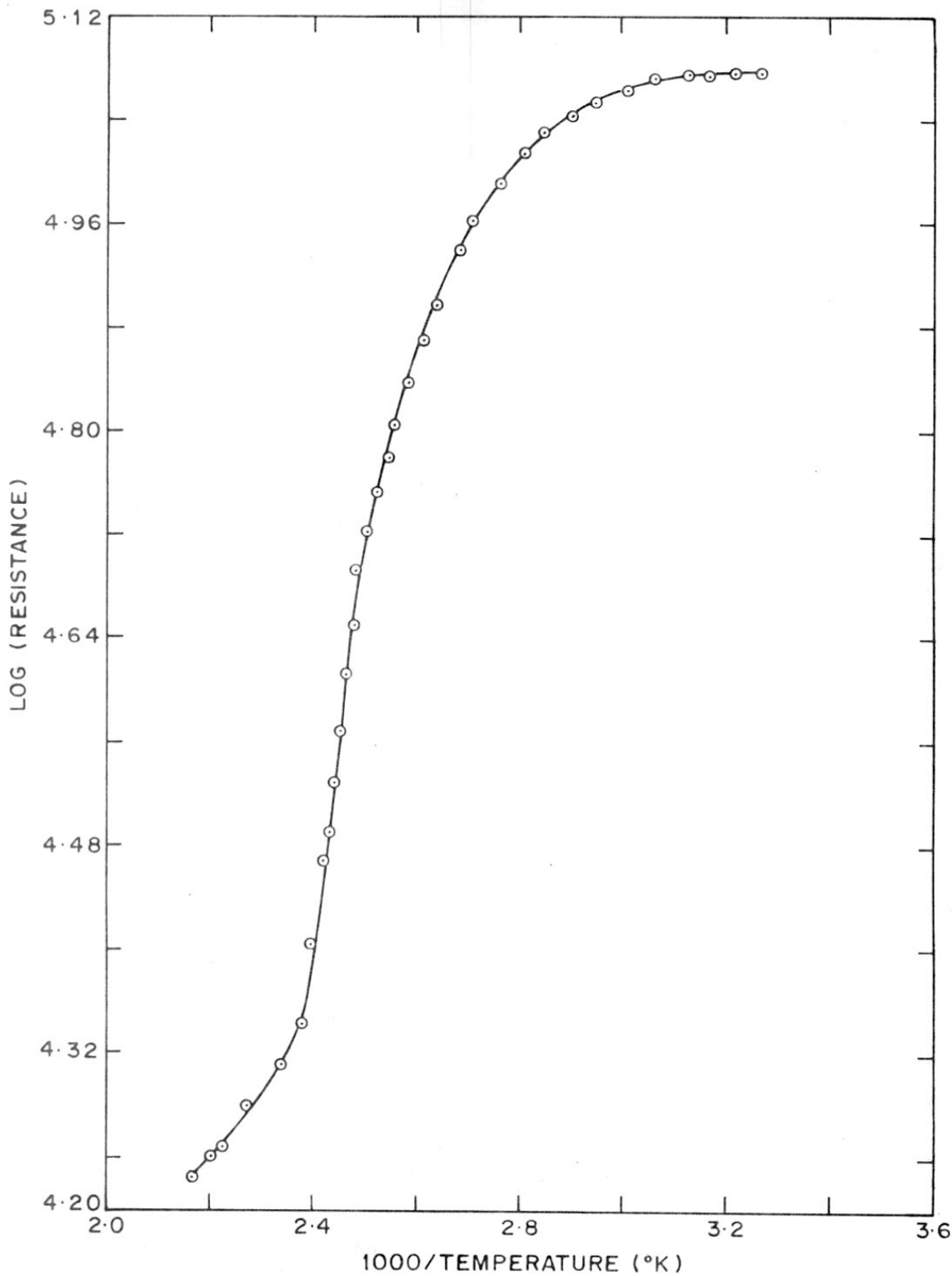


FIG. 3.16: LOG (RESISTANCE) Vs 1000/T FOR $(\text{Cd}_{1.998} \text{Pb}_{0.002} \text{SnO}_4)$
THICK FILM FIRED AT 700 °C

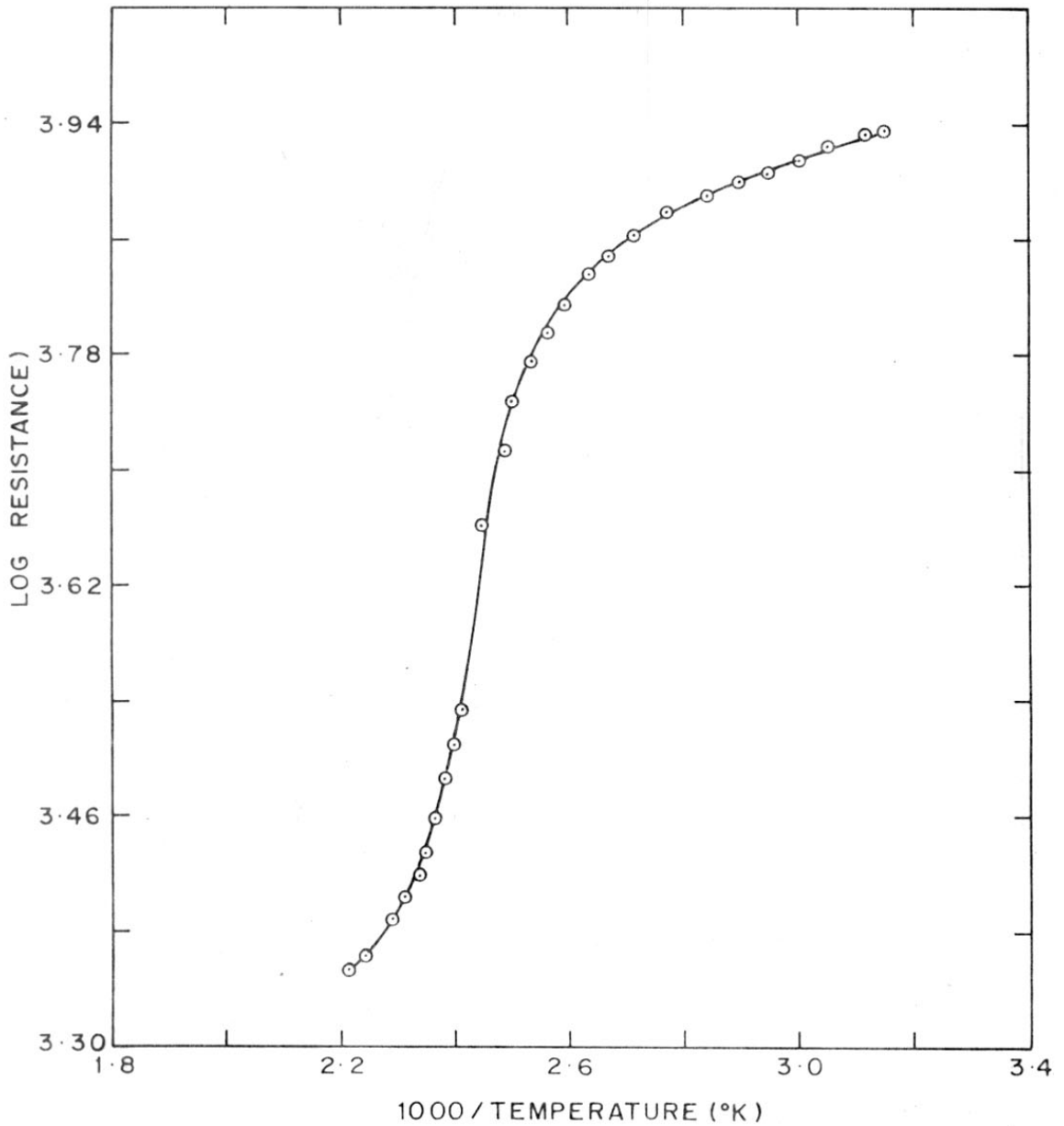


FIG. 3.17: LOG (RESISTANCE) Vs 1000/T FOR $(\text{Cd}_{1.998} \text{Pb}_{0.002} \text{SnO}_4)$ THICK FILM FIRED AT 800 °C

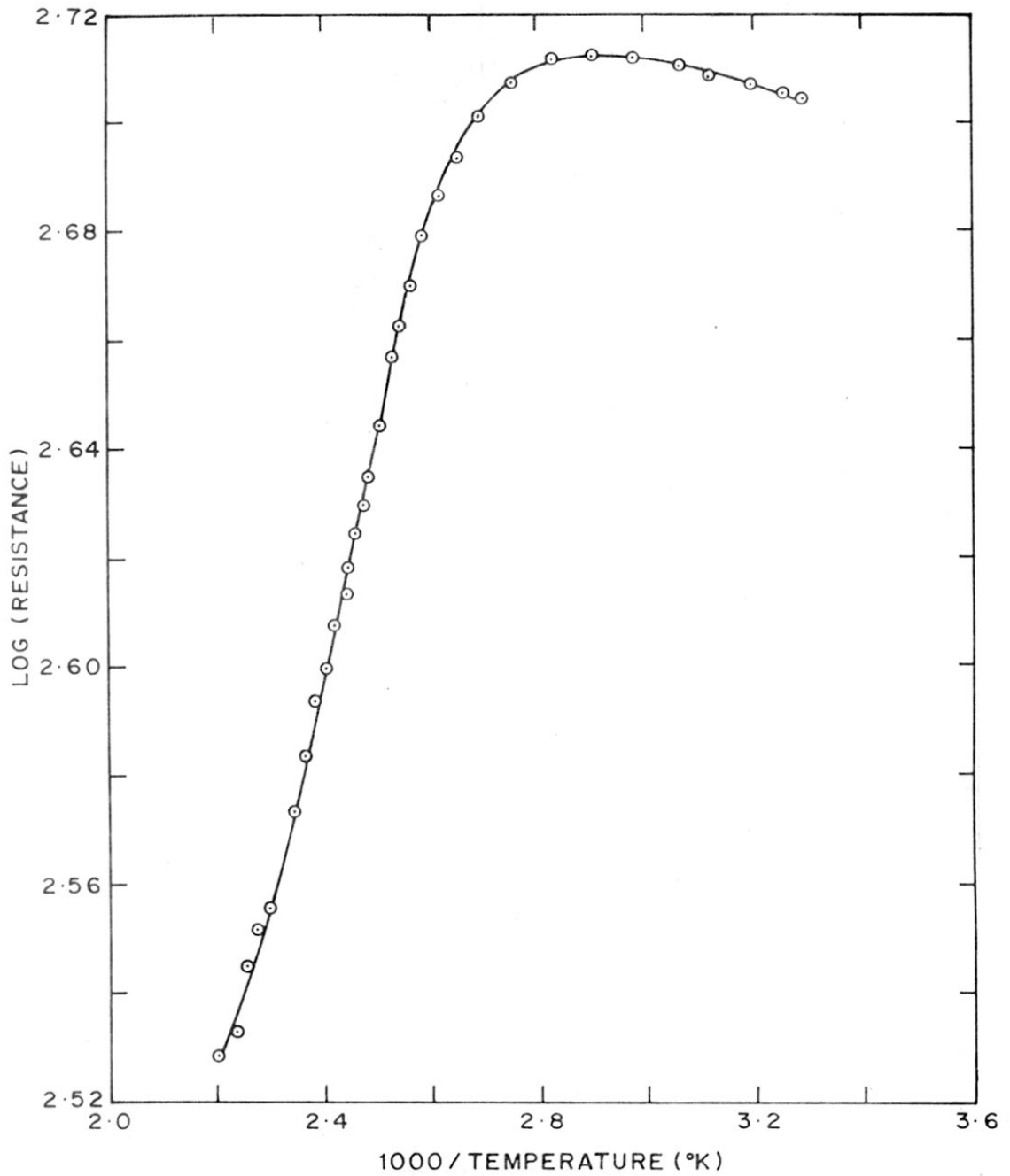


FIG. 3-18: LOG (RESISTANCE) Vs 1000/T FOR $(\text{Cd}_{1.998}\text{Pb}_{0.002}\text{SnO}_4)$
THICK FILM FIRED AT 900 °C

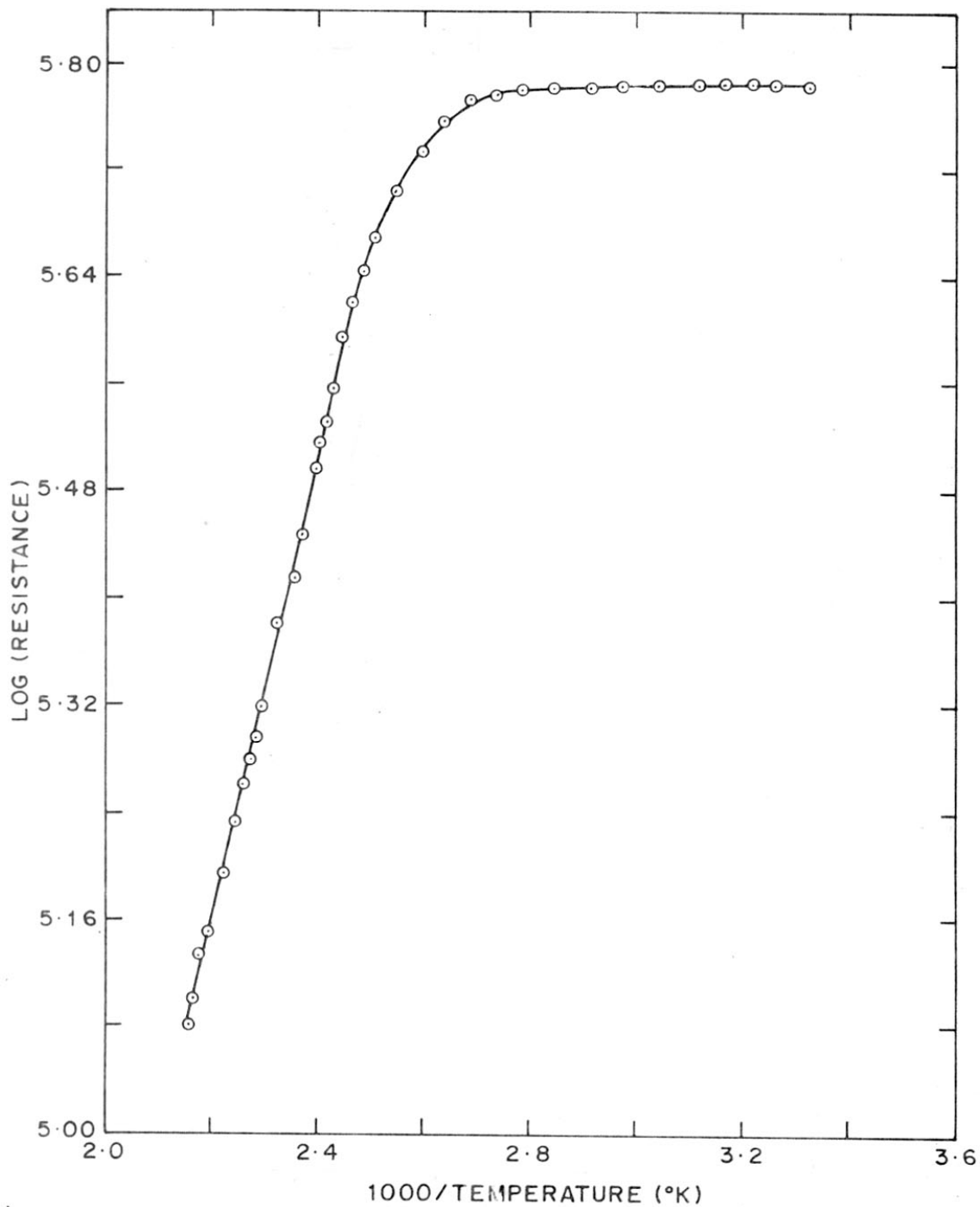


FIG. 3-19: LOG (RESISTANCE) Vs 1000/T FOR $(\text{Cd}_{1.990}\text{Pb}_{0.010}\text{SnO}_4)$
THICK FILM FIRED AT 600 °C

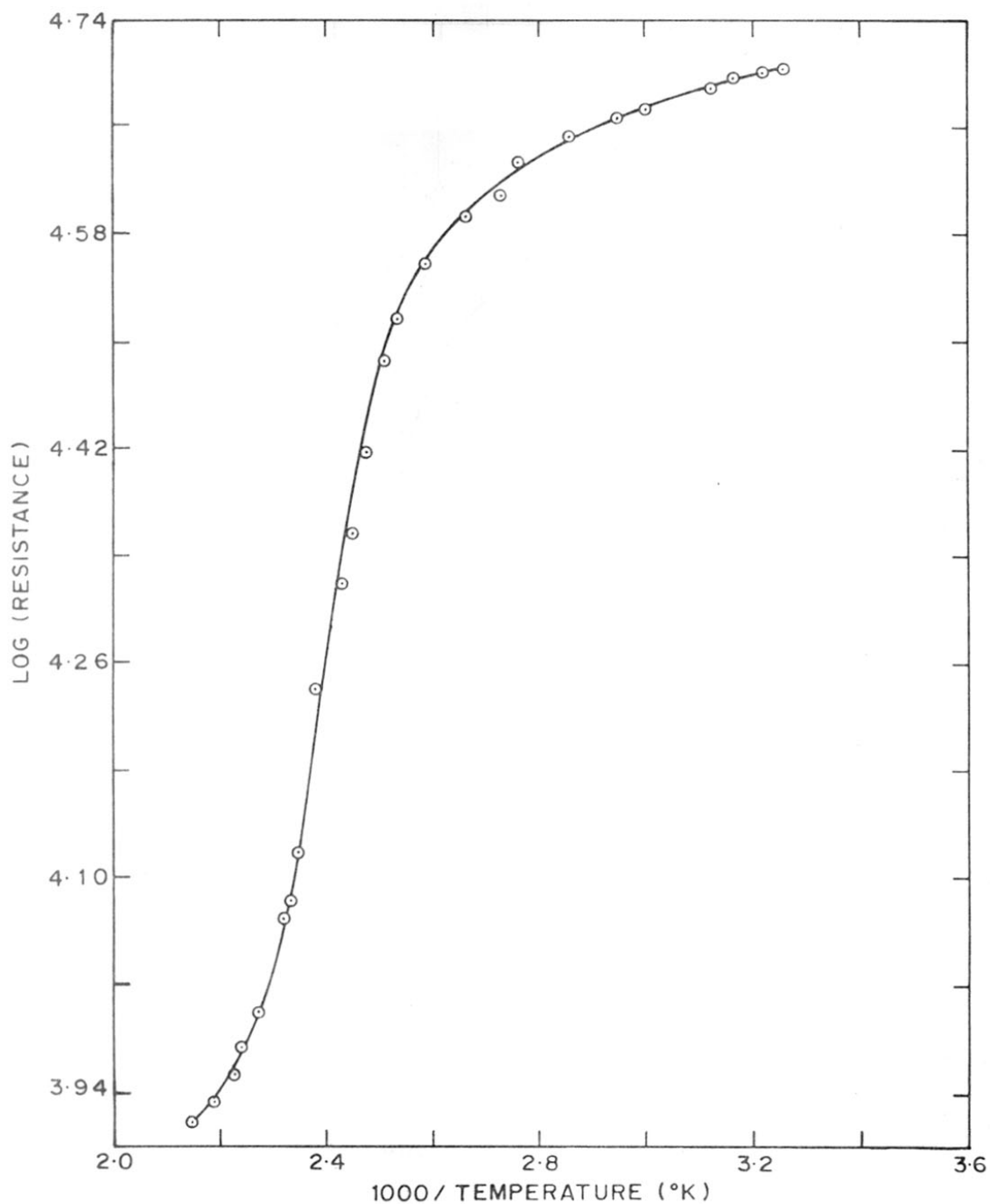


FIG. 3-20: LOG (RESISTANCE) Vs 1000/T FOR (Cd_{1.99} Pb_{0.01} SnO₄) THICK FILM FIRED AT 700 °C

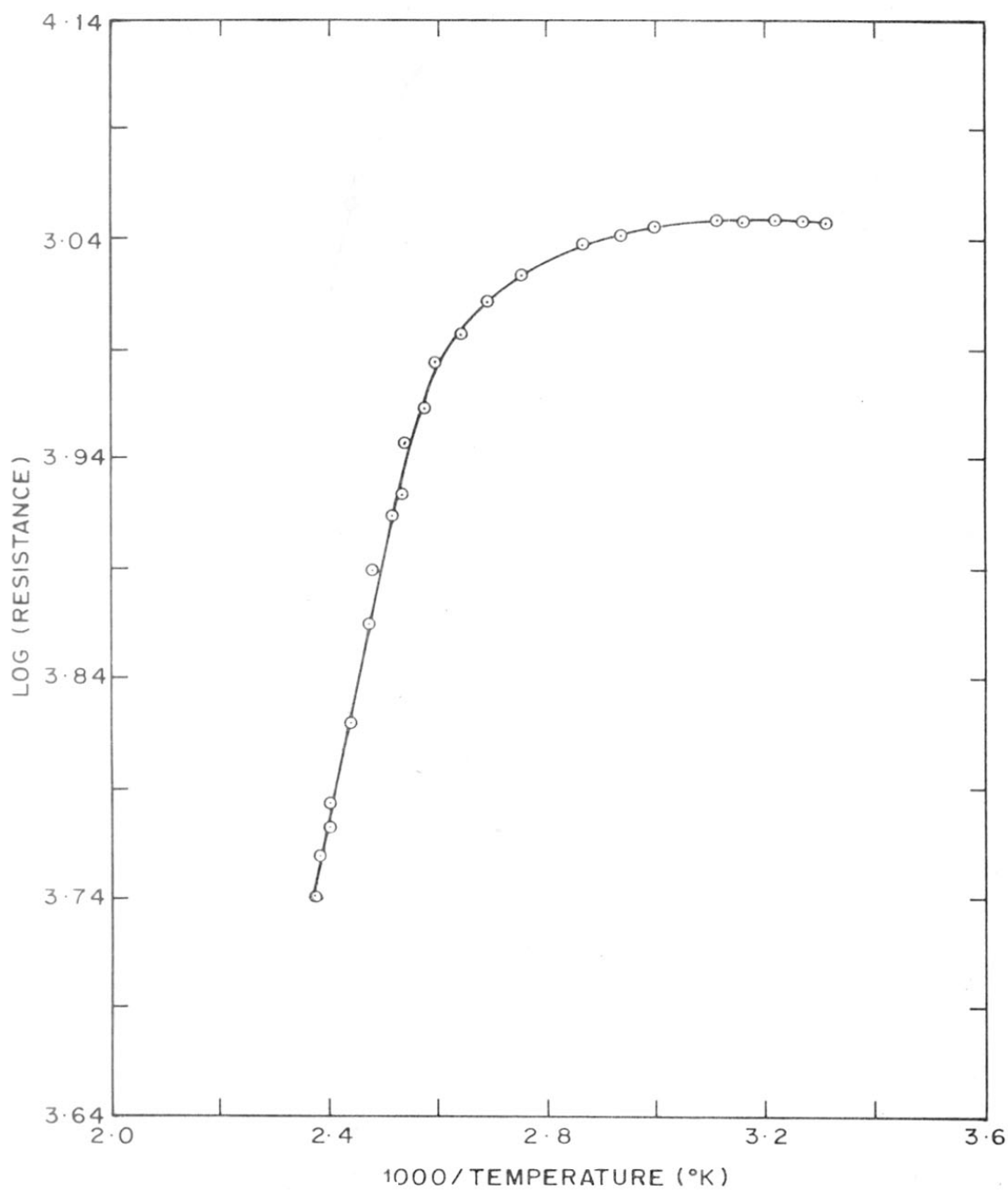
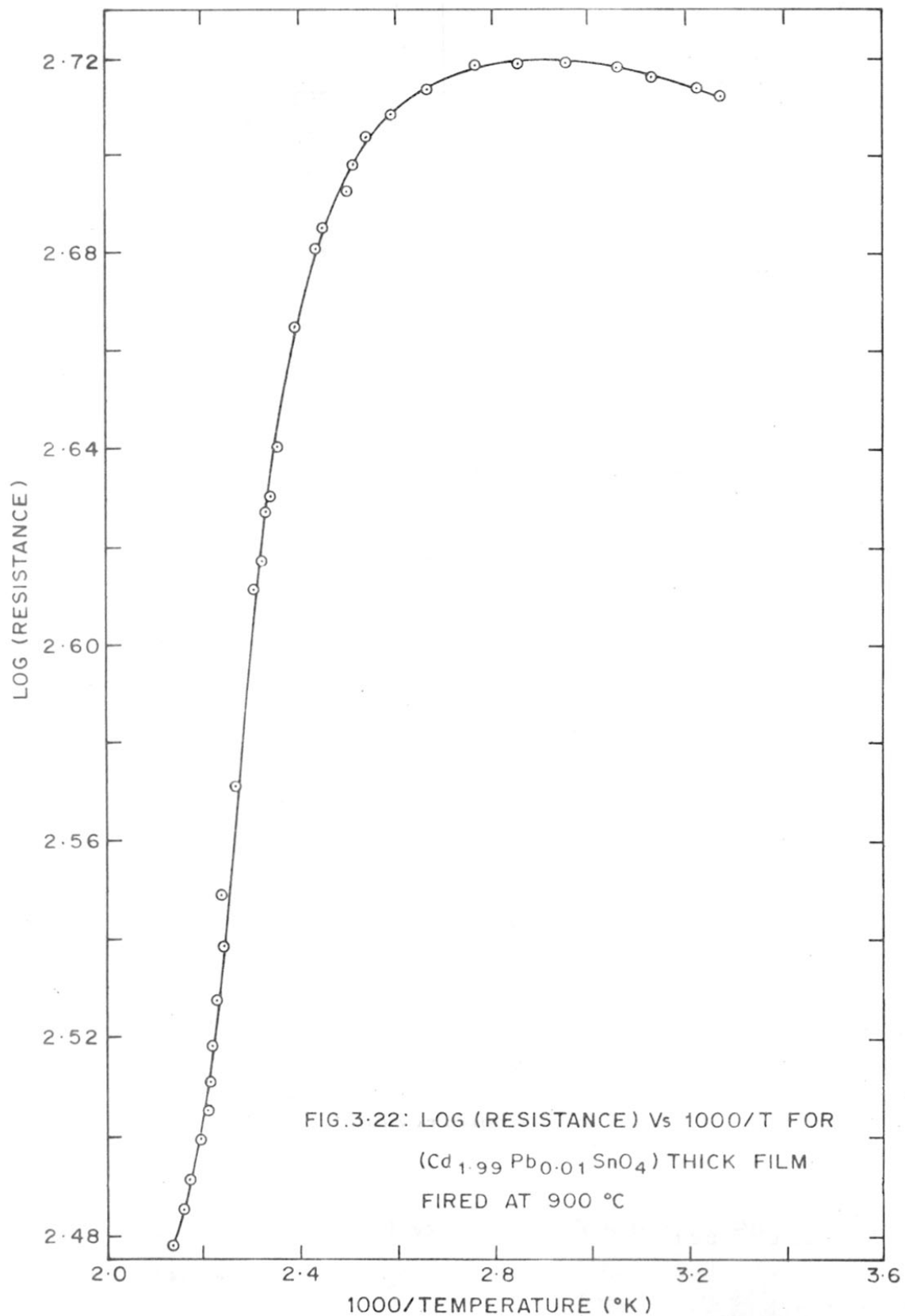


FIG. 3-21: LOG (RESISTANCE) Vs 1000/T FOR $(\text{Cd}_{1.99} \text{Pb}_{0.01} \text{SnO}_4)$
THICK FILM FIRED AT 800 °C



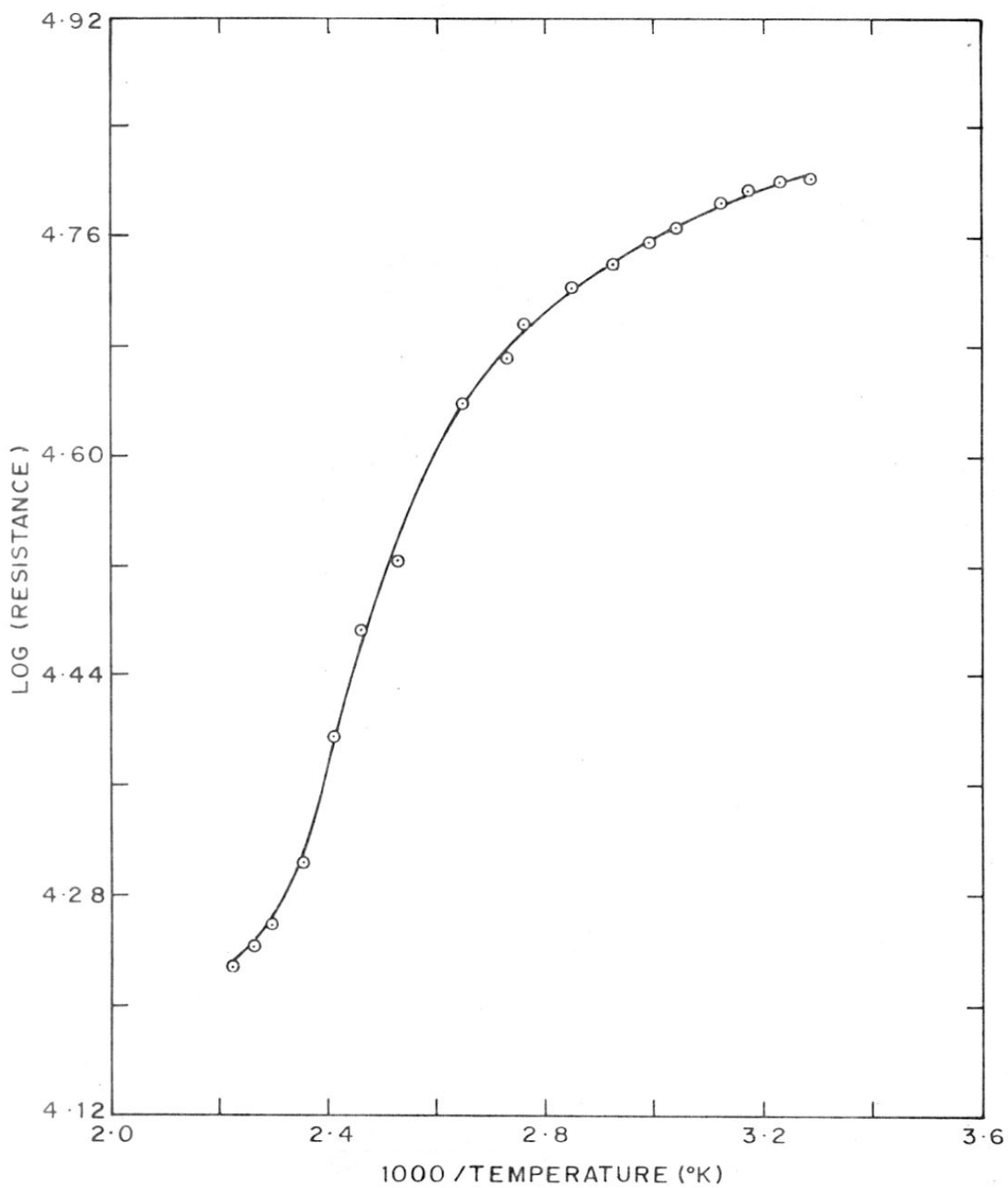


FIG. 3-23: LOG (RESISTANCE) Vs $1000/T$ FOR $(\text{Cd}_{1.98} \text{Pb}_{0.02} \text{SnO}_4)$
THICK FILM FIRED AT 600 °C

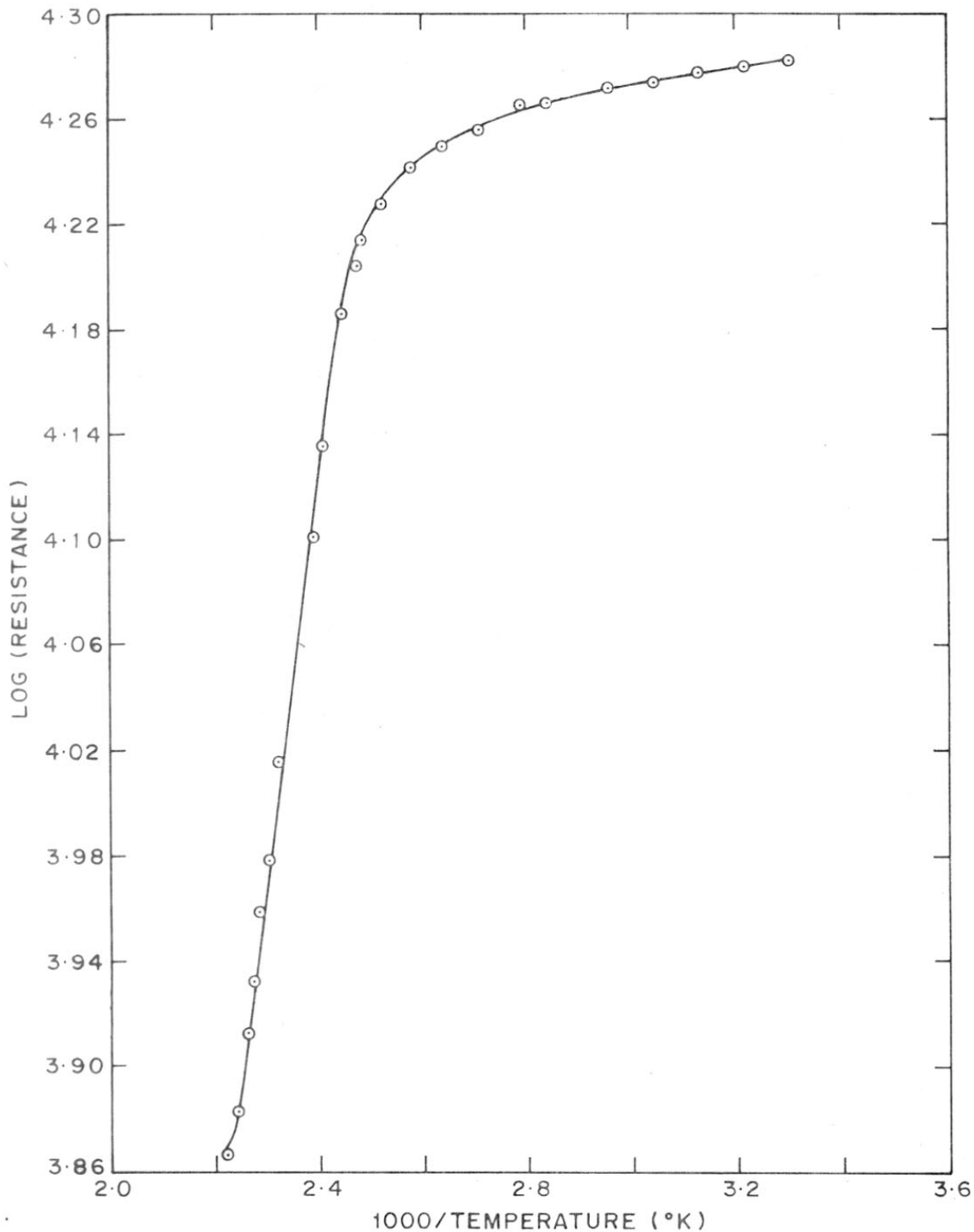


FIG. 3-24: LOG (RESISTANCE) Vs 1000/T FOR $(\text{Cd}_{1.98}\text{Pb}_{0.02}\text{SnO}_4)$
THICK FILM FIRED AT 700 °C

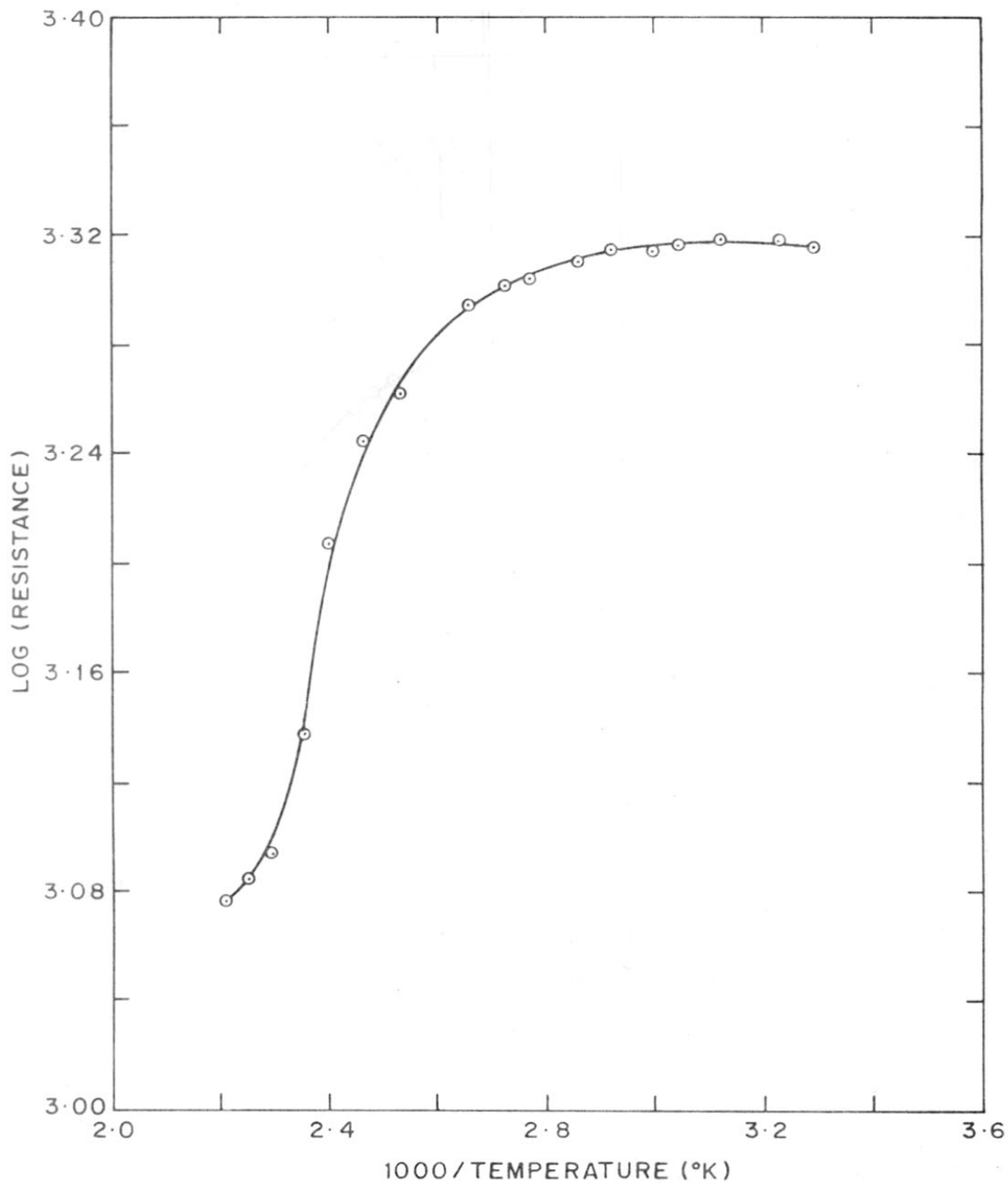


FIG. 3-25: LOG (RESISTANCE) Vs 1000/T FOR $(\text{Cd}_{1.98} \text{Pb}_{0.02} \text{SnO}_4)$ THICK FILM FIRED AT 800 °C

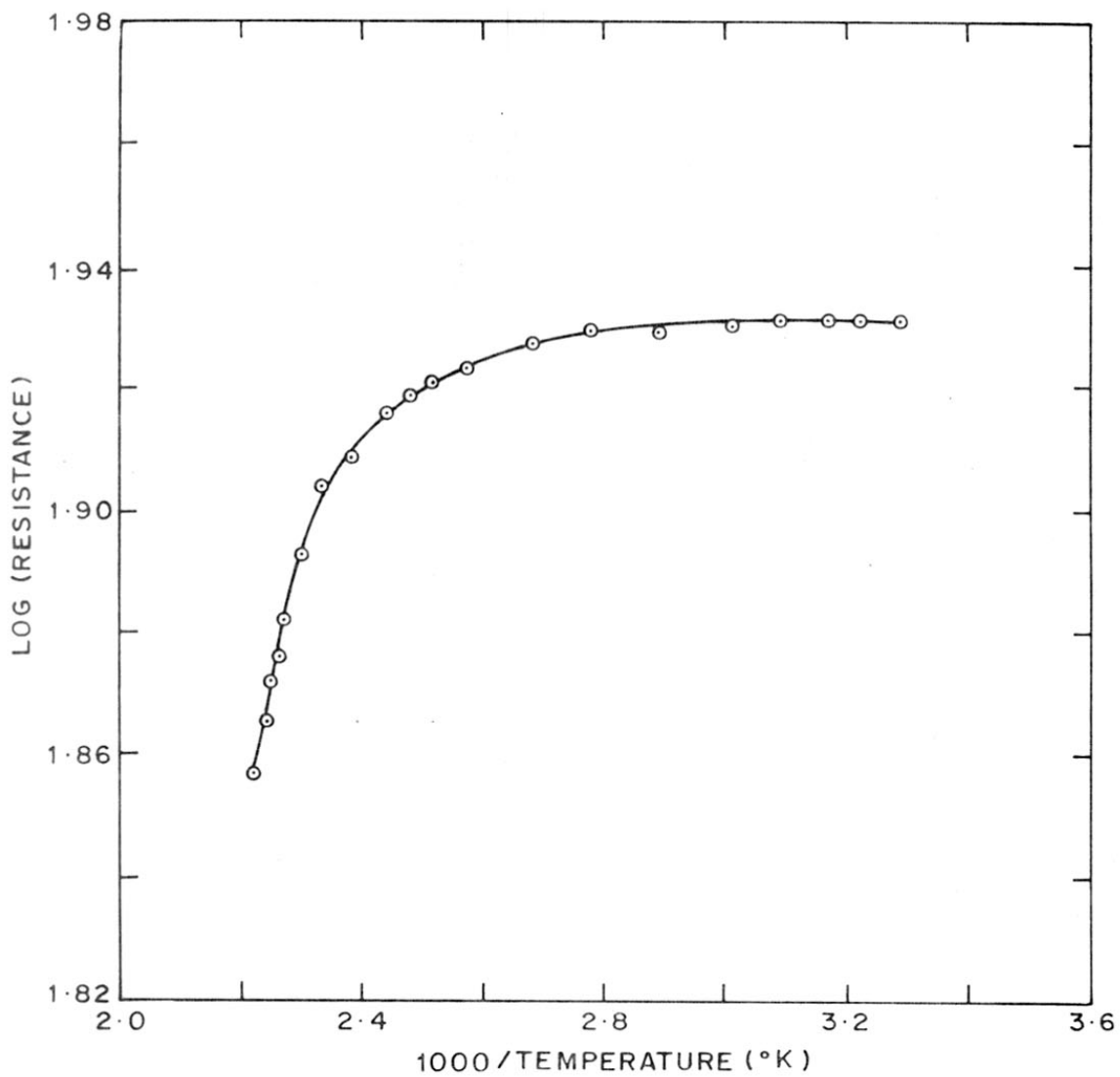
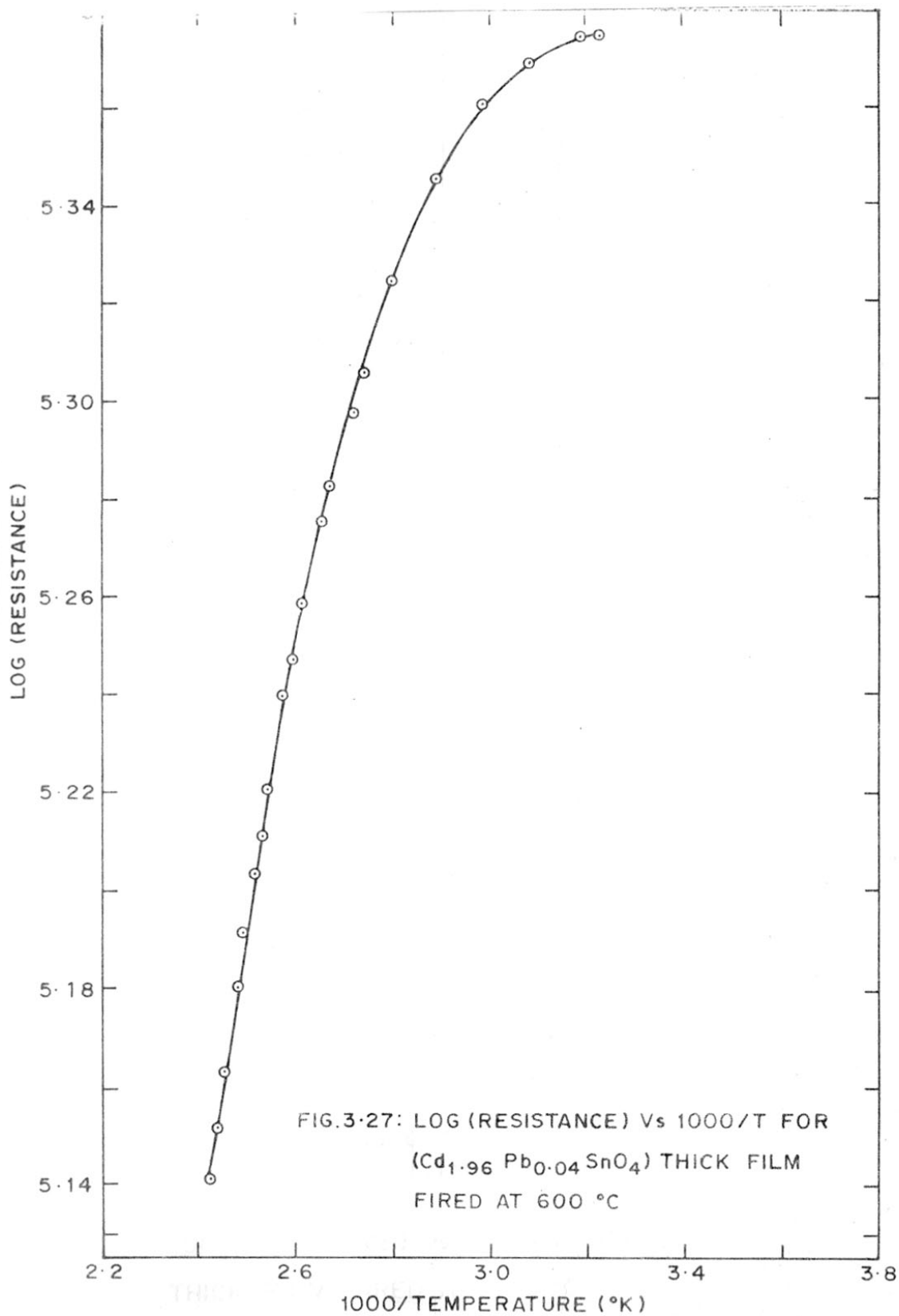


FIG. 3.26: LOG (RESISTANCE) Vs 1000/T FOR $(\text{Cd}_{1.98}\text{Pb}_{0.02}\text{SnO}_4)$
THICK FILM FIRED AT 900 °C



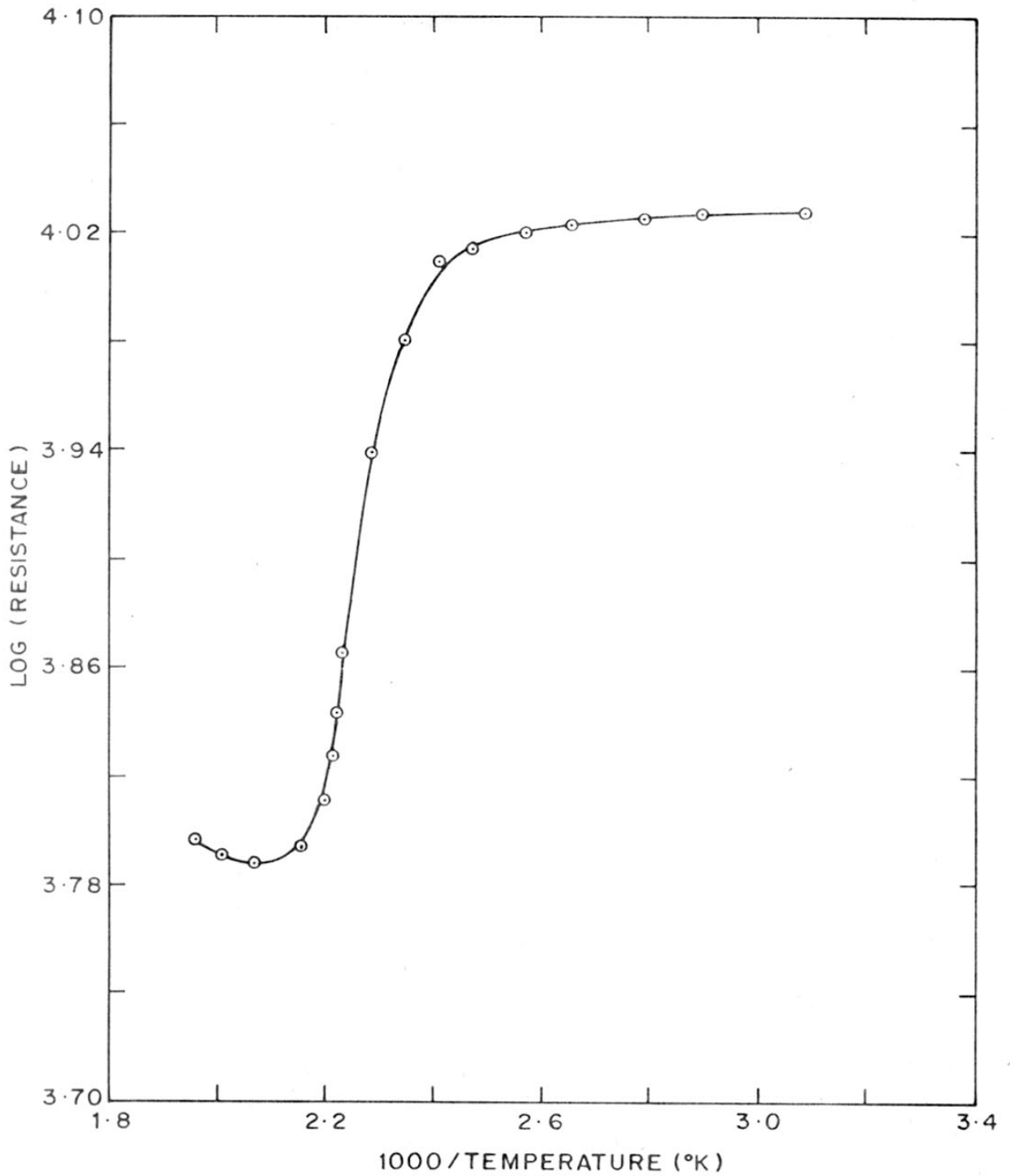
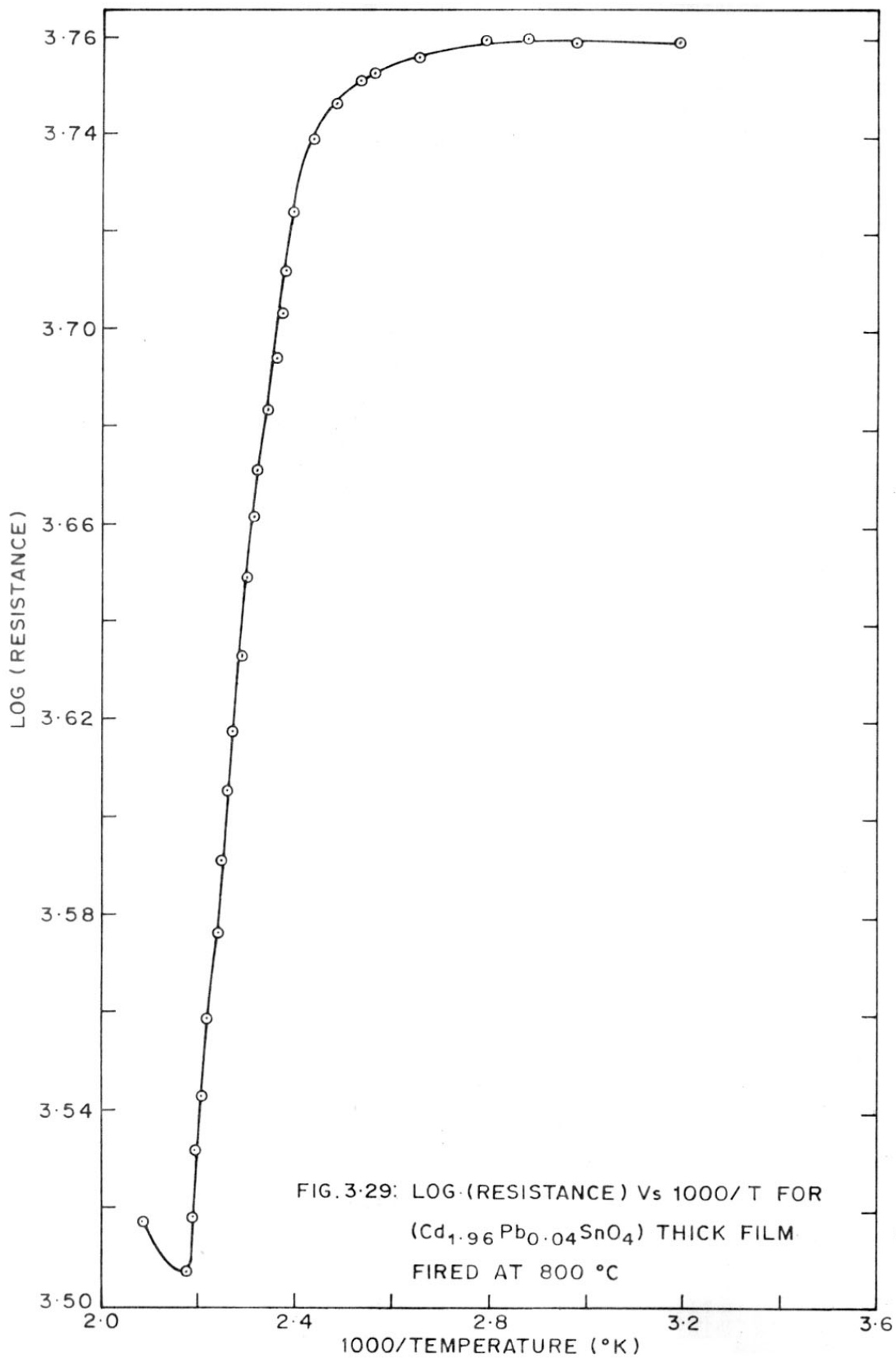


FIG. 3.28: LOG (RESISTANCE) Vs 1000/T FOR $(\text{Cd}_{1.96}\text{Pb}_{0.04}\text{SnO}_4)$ THICK FILM FIRED AT 700 °C



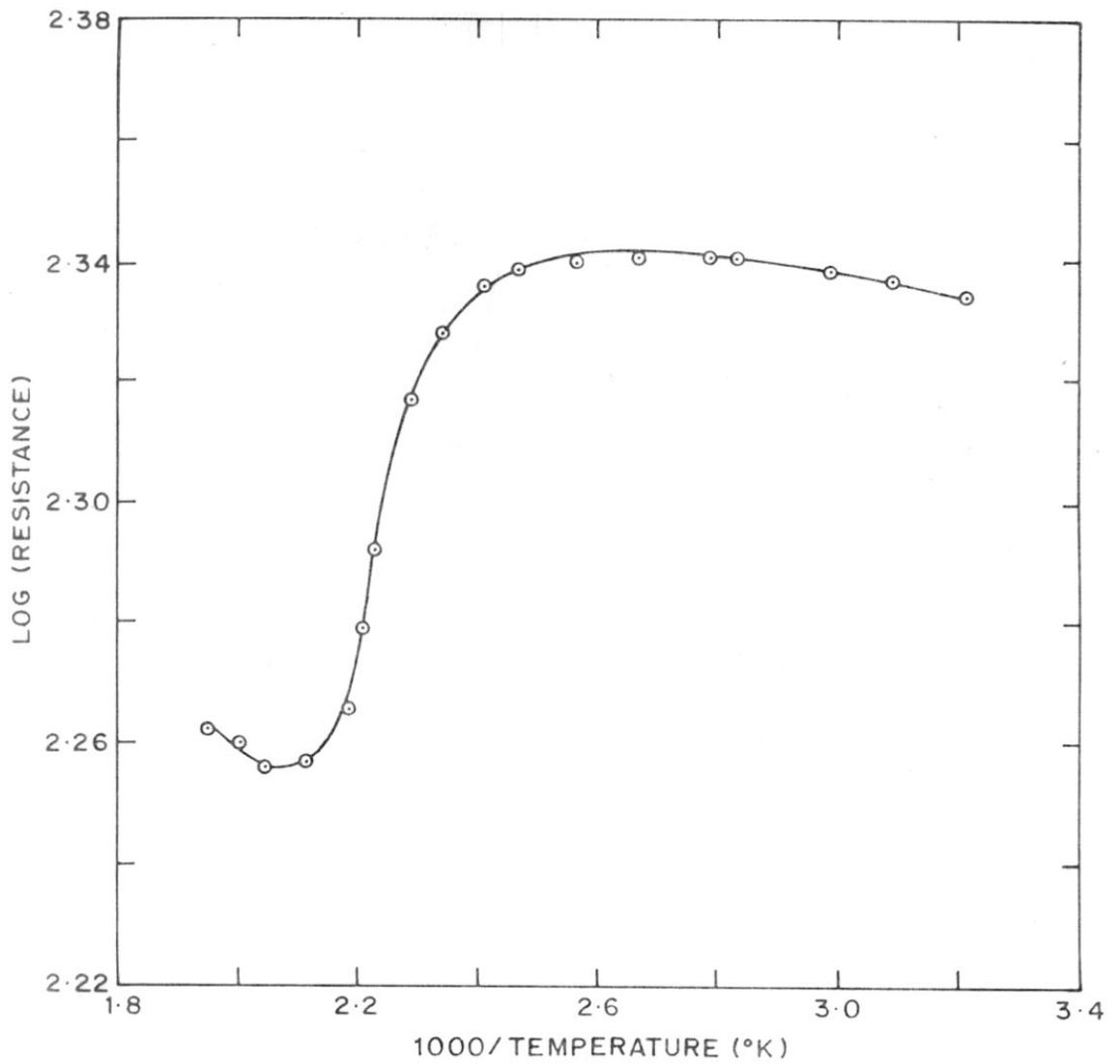
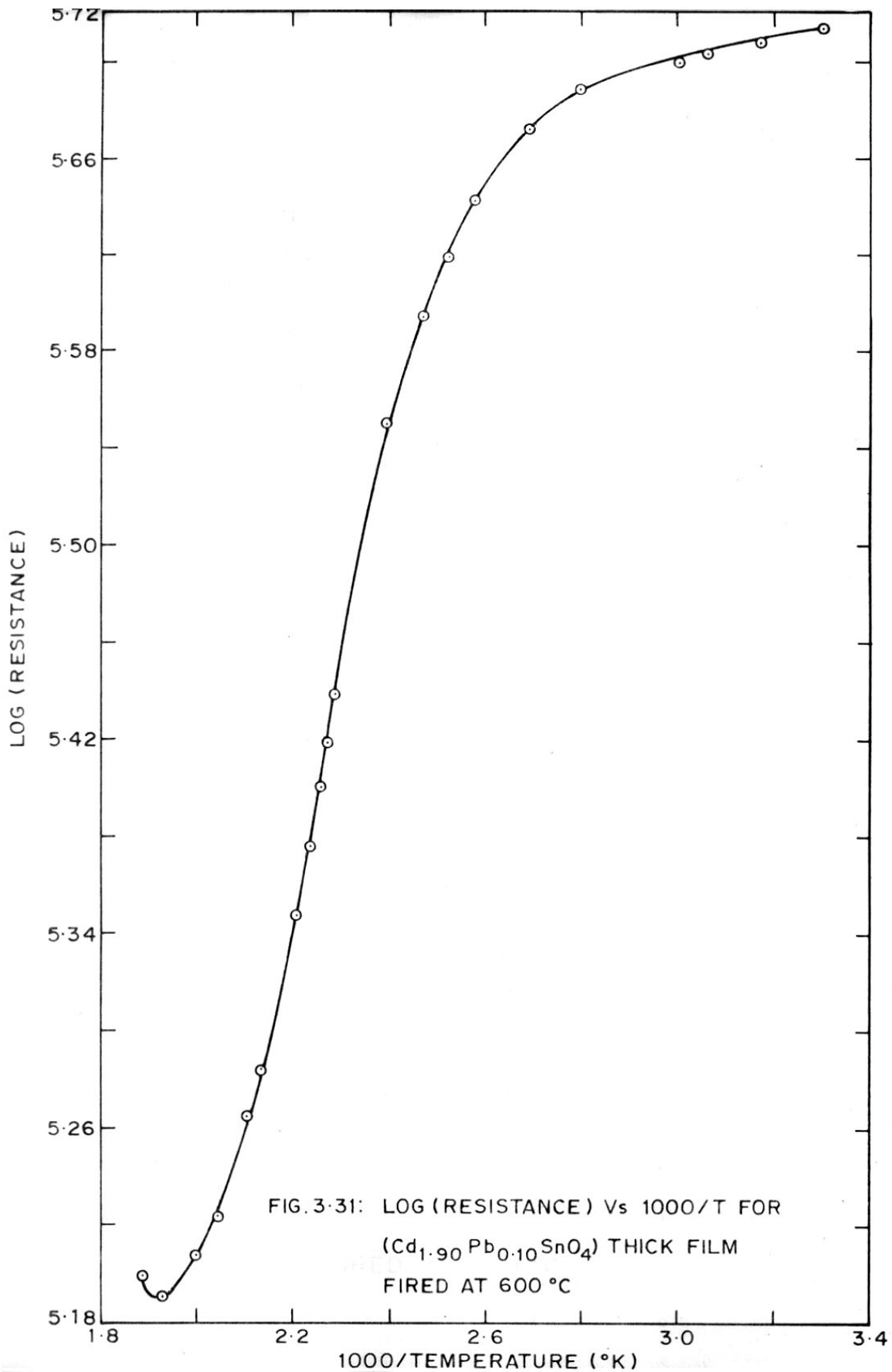


FIG. 3.30: LOG (RESISTANCE) Vs 1000/T FOR $(\text{Cd}_{1.96} \text{Pb}_{0.04} \text{SnO}_4)$
THICK FILM FIRED AT 900 °C



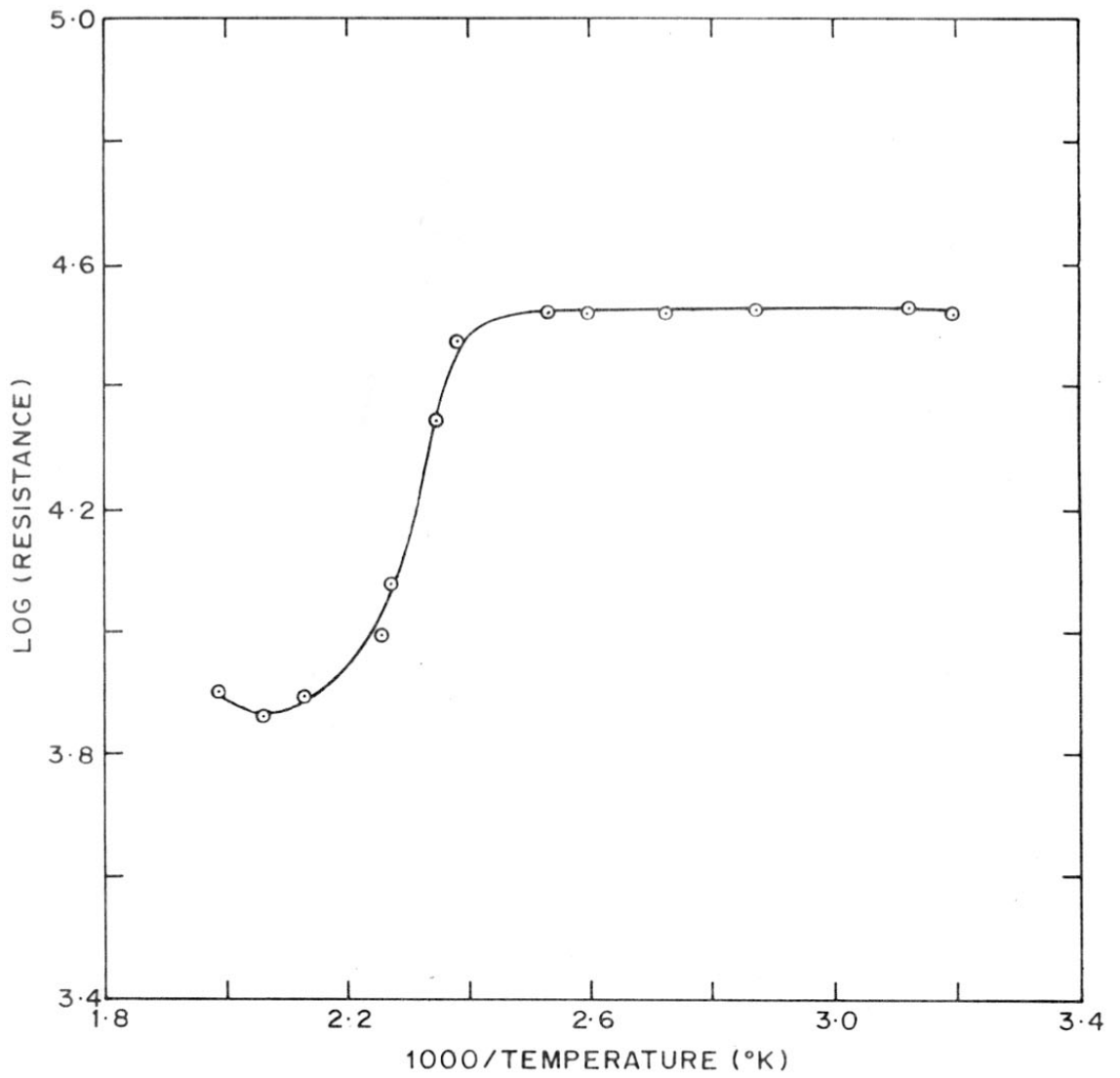


FIG. 3-32: LOG (RESISTANCE) Vs 1000/T FOR $(\text{Cd}_{1.90}\text{Pb}_{0.10}\text{SnO}_4)$ THICK FILM FIRED AT 700 °C

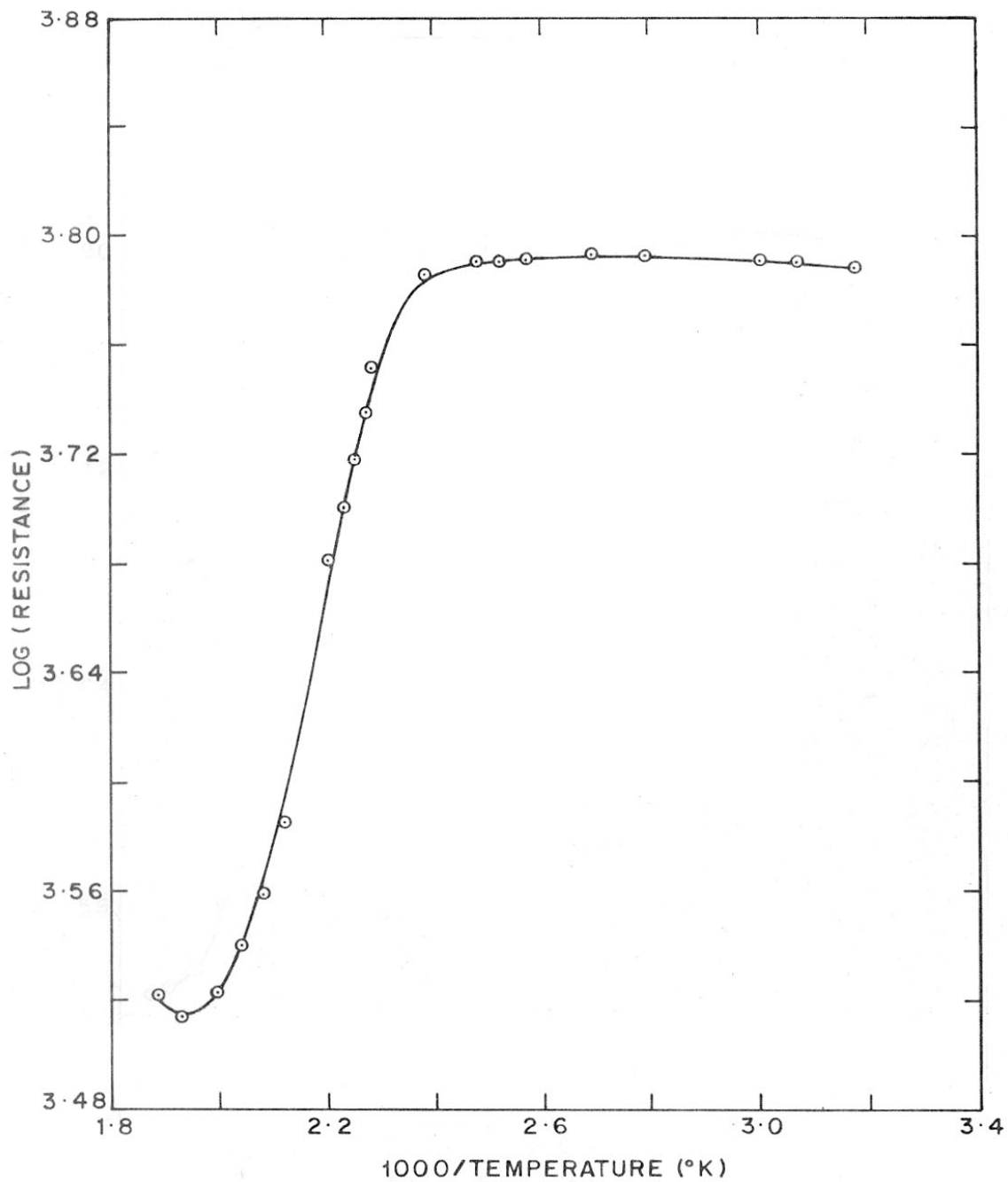


FIG. 3.33: LOG (RESISTANCE) Vs 1000/T. FOR $(\text{Cd}_{1.90}\text{Pb}_{0.10}\text{SnO}_4)$
THICK FILM FIRED AT 800 °C

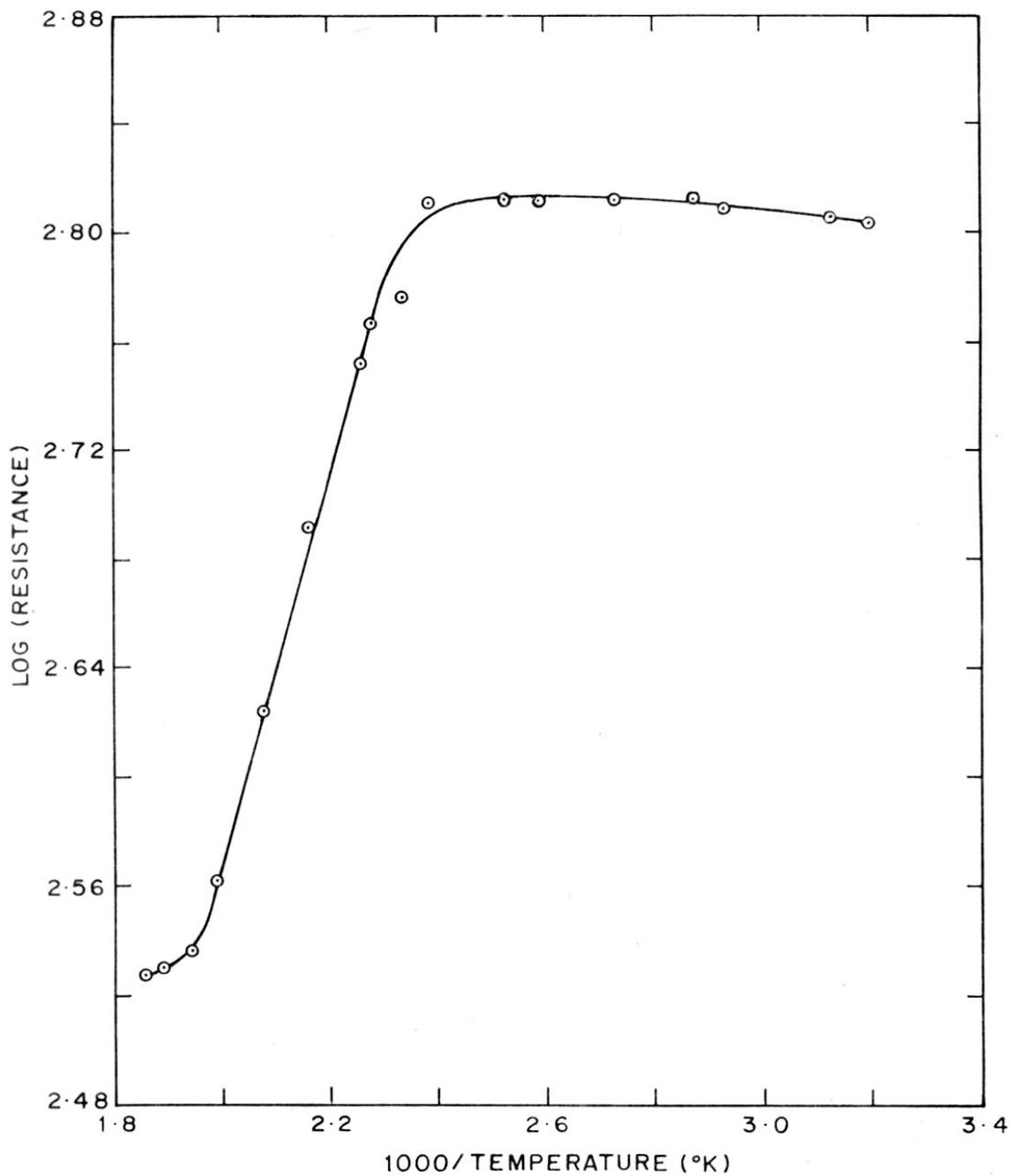


FIG. 3-34: LOG (RESISTANCE) Vs 1000/T FOR $(\text{Cd}_{1.90}\text{Pb}_{0.10}\text{SnO}_4)$
THICK FILM FIRED AT 900 °C

Table 3.10 - Temperature ($^{\circ}\text{C}$) at which the low slope changes to high slope

Dopant concentration	$\text{Cd}_{1-x}\text{Pb}_x\text{SnO}_4$				
	$x = 0.002$	0.01	0.02	0.04	0.10
Firing temperature ($^{\circ}\text{C}$)					
600	84	97	84	84	84
700	84	97	97	127	144
800	84	97	97	127	144
900	84	97	97	127	144

(eV)

Table 3.11 - Activation energy values corresponding
to the low slope values of the log R-1000/T
curves

Firing temperature (°C)	PbO mole (%)				
	0.002	0.01	0.02	0.04	0.10
600	0.12	< 0.01	0.04	0.03	< 0.01
700	0.04	0.02	< 0.01	< 0.01	< 0.01
800	0.03	< 0.01	< 0.01	< 0.01	< 0.01
900	< 0.01*	< 0.01*	< 0.01*	< 0.01*	< 0.01*

* slopes are of opposite sign.

(ev)

Table 3.12 - Activation energy values corresponding to the high slope values of the log R-1000/T curves

PbO mole (%)	0.002	0.01	0.02	0.04	0.10
Firing temperature (°C)					
600	0.76	0.33	0.24	0.12	0.20
700	0.65	0.44	0.27	6.22	0.72
800	0.46	0.19	0.16	0.20	0.18
900	0.08	0.17	0.06	0.09	0.14

temperature and the dopant concentration.

The slopes of the curves between the temperature 400-450°K (table 3.12) correspond to the higher activation energy values. For a given composition, the activation energy decreases with the firing temperature.

Additionally, we have carried conductivity measurements during the heating - cooling cycles.

We selected $\text{Cd}_{1.9}\text{Pb}_{0.1}\text{SnO}_4$ as a typical composition for the purpose. The thick film samples were fired at 600, 700, 800 and 900°C.

The results showed that the room temperature resistance value decreased progressively with the number of heating - cooling cycle. Also, the difference in the resistance value at any temperature between heating and cooling cycles gradually decreased. After more than five cycles, the heating and cooling curves were almost identical. Further, it was seen that the resistance increased with the increase in temperature from room temperature. This was very much in evidence particularly in the case of the sample fired at 900°C. In other cases, such a situation occurred after a few heating-cooling cycles.

The decrease in the conductivity with the rise in temperature in the samples is a typical behaviour of degenerate semiconductor. The activation energy is very low, < 0.01 eV.

The conductivity measurements, described above, indicate that our samples are degenerate. To obtain high degree of degeneracy, one needs either to impart high impurity concentration or create a large number of defects.¹¹¹ In our doped samples, it is seen from the data presented in the table (3.9) that the conductivity increases with the firing temperature for all the concentrations of the dopant. Likewise, the colour of the samples also changes from bright yellow to green.

Resistance values are plotted against the dopant concentration for all the four firing temperatures (figures 3.35 - 3.38) present this data. The resistance - PbO (%) relation is similar for the samples fired at 600 and 700°C. Gradual decrease of resistance shows a minimum at PbO = 0.66% (600°C) and PbO = 1.32% (700°C). It increases further with further increase of PbO. Whereas in the cases of 800 and 900°C, the trend is almost identical. A minimum is shown at PbO = 0.66%.

The resistance values are very high in the as-fired samples, notwithstanding the dopant concentration, and other preparation conditions. The values decreased by 1 - 2 orders of magnitude after annealing at 180°C. Even in the sputtered films of Cd_2SnO_4 , whether doped or undoped, there is wide variation of resistance.⁵²

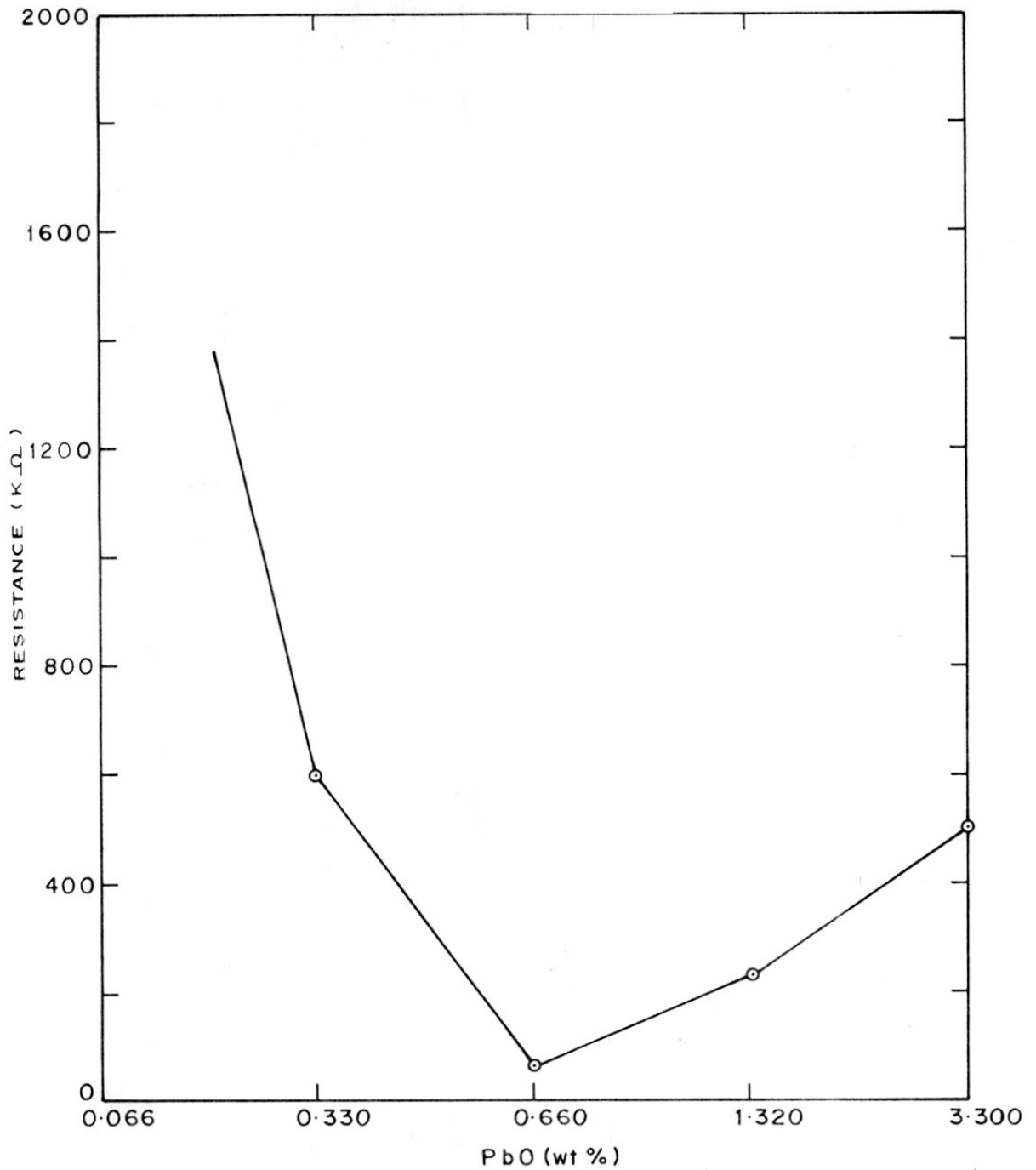


FIG. 3·35: RESISTANCE Vs. DOPANT (PbO) CONCENTRATION FOR THICK FILMS FIRED AT 600 °C

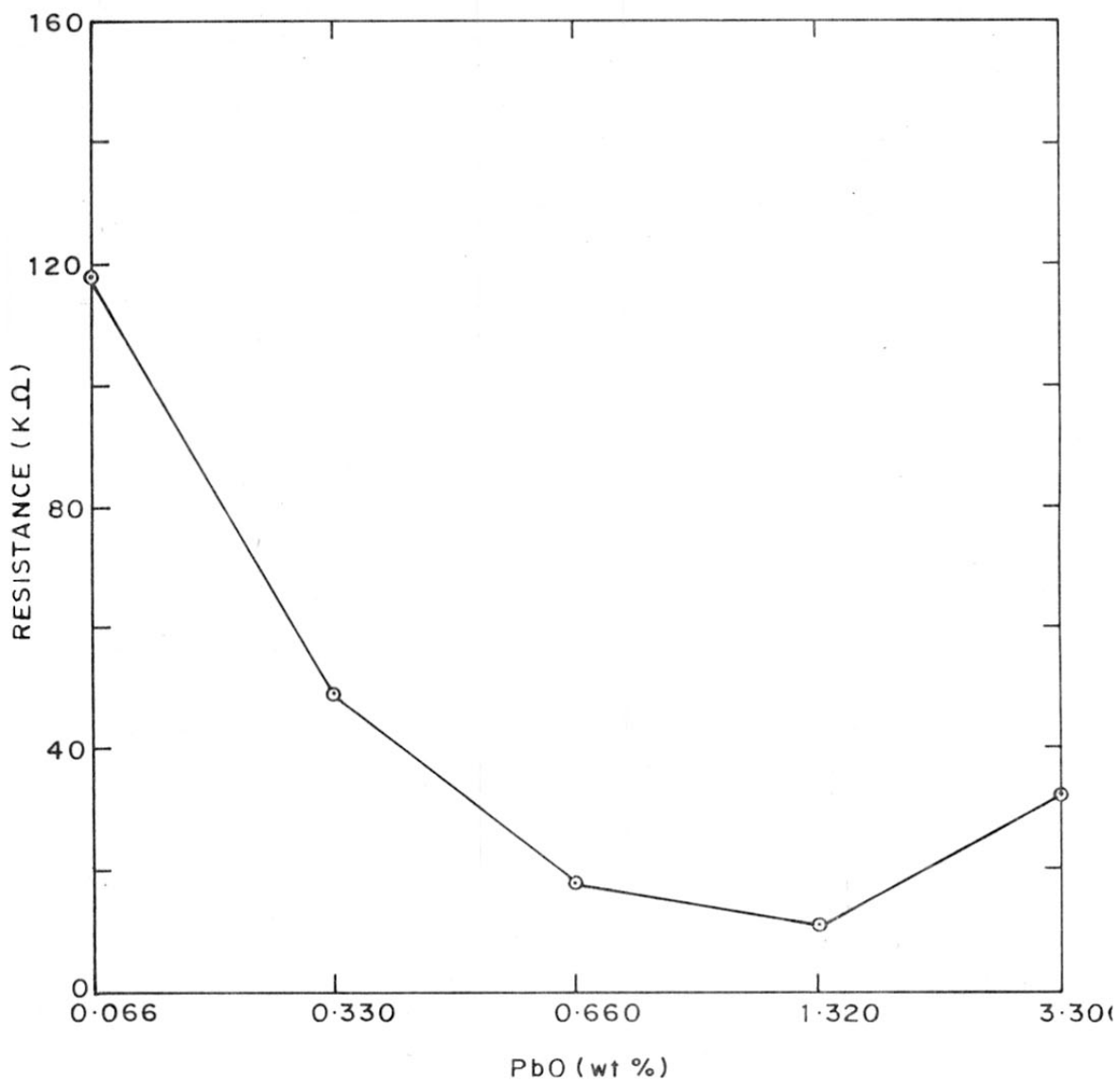


FIG. 3.36: RESISTANCE Vs. DOPANT (PbO) CONCENTRATION FOR THICK FILMS FIRED AT 700 °C

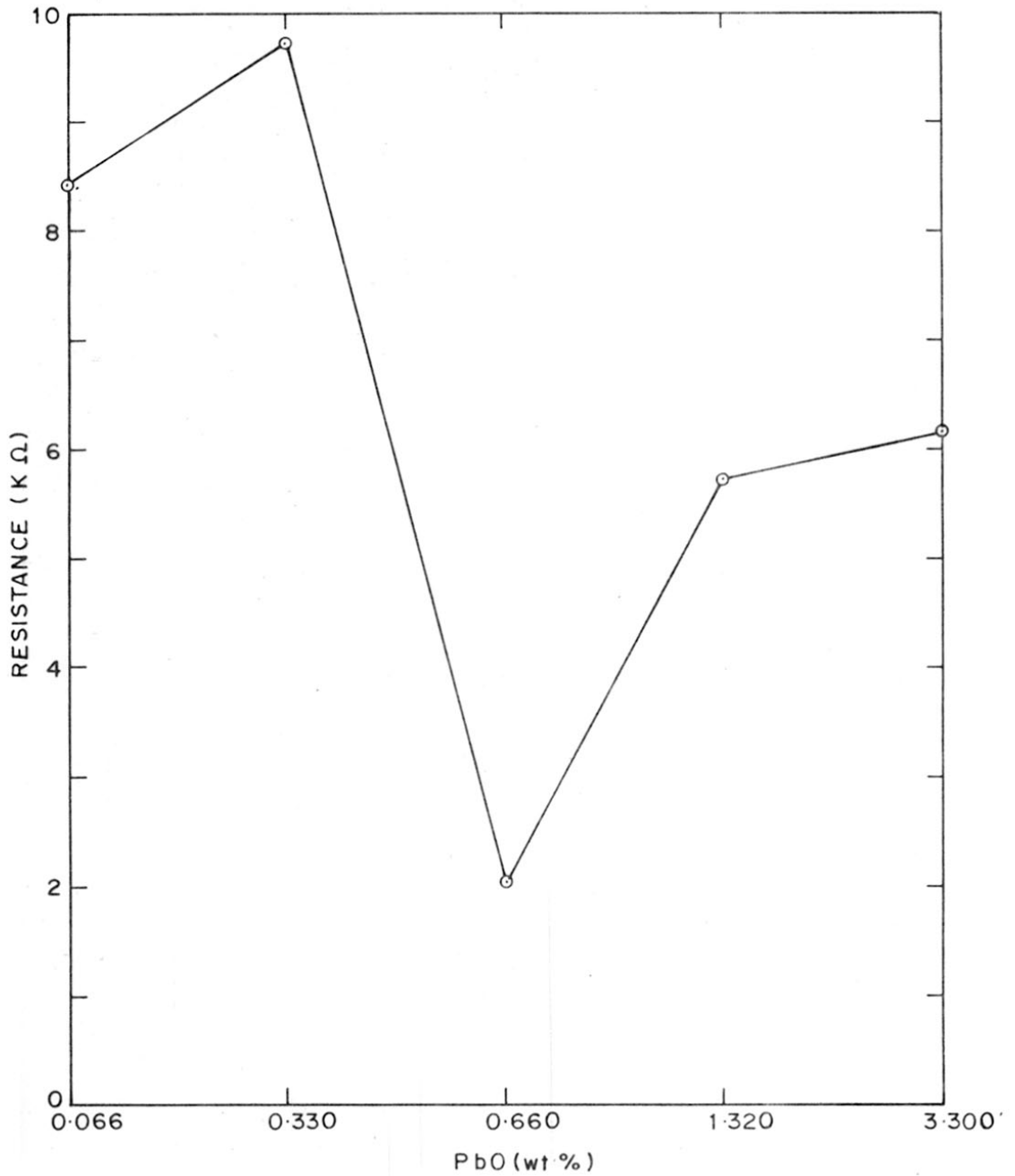


FIG. 3-37: RESISTANCE Vs. DOPANT (PbO) CONCENTRATION FOR THICK FILMS FIRED AT 800 °C

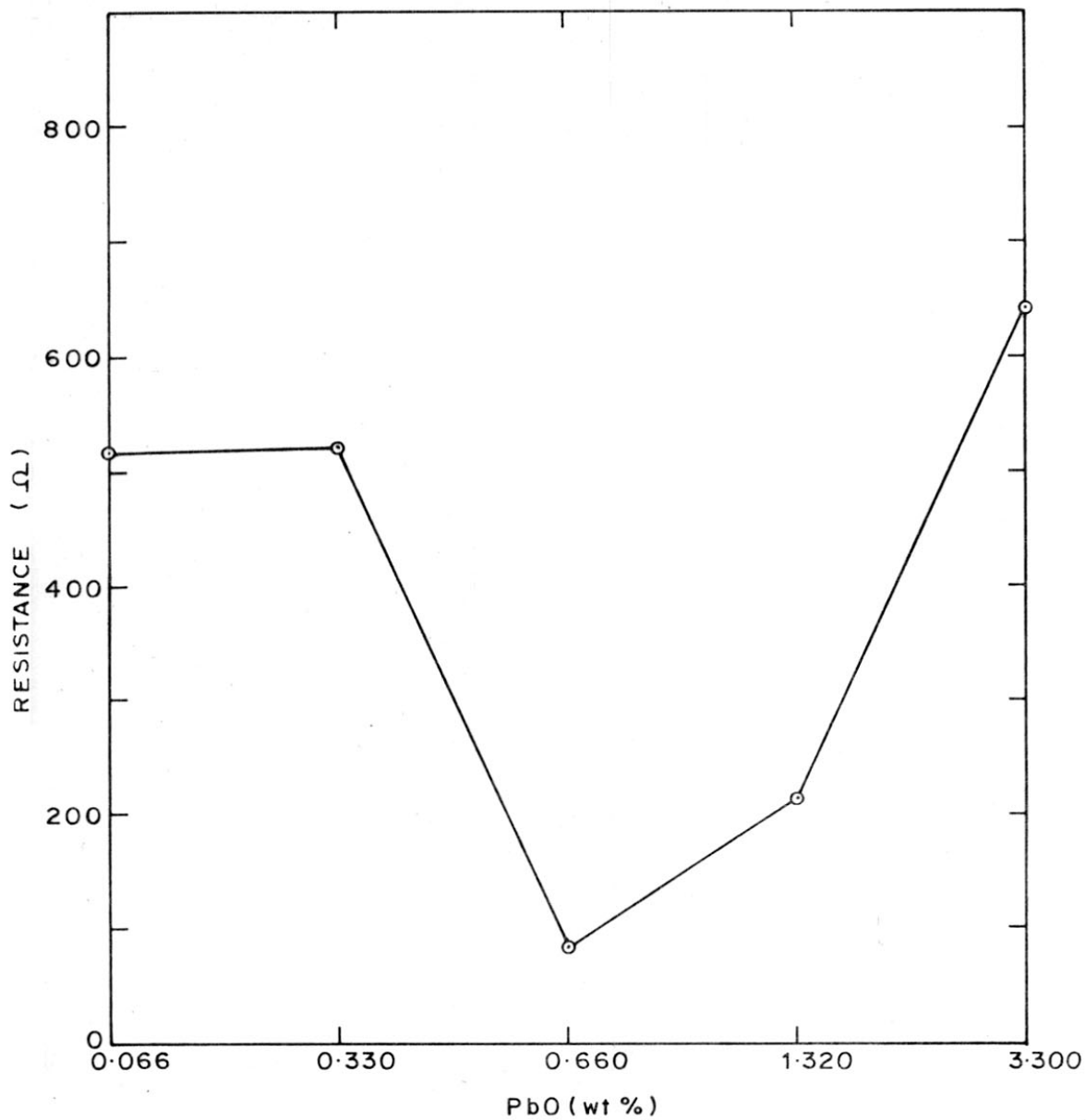


FIG. 3-38: RESISTANCE, Vs. DOPANT (PbO) CONCENTRATION FOR THICK FILMS FIRED AT 900 °C

This seems to be a common phenomenon in all n-type, oxygen deficient semiconductors (e.g. In_2O_3 , SnO_2 , CdO etc).

Heat treatment of the sample films under vacuum and in "forming atmosphere" show conductivity increase and is highly temperature-dependent.⁶⁸ The value can be frozen at that temperature. Probably, the adsorbed oxygen on the surface is removed and this contributed donor electrons for conduction.

Thornton and Hedgoth⁴⁶ suggested that the carriers were liberated from the compensation traps during the heat treatment. Presence of interstitial cadmium also provided carriers, but mobility values fell. The mobility increased during annealing because the structural disorder disappeared. Similar situation was prevalent in our Cd_2SnO_4 thick films also.

The controlling factors influencing the electrical properties can be different. Surface processes like dissociation of the oxide, creation of oxygen vacancies, presence of cation interstitials, adsorption of oxygen, diffusion of the defects, sintering of the particles etc. have been reported.

Evaporation of cadmium as cadmium oxide is negligible^{35,112} in the temperature range 1150-1374°K.

But evaporation of cadmium by dissociation of CdO is possible. The defect comprises of 'D' centres or paired vacancies with two trapped electrons, together with anion vacancies.¹²⁷ The binding energy of the second electron in the 'D' centre is low and therefore acts as an effective electron donor. If the donor states provided by oxygen vacancies are considered as doubly ionised, then the ionisation energy is less.¹²⁸

The different mechanisms suggested earlier which were responsible for the increased conductivity are briefly explained here.

a) Oxygen vacancies:

Choi et al¹¹¹ proposed the transport-mechanism involving vacancies in the anion sublattice. Oxygen vacancies ($V_O^{\bullet\bullet}$) and electrons are formed by the following disorder reaction, obtained from conductivity - oxygen partial pressure studies.



These electrons are available for conduction. Many workers^{23,34} reported that oxygen vacancies in Cd_2SnO_4 provided donor states. Large conductivities could be obtained by increasing oxygen vacancies. Our conductivity

measurements also present the results supporting the presence of oxygen vacancies.

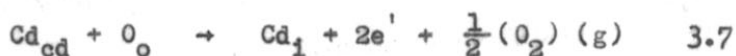
b) Cadmium interstitials:



Ionised cation interstitials, Cd_1^{\cdot} were formed. This amounted to transferring a neutral cadmium atom from the vapour phase to an interstitial position. According to Koffyberg¹¹³, Cd_1^{\cdot} was completely ionised.



The equilibrium condition, where doubly ionised Cd_{cd} existed in CdO of Cd_2SnO_4 could be written as



Dale Hall⁵⁸ also opined that conduction electrons were provided by cadmium interstitials in addition to oxygen vacancies in Cd_2SnO_4 sputtered films. In the case of In_2O_3 ⁵², the conduction was reported to be due

to In interstitials. ESCA and X-ray results discussed elsewhere provide supporting evidence for the presence of Cd interstitials.

e) The possibility of adsorption of gases is supported by our thermal analysis results. TG curve shows gain in weight during the heating of the sample in oxygen atmosphere because of adsorption. Desorption of oxygen leaves two electrons associated with each oxygen atom. These electrons participate in conduction.

d) Sintering effects and network formation:

Very high conductivity values for all compositions were obtained when the samples were fired at 900°C. This might be attributed to some kind of coalescing or sintering of the particles leading to an increase in contact area¹¹² of the microcrystals of the polycrystalline thick films. The SEM photomicrographs, Figures (3.9 - 3.14) indicate the existence of sintering and network formation when the sample films were fired from 500 to 900°C. The void spaces were much smaller by comparison than the sizes of the connecting necks. Moreover, shortening of the necks was also seen for the sample fired at 900°C (figure 3.14).

The total resistance of the sample film was the sum of the outer sheath (high value) and the inner sheath

(low value). The first one might be attributed to the adsorbed oxygen. The second might be due to the defects. With the increase in temperature, the resistance increase resembled like that in metals in having similar electronic properties. The increase was because of the lower values of mobility of the charge carriers due to the scattering effects.

The resistance decreased with further increase in temperature. This variation was time-dependent in all our samples, particularly at higher temperatures.

Fall in resistance over a number of cycles of heating and cooling was mentioned earlier. This was indicative of slow diffusion of oxygen outwards and a rapid decrease of oxygen content in the thin surface 'skin'.

The increase in conductivity in the samples fired at 900°C was attributed to the increase in surface mobility of the charge carriers. The carrier concentration was controlled by the dopant percentage. At 700°C and above, the conductivity increase might additionally be due to $\text{Pb}^{2+} \rightarrow \text{Pb}^{4+} + 2\text{e}'$. The electrons were thus added to enhance the conductivity. ESCA results show supporting evidence to this reasoning.

Long periods were required for the attainment of

equilibrium with the gaseous oxygen at annealing temperature to get back the original electrical properties. The reason for this was that although the surface equilibrium might be rapid but the lattice diffusion was extremely slow. That is how the electrical properties of our samples are influenced, by the combination of 'adsorption' and 'structure' of the polycrystalline thick films.

3.5 THERMOELECTRIC MEASUREMENTS

Thermoelectric power (θ) plotted against temperature for the samples are presented in the figures (3.39-3.42).

Before starting the measurements, it was ensured that the emf value was zero when the temperature at the ends of the sample was same.

Thermoelectric power or Seebeck coefficient was calculated for the samples using the formula

$$\theta = \frac{P.D}{(T_1 - T_2)} \quad 3.8$$

where P.D. is the potential difference, T_1 and T_2 are the temperatures at the ends of the sample.

The Cd_2SnO_4 thick film samples used for the measurements corresponded to the composition $Cd_{1.9}Pb_{0.1}SnO_4$.

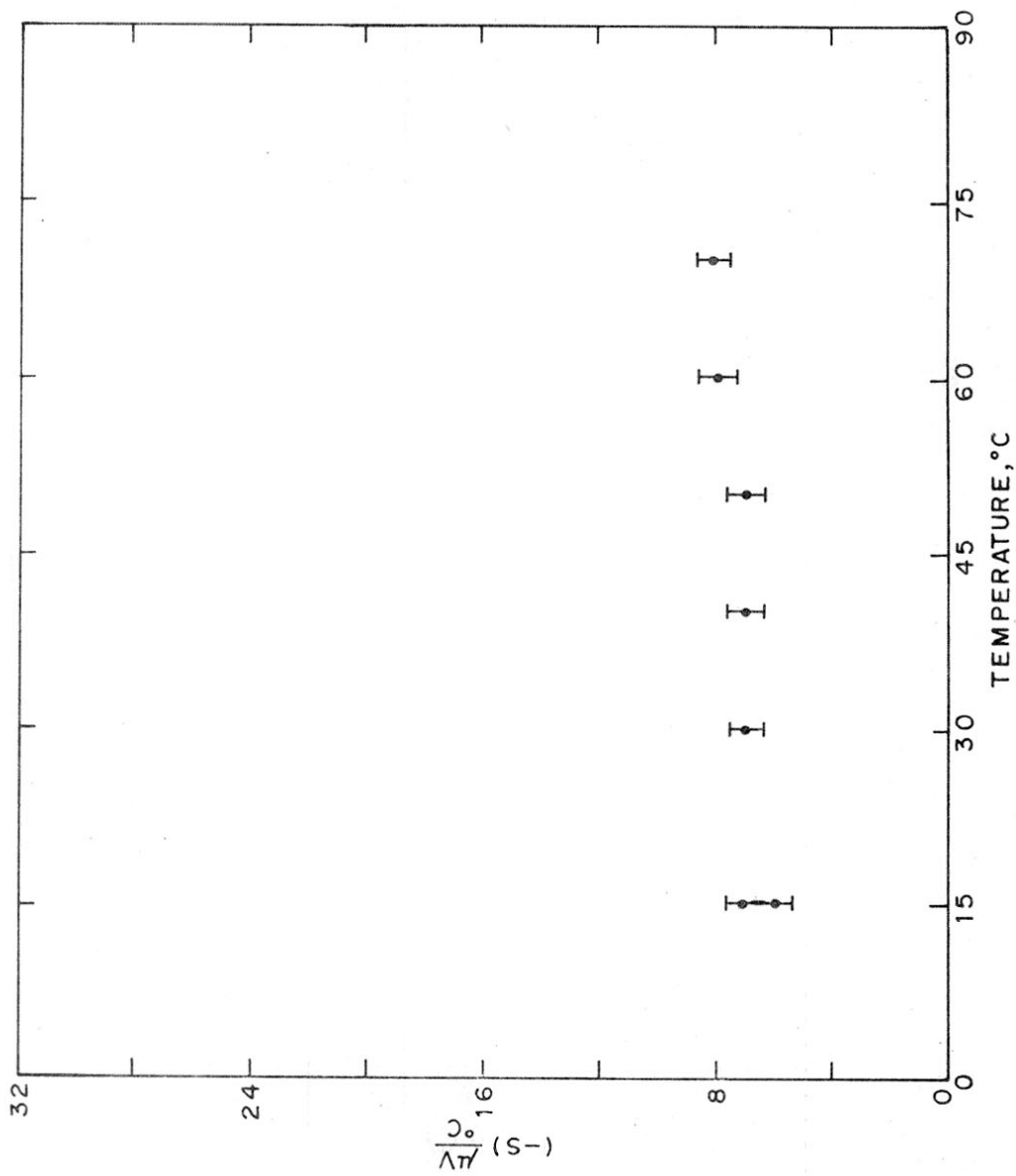


FIG. 3-39: VARIATION OF SEEBECK COEFFICIENT (S) WITH TEMPERATURE FOR $(Cd_{1.9}Pb_{0.1}SnO_4)$ THICK FILM FIRED AT 600 °C

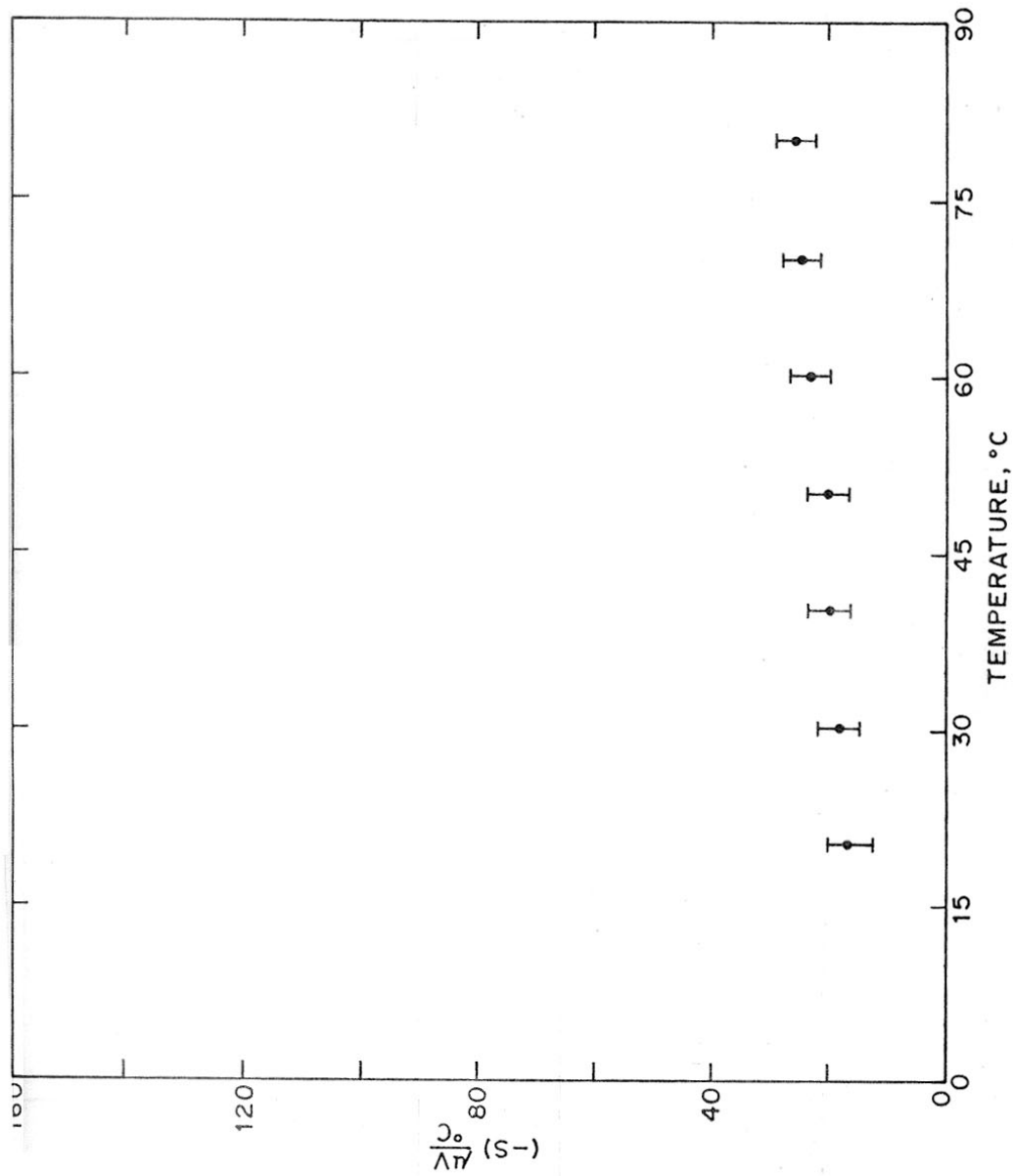


FIG. 3-40: VARIATION OF SEEBECK COEFFICIENT (S) WITH TEMPERATURE FOR $(\text{Cd}_{1.9}\text{Pb}_{0.1}\text{SnO}_4)$ THICK FILM FIRED AT 700°C

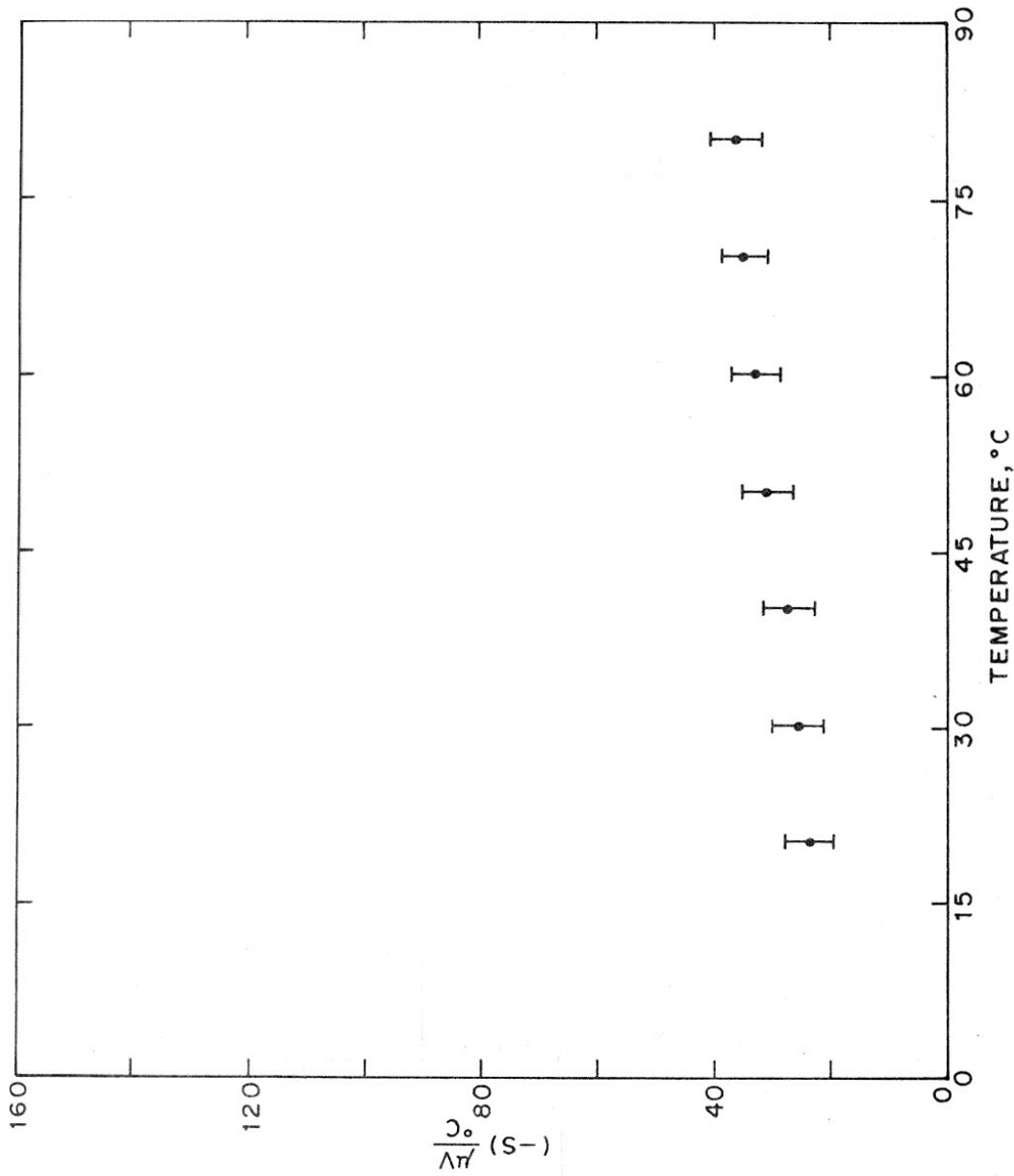


FIG. 3-41: VARIATION OF SEEBECK COEFFICIENT (S) WITH TEMPERATURE FOR $(Cd_{1.9}Pb_{0.1}SnO_4)$ THICK FILM FIRED AT $800^{\circ}C$

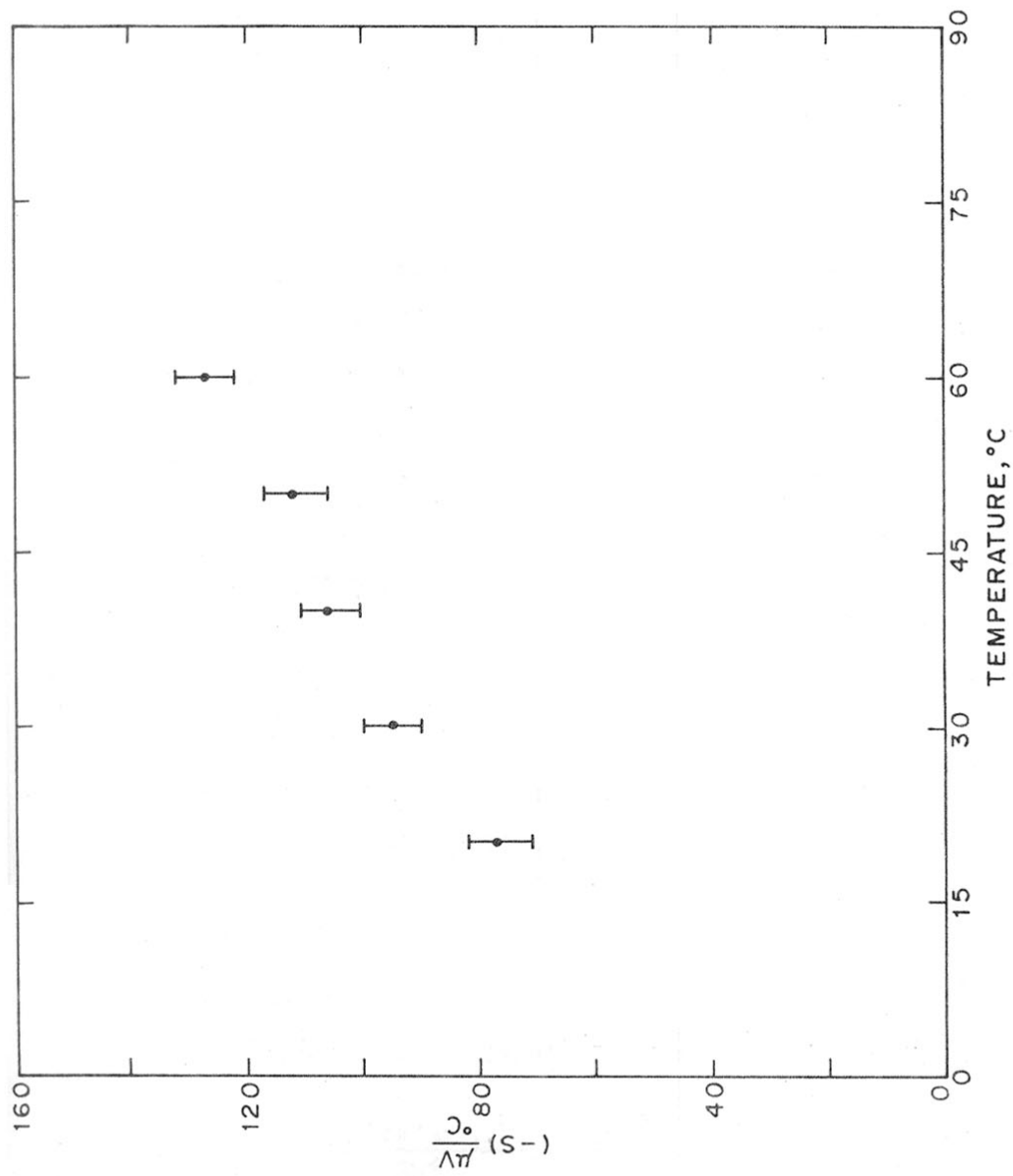


FIG. 3.42: VARIATION OF SEEBECK COEFFICIENT (S) WITH TEMPERATURE FOR (Cd_{0.5}Pb_{0.5}SnO₃) THICK FILM FIRED AT 900 °C

The peak firing temperature was 600-900°C.

Table (3.13) presents the thermoemf data.

It is seen from the above table that all the samples are n-type semiconductors. The thermoemf is negative. The results indicate a trend in the Seebeck coefficient values for the doped Cd_2SnO_4 thick films fired at different temperatures. The ' θ ' values increase with the sample firing temperature.

It has been reported in literature that Cd_2SnO_4 is always an n-type semiconductor.^{23,57,61,75} Shannon et al⁵⁷ reported the Seebeck coefficient values for antimony doped Cd_2SnO_4 samples, $(Cd_2Sn_{1-x}Sb_xO_4)$ as $-170 \mu V/^\circ K$ and $-50 \mu V/^\circ K$. We have obtained a value of $-127 \mu V/^\circ K$ for Seebeck coefficient for our sample $Cd_{1.9}Pb_{0.1}SnO_4$ fired at 900°C.

The value of thermoemf and the nature of its dependence on the temperature indicate that the samples are in a degenerate state (metal-like thermoemf and conductivity) in the temperature 293-350°K.

The linear dependence of ' θ ' on T is in conformity with the equation of Wright^{114,115} derived by him for CdO,

$$\theta = \frac{16\pi^2 m^* k^2}{3h^2} \pi/3 \quad T^{2/3} \quad \frac{T}{N^{2/3}} \quad . \quad 3.9$$

Table 3.13 - Variation of Seebeck coefficient with the temperature for the samples fired at different temperatures

Temperature (°K)	Measured Seebeck coefficient ($\mu\text{V}/^\circ\text{K}$)			
	600°C	700°C	800°C	900°C*
293	-7	-17	-24	-77
303	-7	-18	-26	-95
313	-7	-20	-28	-106
323	-7	-20	-31	-112
333	-8	-23	-33	-127
343	-8	-25	-35	-
353	-	-26	-37	-

* Sample firing temperatures.

From the above equation, it is seen that low value of θ is indicative of high carrier concentration and/or low effective electron mass. Our diffuse reflectance results supports the view that the increase in conductivity is because of low effective electron mass.

Surprisingly the emf increases as the firing temperature is increased. This shows that for the same dopant level the carrier concentration decreases (or not increased) as the firing temperature is increased. It has also been observed that the conductivity increases with the increase in firing temperature. This leads us to the conclusion that the carrier mobility increases, for a given composition, at higher firing temperature. High temperature mobility measurements should confirm the above reasoning.

3.6 DIFFUSE REFLECTANCE SPECTRA RESULTS

The diffuse reflectance spectra for the doped Cd_2SnO_4 thick films fired at 500, 600, 700, 800 and 900°C are presented in the figure (3.43).

The optical edge has shifted towards the uv region from 534 to 513 nm, wavelength for the samples from A to E. The absorption edge is taken at the wavelength (λ_e) at which the slope of the diffuse reflectance curve is maximum.²³

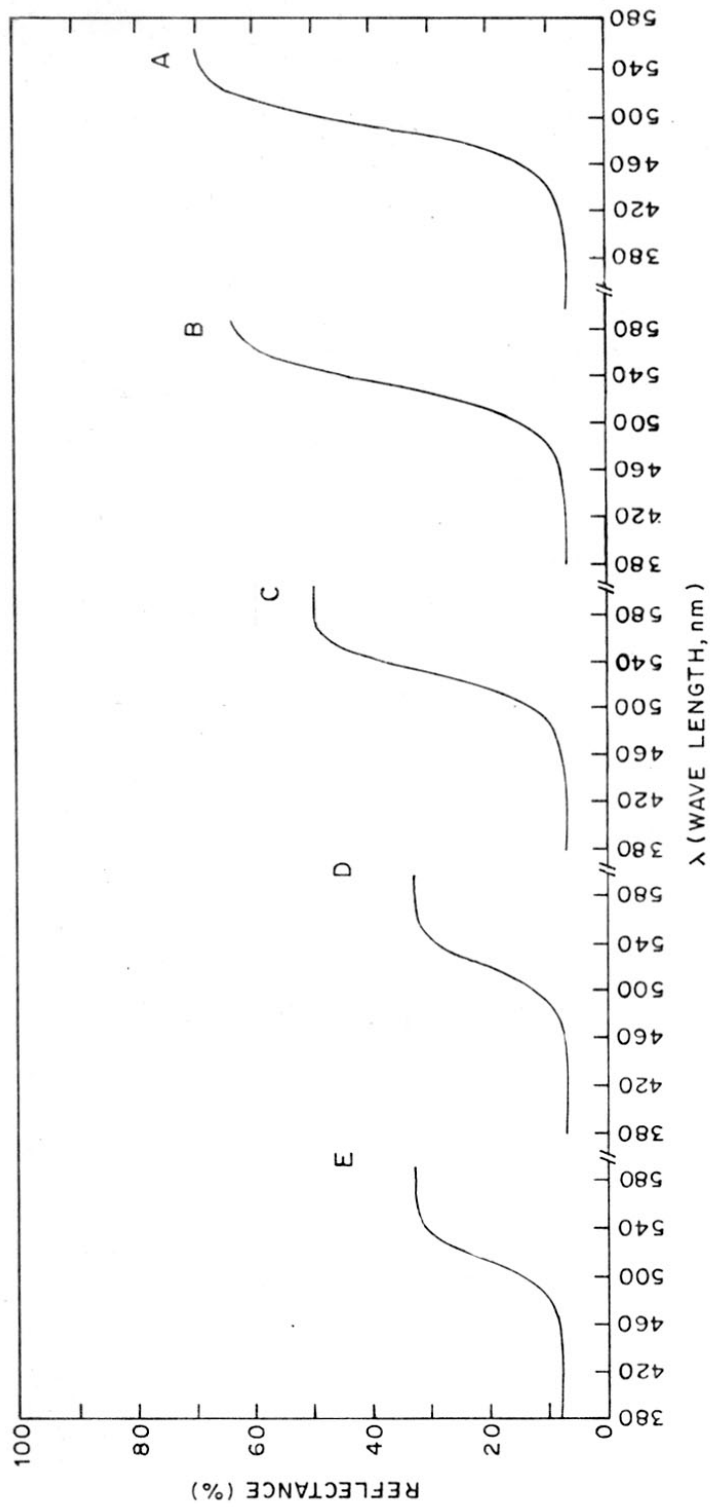


FIG. 3-43: DIFFUSE REFLECTION SPECTRA OF $(\text{Cd}_{1.9}\text{Pb}_{0.1}\text{SnO}_4)$ THICK FILMS FIRED AT VARIOUS TEMPERATURES. A (500 °C), B (600 °C), C (700 °C), D (800 °C) AND E (900 °C)

The approximate band gap is calculated from the formula

$$E = \frac{hc}{\lambda_e} \quad 3.10$$

where E = energy in ergs

h = plank's constant (6.62×10^{-27} erg sec)

c = velocity of light (2.998×10^{10} cm/sec)

λ_e = wavelength in Å units at the absorption edge.

Energy in eV is calculated from $1 \text{ eV} = 1.602 \times 10^{-12}$ erg.

The results are presents in the table (3.14).

It is seen from the above table that the reflectance decreases from 40 to 35, 39, 20 and 20% as we go from the sample A to E. Higher the sample firing temperature, lower is the reflectance. The band gap increases from 2.32 to 2.41 eV correspondingly. The colour of the sample changes with the band gap value, the one with highest energy gap is green.

The samples are degenerate semiconductors as revealed by conductivity measurements. The Pb addition has increased the conductivity. The fact that PbO is incorporated in Cd_2SnO_4 is supported by X-ray and ESCA results.

Table 3.14 - Effects of the preparative conditions
on the optical properties of Cd₂SnO₄ thick
films.

Sample	Firing temperature (°C)	Colour	D.R.* (%)	Approximate absorption edge (Å)	Apparent energy gap (eV)
A	500	Bright yellow	40	5340	2.32
B	600	Yellow	35	5298	2.33
C	700	Yellow ochre	29	5250	2.36
D	800	Green	20	5178	2.39
E	900	Green	20	5138	2.41

* Diffuse reflectance.

The shift of the optical absorption edge is the well-known Burstein shift.²⁸ The sample having increased conductivity will have higher optical gap and large absorption shift. This indicates that the effective electron mass is small in the doped Cd_2SnO_4 ($\text{Cd}_{1.9}\text{Pb}_{0.1}\text{SnO}_4$) and the conduction band has high curvature with low density of states at the bottom. These can be saturated easily by a small free-carrier concentration. This occupation by the carriers forces the fundamental optical absorption edge towards the higher energy.

From the figure (3.43), the effect of free-carrier absorption is evident. Highly conductive sample has large shift and has resulted in the decreased reflectance in the red.

Nozik²³ observed Burstein shift in Cd_2SnO_4 crystalline samples prepared under vacuum and also, for the first time, in amorphous Cd_2SnO_4 sputtered films. In the latter case, the reduced transmission was in the red and infrared regions. On the basis of some indirect evidence, Nozik²³ felt that it could be an indirect band gap material.

Burstein effect has been observed in thick films of doped Cd_2SnO_4 (present work) for the first time.

3.7 X-RAY PHOTOELECTRON SPECTROSCOPIC STUDIES

XPS spectra for the samples are presented in the figures (3.44) and (3.45). The thick films scanned are (i) Cd_2SnO_4 , (ii) $\text{Cd}_{1.9}\text{Pb}_{0.1}\text{SnO}_4$ unfired thick film, fired at (iii) 500° , (iv) 600° , (v) 700° (vi) 800° and (vii) 900°C .

Figure (3.44) shows the ($3d_{5/2}$) peaks of Cd and Sn, ($4f_{7/2}$) peaks of Pb and (1s) peaks of oxygen for the samples. Figure (3.45) presents the corresponding peaks for (i) cadmium metal (ii) CdO and (iii) SnO_2 .

The instrument was calibrated using Au($4f_{7/2}$) line (83.96 eV) binding energy value.

The spectra recorded by the instrument gave the direct B.E. values for the various core electrons of Cd, Sn, Pb and O atoms. These values were found to vary depending on the surface charging of the sample. This charging effect was corrected by carrying out a simultaneous kinetic energy measurement on carbon. This was taken as a reference substance. The C (1s) electron has binding energy value of 285.0 eV, a standard generally accepted in XPS studies.

Table (3.15) presents the directly measured and corrected BE values. The corrected values obtained by

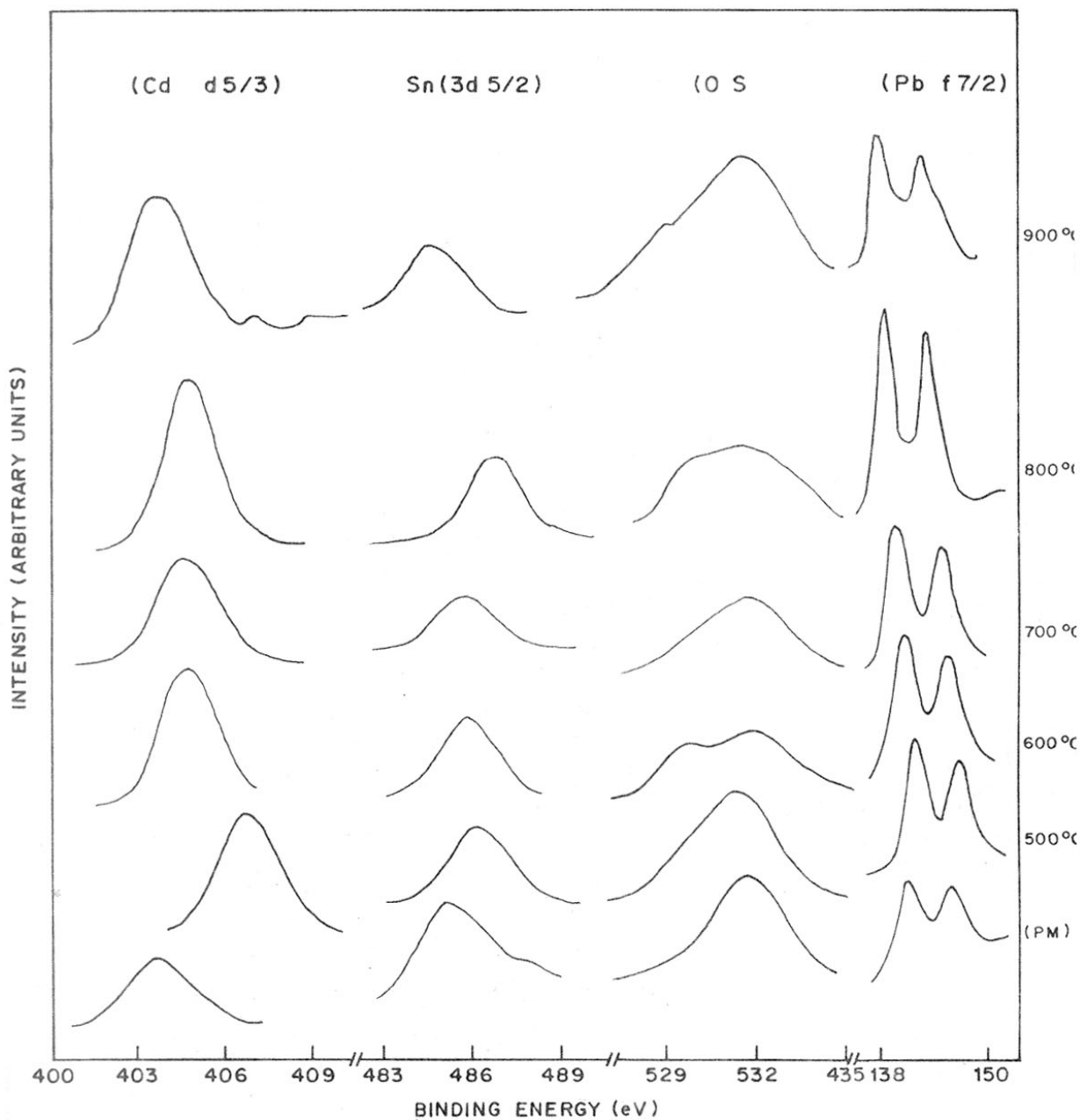


FIG. 3-44: XPS SPECTRA FOR $\text{Cd}_{1.9}\text{Pb}_{0.1}\text{SnO}_4$ THICK FILM FIRED AT VARIOUS TEMPERATURES

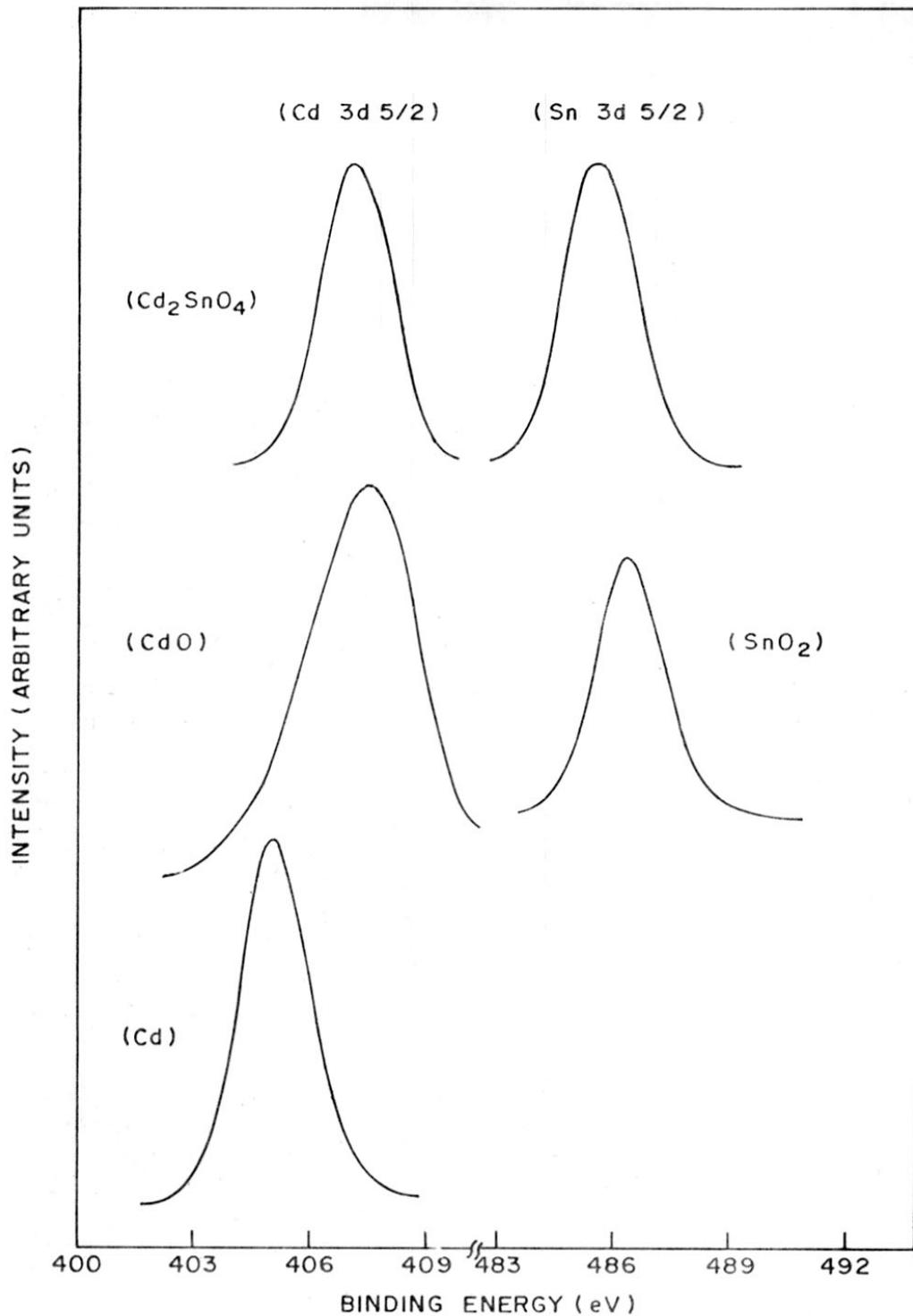


FIG. 3-45: XPE SPECTRA FOR (i) Cd, (ii) CdO, (iii) SnO₂ AND (iv) Cd₂SnO₄

Table 3.15 - Experimental B.E.'s of various compositions

Sample	Cd(3d _{5/2})		Sn(3d _{5/2})		Pb(4f _{7/2})		O(1s)		C(1s)	
	Direct eV	Corrected eV	Direct eV	Corrected eV	Direct eV	Corrected eV	Direct eV	Corrected eV	Direct eV	Corrected eV
F	405.16	403.68	486.66	485.18	140.4	138.92	533.28	531.80	286.48	285.0
A	408.64	404.88	489.96	486.20	145.5	141.86	535.20	531.44	288.76	285.0
B	404.8	404.76	486.0	485.96	140.5	140.46	529.8 531.6	529.76 531.56	285.04 287.2	285.0 287.16
C	408.4	404.70	489.48	485.78	143.2	139.5	534.24 535.08	530.54 531.38	285.4 288.7	285.0 285.0
D	405.28	404.76	487.36	486.84	139.0	138.48	530.52 532.08	530.0 531.56	285.52	285.0
E	405.28	403.68	486.36	484.76	139.8	138.2	530.88 533.28	529.28 531.68	286.6	285.0
Cd ₂ SnO ₄ (basic)	405.10	404.34	486.48	485.72	-	-	530.14 531.4	529.38 530.64	285.76	285.0
CdO	408.46	407.58	-	-	-	-	532.24 534.76	531.36 533.88	285.88 288.04	285.0 287.16
Cd	404.98	-	-	-	-	-	-	-	285.0	-
SnO ₂	-	-	487.02	486.44	-	-	531.1	530.52	285.58	285.0

subtracting from the directly measured values for the various constituents of the samples, i.e. Cd, Sn, Pb and O, the difference between the measured (direct) C ($1s$) B.E. and the assumed value of 285.0 eV. Additionally, silver paste¹⁰⁵ was also applied to the samples connecting them electrically to the ESCA metal sample holder.

It is reported¹¹⁶ that the presence of more electronegative substituents leads to a greater surface charging corrections. Oxides generally present charging problems.

The difference between the corrected B.E. of core electrons of a particular atom of a given compound and that of another composition is termed as the chemical shift of the atom of the former compound with respect to the latter.

Table (3.16) presents the chemical shift values for Cd ($3d_{5/2}$) core electrons in relation to Cd metal for our samples.

A chemical shift of 2.6 eV between cadmium metal and CdO is seen from the table (3.16). This value exactly matches with the reported value in literature.¹¹⁷

Table 3.16 - B.E. values of the Cd, Sn, O and Pb peaks
and chemical shift for Cd(3d_{5/2})

No.	Sample	Binding energy values (eV)				Shift based on Cd. (eV)
		Cd(3d _{5/2})	Sn(3d _{5/2})	O(1s)	Pb(4f _{7/2})	
1	Cd	404.98	-	-	-	0
2	CdO	407.58	-	531.36 533.88	-	2.60
3	SnO ₂	-	486.44	530.52	-	-
4	Cd ₂ SnO ₄	404.34	485.72	529.38 530.64	-	-0.64
5	F*	403.68	485.18	531.8	138.94	-1.30
6	A	404.88	486.20	531.44	141.86	-0.10
7	B	404.76	485.96	529.76 531.56	140.46	-0.22
8	C	404.70	486.78	530.54 531.38	139.50	-0.40
9	D	404.76	486.84	530.00 531.56	138.48	-0.22
10	E	403.68	484.76	529.28 531.68	138.20	-1.30

* Composition - Cd_{1.9}Pb_{0.1}SnO₄

In Cd_2SnO_4 samples, the B.E. of 407.58 eV for $\text{Cd}(3d_{5/2})$ electrons indicates that the cadmium is present as Cd^{++} , whereas the B.E. value less than 405.0 eV indicates that the cadmium to be Cd^0 . In all our samples, the $\text{Cd}(3d_{5/2})$ electrons have B.E. value < 405.0 eV.

In other words, the B.E. of $\text{Cd } 3d_{(5/3)}$ electrons is closer to that in metal than that in CdO . This shows the highly metallic character of the material and decrease in the ionic character of the bond.

This could arise from the presence of cadmium interstitials on the surface of the Cd_2SnO_4 thick films. For the samples fired at 900°C , the B.E. of $\text{Cd}(3d_{5/2})$ electrons is 403.68 eV. It is less by 1.3 eV compared to Cd peak in Cd metal. This may be due to the increased electron density around the Cd sites.

The B.E. values for $\text{Sn}(3d_{5/2})$ electrons does not show any systematic variation. The value for the samples show more or less the same B.E. values as in SnO_2 . Again for the sample E, the B.E. is lower indicative of increased electron density around the metal sites.

The Cd/Sn ratio is affected by the firing temperature of the thick films as is seen from the figure (3.44). The ratio of the peak heights for Cd and Sn increases with

the firing temperature. We take this as suggestive of preferential migration of Cd to the surface.

There are two oxygen peaks, particularly for those fired at 600°C and above. The main peak remains unchanged at ~ 531.5 eV but the shoulder which appears for the samples from B onwards show a systematic drift to lower energy values with increasing in the firing temperature. With the argon ion bombardment, the spectra showed the disappearance of the peaks due to adsorbed oxygen or a reduction in the peak heights. The shoulder may, therefore, be associated to oxygen loss and non-stoichiometry. In non-stoichiometry samples two types of oxygen surroundings is not unlikely.

There is decrease in the B.E. value for $Pb(4f_{7/2})$ electrons from sample A to E. The E_p values for Pb in PbO_2 and PbO are 137.4 eV and 140.0 eV respectively.¹¹⁶ The lowering of B.E. value is indicative of increased electron density around Pb sites.

Since the increase in electron density around Cd, Sn and Pb sites is shown by the results, one can visualise that the increased free electron density in the samples arises from the loss of oxygen leading to non-stoichiometric samples. In oxygen deficient compounds, one has excess of

electrons to maintain charge neutrality. They are bound to the oxygen vacant sites at low temperatures. But at room temperature, they would be free and get delocalised to create appreciable electron density around metal sites.

The XPS results suggest the presence of both cadmium interstitials and oxygen vacancies. They together contribute to the electrical conductivity of the films. The lead dopant perhaps has catalysed the processes. It is, of course, not very definite which of the two agencies is dominant in a sample fired at a particular temperature. Moreover, sintering also contributes in getting higher mobility values which contributes to the enhanced electrical conductivity ($\sigma = ne\mu$). This, therefore, again reminds us that high temperature mobility measurements are essential to further substantiate the results.

3.8 MOSSBAUER SPECTROSCOPIC RESULTS

Figure (3.46) presents the Mossbauer spectra for the samples of composition, $Cd_{1.9}Pb_{0.1}SnO_4$, fired at temperatures 500-900°C.

The Mossbauer spectra show a single line pattern upto 700°C and at high temperatures (800, 900°C), they show the presence of discernably small quadrupole splitting.

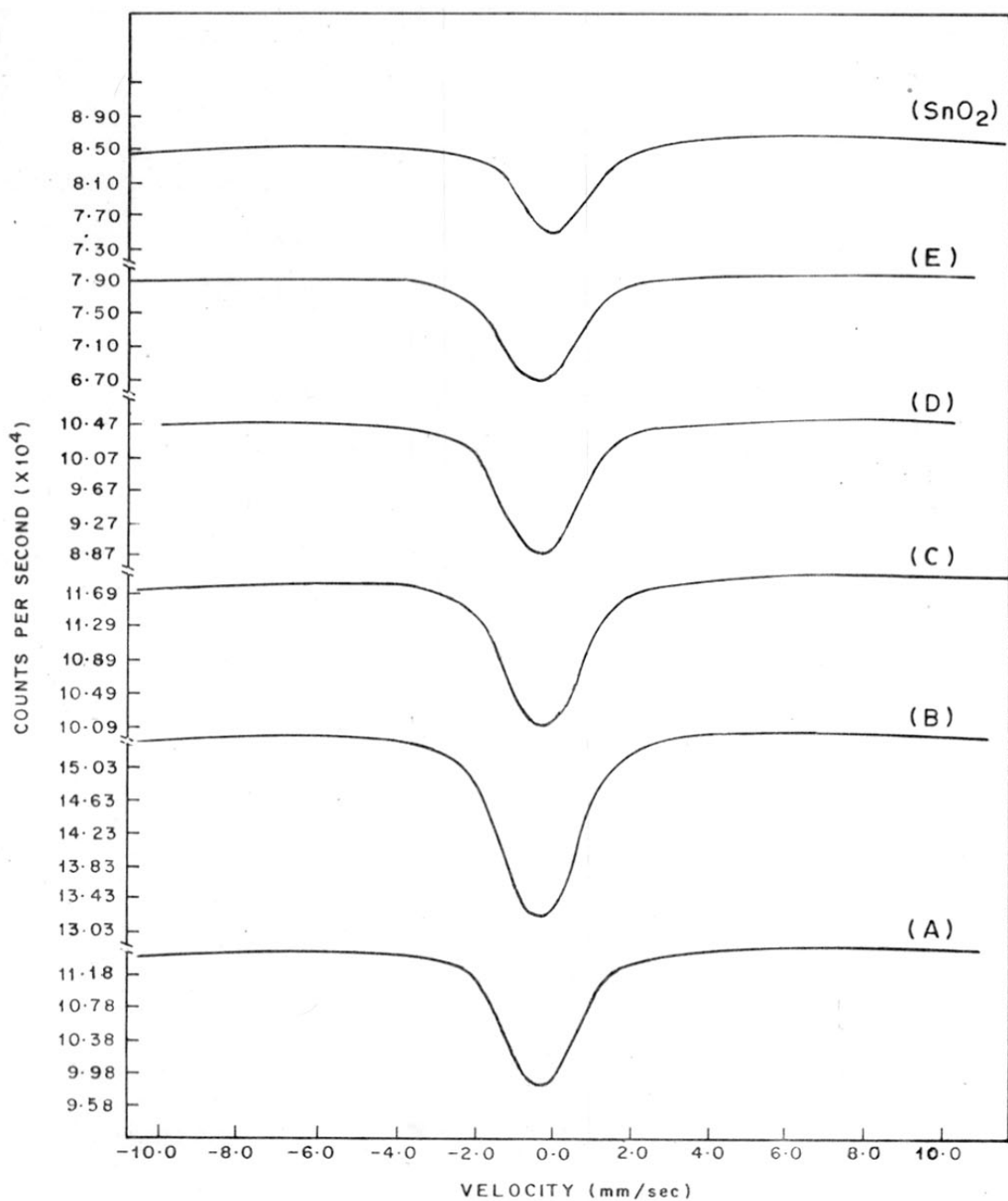


FIG. 3.46: CHARACTERISTIC MÖSSBAUER SPECTRA OBTAINED WITH $\text{Cd}_{1.9}\text{Pb}_{0.1}\text{SnO}_4$ SAMPLES FIRED AT DIFFERENT TEMPERATURES AND SnO_2

The results of isomer shifts and line widths are given in the table (3.17).

The interest in this study was to see whether tin undergoes a reduction during the induction of PbO in the Cd_2SnO_4 matrix. The Mössbauer spectra clearly show the absence of divalent tin in the samples fired at 500-900°C of the composition $\text{Cd}_{1.9}\text{Pb}_{0.1}\text{SnO}_4$.

Metal oxide bonds are predominantly of ionic in character. Covalent bond lengths change depending on the chemical environment of the atoms.

Comparing the isomer shifts with that for SnO_2 , samples A and B are more covalent and C, D and E have less covalent character. The shift is more positive in the case of A and B. This means that oxygen removes fewer electrons from the cations. In other words, the electron density around the cation site is increased. This is consistent with the results of other measurements which point towards the same conclusion i.e. of increased free electron density in the samples fired at 700°C and above.

Table 3.17 - Variation of the isomer shifts and the line widths with respect to the sample firing temperature

Sample	Firing temperature (°C)	Isomer shift	(FWHM) mm/sec.
A	500	0.26 ± 0.04	2.26
B	600	0.26 ± 0.04	2.26
C	700	0.09 ± 0.04	2.18
D	800	0.13 ± 0.04	2.31
E	900	0.09 ± 0.04	2.31
SnO ₂	-	0.00 ± 0.04	2.26

APPENDIX - I : I-V CHARACTERISTICS

APPENDIX - IA. I-V CHARACTERISTICSA.1 PREPARATION OF THE SAMPLES

95 parts of Cd_2SnO_4 and 5 parts of lead-borosilicate glass were mixed together under distilled acetone. The powder was pelleted using 10 mm diameter die set in the Carver Laboratory hydraulic press at an applied load of 10,000 lbs. The pellets were then fired in the thick film furnace under identical conditions as was done for thick films.

A-2 SAMPLE HOLDER

The sample holder is shown in the figure (A.1). It was fabricated in the laboratory. The pellet was placed between stationary and movable brass disc. The movable arm was fitted with a spring inside it. This gave a perfect pressed contact and held the pellet in position. Both the discs were electrically separated by teflon block. Shielded wires were soldered to the two arms for electrical measurements.

A-3 EXPERIMENTAL SET UP

D.C. regulated power supply (Aplab 0-60 V, 0-2.5 A, Model 7122) was used for applying voltage across the sample. The current was measured by the multimeter (Simpson 620) (Figure A-2).

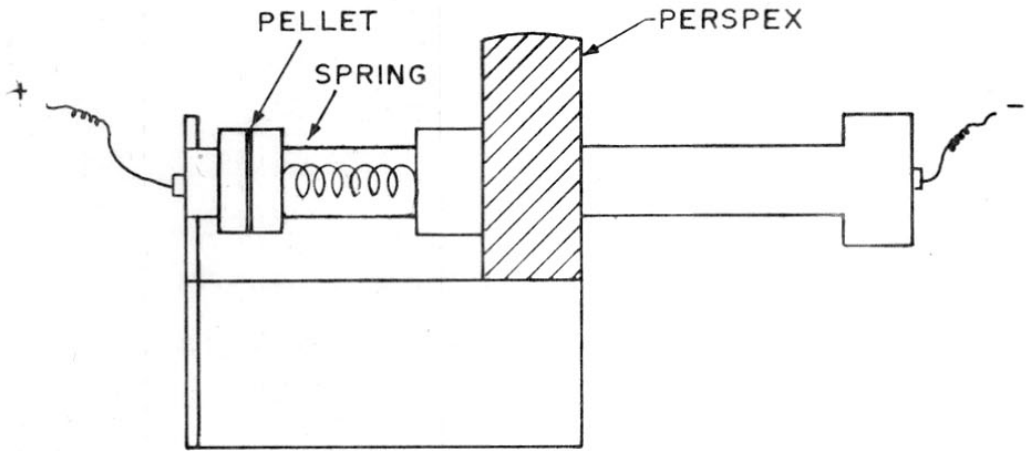
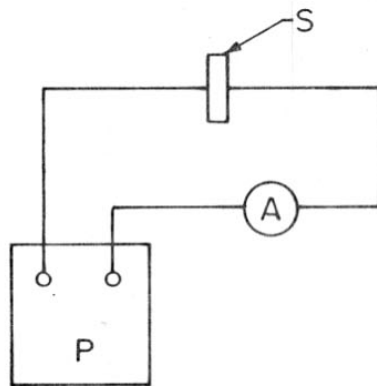


FIG. A-1: SAMPLE HOLDER FOR CURRENT-VOLTAGE MEASUREMENTS.



S- SAMPLE
P- POWER SUPPLY
A- CURRENT METER

FIG. A-2: SCHEMATIC DIAGRAM FOR I-V MEASUREMENTS

A-4 RESULTS AND DISCUSSION

A sudden drop in the resistance of the samples at around 180°C was observed during our conductivity measurements. It was thought that some filamentary action or conductive paths were created because of heating. It was, therefore, decided to see the effect of applied voltage across the sample and check whether conductivity increased due to Joule heating.

The colour of the sample pellets fired at $600-900^{\circ}\text{C}$ was same as it was with the thick films. A glassy appearance was observed on the alumina substrates after removing the pellets from the furnace. This could be due to the melting and flowing down of the glass content in the pellet. The glass mark was colourless. The pellets were found to be hard, probably due to sintering.

Air drying silver paste¹⁰⁵ was brushed at the faces of the pellet for electrodes.

The pellet samples were kept between the arms of the sample holder. Voltage was applied at 2 V increments. The current value was noted at every voltage increment. The I-V characteristics are shown in the figures (A-1 to A-4).

The current increased slowly with the applied voltage in the initial stages and soon it had non-linear

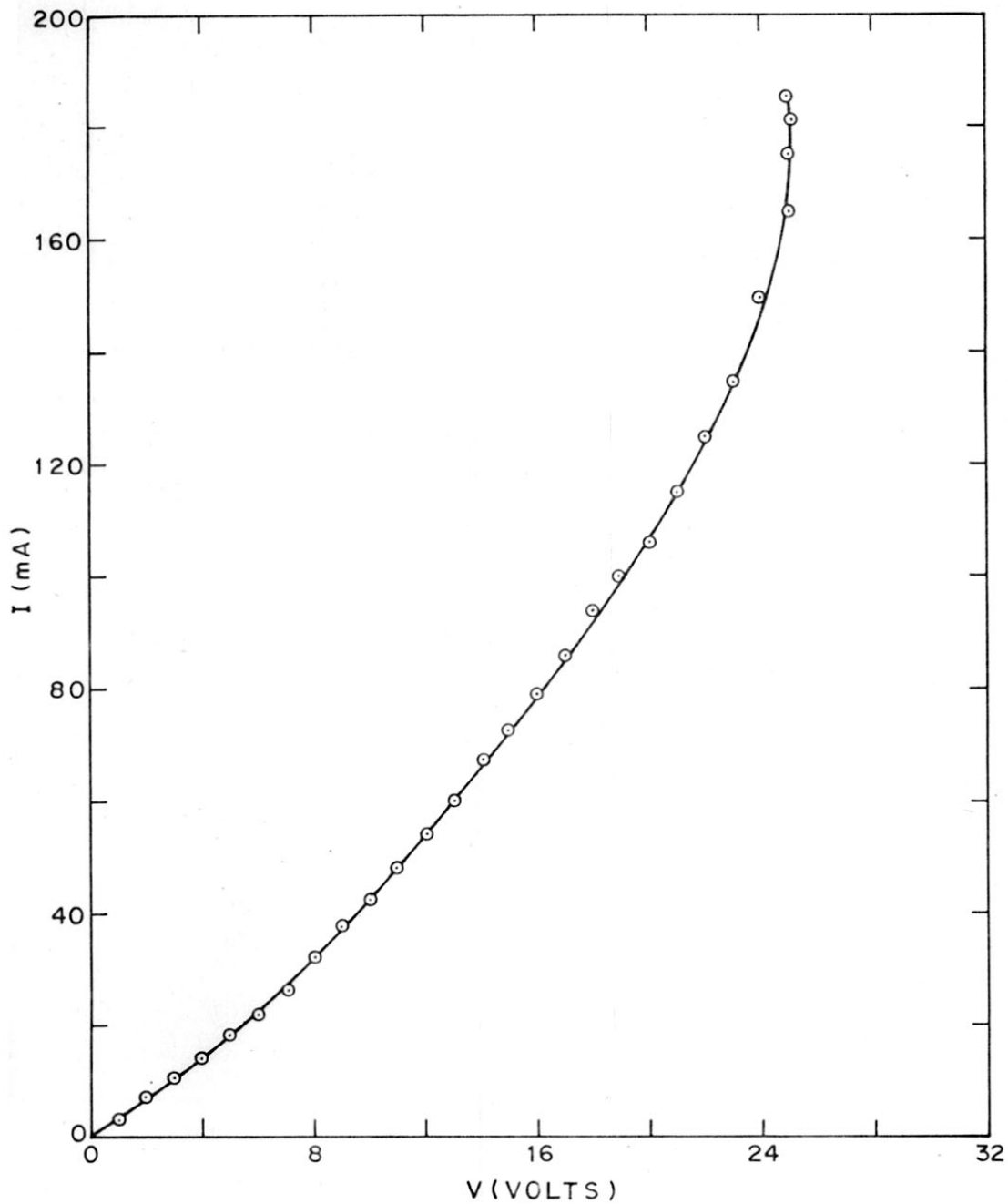


FIG. A.1: I-V. CHARACTERISTIC OF $(\text{Cd}_{1.90} \text{Pb}_{0.10} \text{SnO}_4)$
PELLET FIRED AT 600 °C

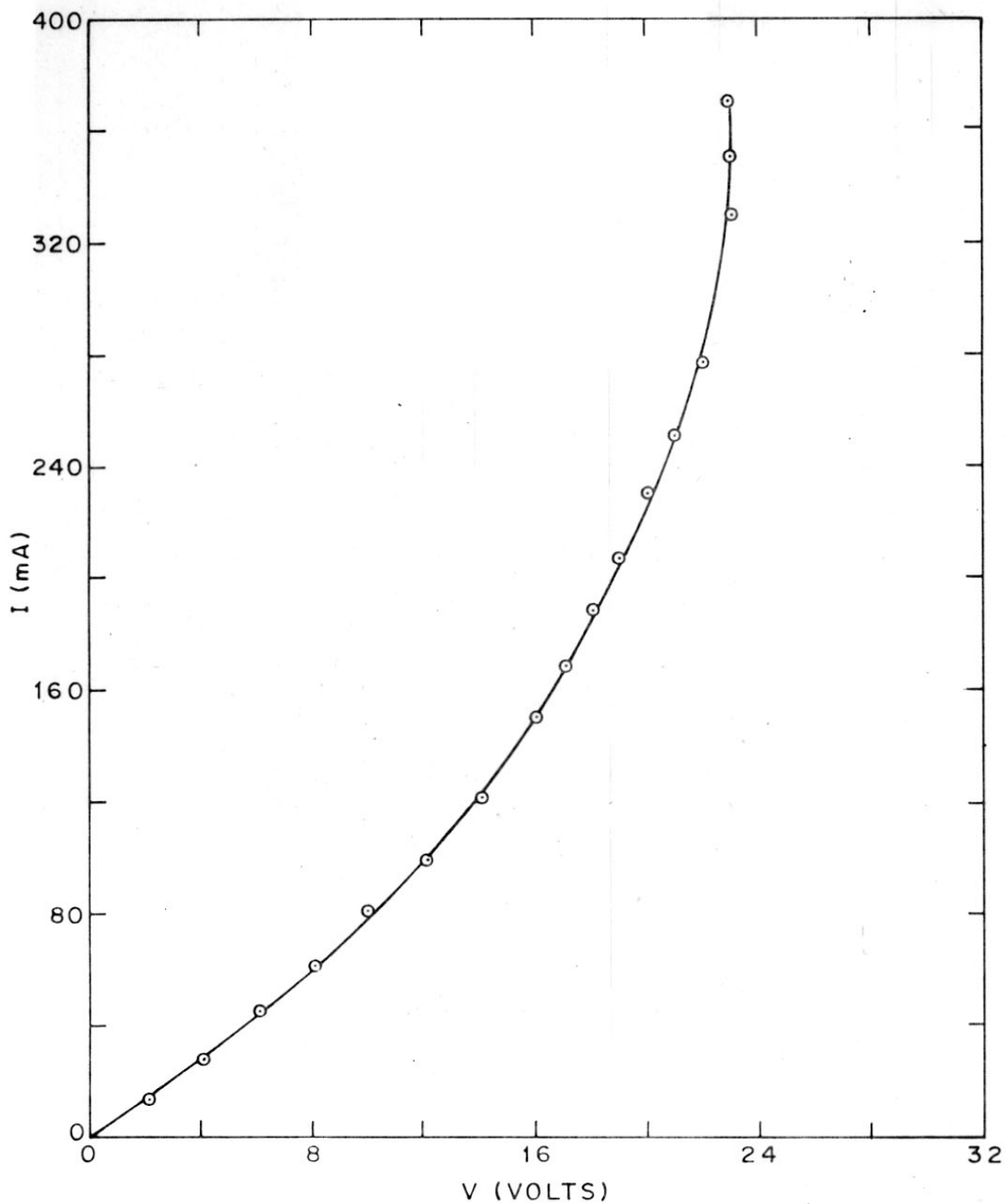
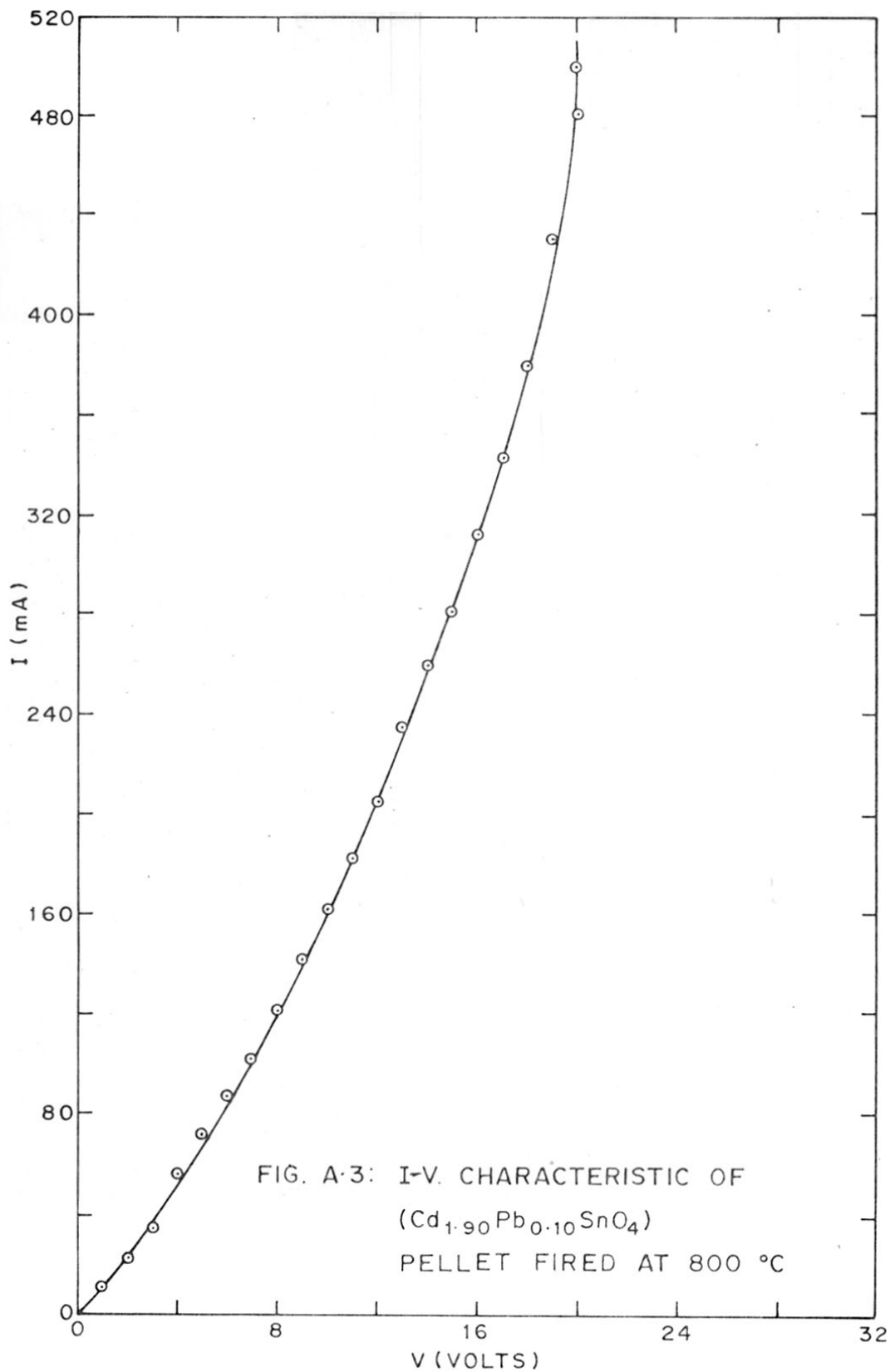


FIG. A-2: I-V. CHARACTERISTIC OF $(\text{Cd}_{1.90} \text{Pb}_{0.10} \text{SnO}_4)$
PELLET FIRED AT 700 °C



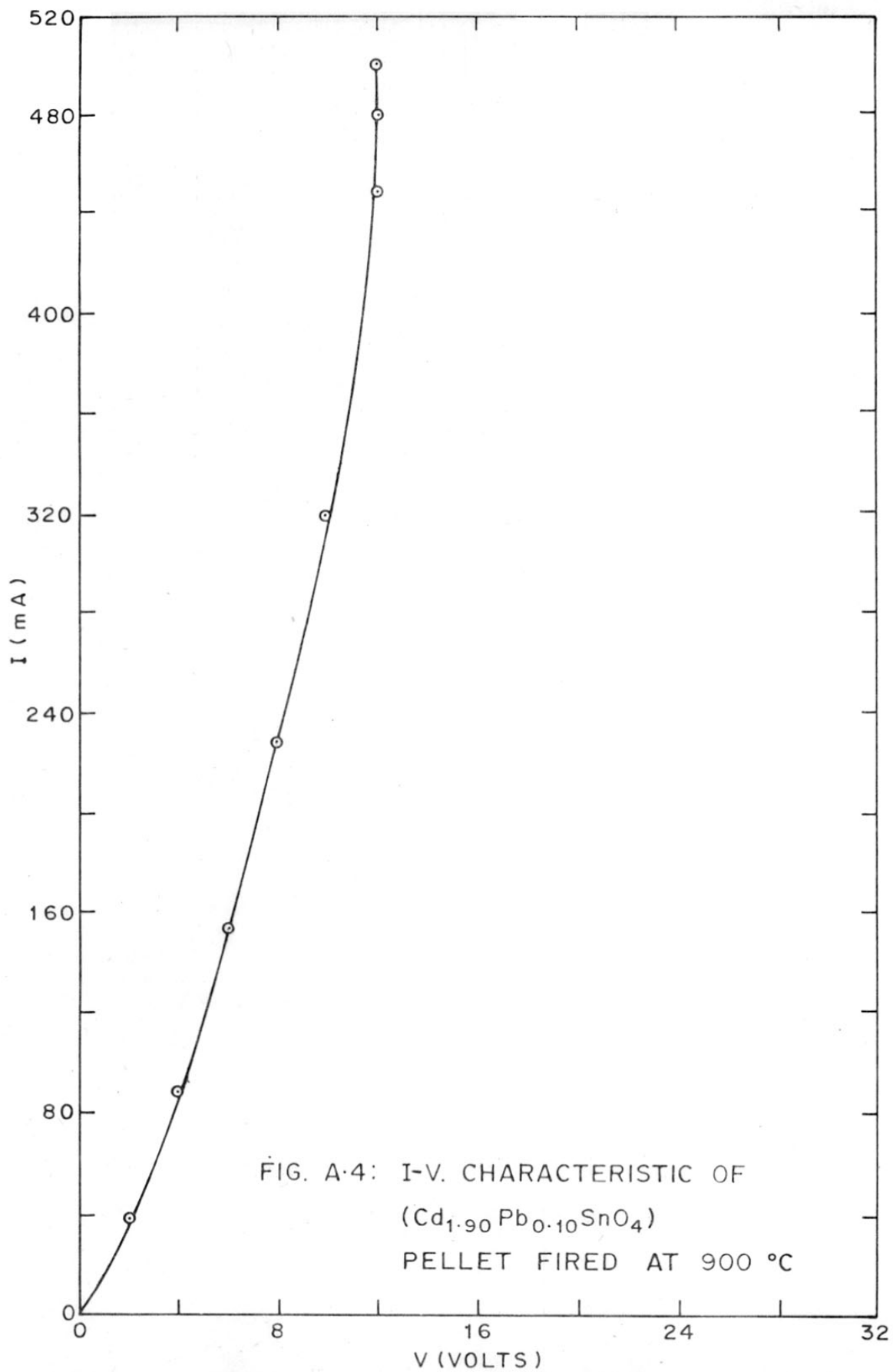


FIG. A-4: I-V. CHARACTERISTIC OF
($\text{Cd}_{1.90}\text{Pb}_{0.10}\text{SnO}_4$)
PELLET FIRED AT 900 °C

relation with the voltage. The pellets became hot and thermal switching took place.

The threshold voltage (V_{Th}) and holding current values are presented in the table A-1.

The threshold voltage (V_{Th}) and the voltage gradient values decrease with the increase of the sample firing temperature. Several cycles of I-V measurements were carried out for each sample. Thermal switching took place at a slightly lower threshold voltage than the previous value at every successive cycle in all the samples. In the case of the last sample (900°C), switching took place more or less at the same voltage, but the holding current value had increased in each cycle.

For one of the samples, the spot at which arching occurred was polished with a fine emery paper. The surface had become hard and scratch resistant. The thermal switching occurred again at the same threshold voltage. The 'glow' also appeared at the same spot.

The studies further indicated that there was some time lag for the sample to return to the original state after removing the applied voltage. It took 5-6 hours in the case of the sample fired at 900°C . The other samples could not be brought back to the original state even after keeping them for longer time.

Table A-1 - Variation of I-V characteristics with the sample preparation conditions

Sample firing temp. (°C)	Threshold voltage (V_{Th})	Pellet Dimensions (mm)		Voltage gradient V/cm	Holding current (mA)
		Diameter	Thickness		
600	25	8.60	2.5	10.0	150
700	23	8.60	2.5	9.2	330
800	20	8.60	3.0	6.7	480
900	12	8.60	2.0	6.0	440

The heat is generated due to Joule heating. The heat dissipated by the sample depends on several factors. During the Joule heating, the adsorbed oxygen gets ionised leaving behind the charge carriers. The diffused oxygen also migrates to the surface and gets desorbed. This phenomenon contributes to the conductivity which is clearly observed during our conductivity measurements. Perhaps the conductivity increase at a particular voltage (V_{Th}) is because sufficient quantity of thermal energy is supplied equal to the ionisation energy of oxygen. Thus, I-V characteristics studies provided supporting evidence to the conclusions arrived at with respect to conductivity measurements.

REFERENCES

1. J. Weber, U.S. Pat. 1,181,944 (1916)
(CA, 10:1701).
2. Eugene Wainer, U.S. Pat. 2,399,082 (1946)
(CA, 40:4190^B).
3. Eugene Wainer, U.S. Pat. 2,402,515 (1946)
(CA, 40:554¹¹).
4. Eugene Wainer, U.S. Pat. 2,402,518 (1946)
(CA, 40:554¹¹).
5. Eugene Wainer, U.S. Pat. 2,452,532 (1948)
(CA, 43:6803d).
6. Chandler Wentworth, U.S. Pat. 2,529,719 (1950)
(CA, 45:838a).
7. C. Schusterius, Z.tech.Phys. 16(12)
640-42 (1935).
8. F.A. Kröger, "Some Aspects of the Luminescence of Solids",
Elsevier Publishing Co. Inc., New York, (1948), p.310
(CA, 42:5778c).
9. F.A. Kröger and J.T. Gerard Overbeek,
U.S. Pat. 2,542,336 (1951), (CA, 45:5028c).
10. W.W. Coffeen, J.Am.Ceram.Soc. 36(7), 207-14 (1953).
11. W.W. Coffeen, J.Am.Ceram.Soc. 37(10), 480-89 (1954).
12. I. Naray-Szabó, Naturwiss, 31, 202 (1943).
13. H.D. Megaw, Proc.Phys.Soc.Lond, 58, 133-52 (1946).
14. A.J. Smith, Acta Crystallogr., 13,749-752 (1960).
15. Irene Morgensterne-Badarau, Paul Poix and
Andre Michel, Compt.Rend. 256,692-3 (1963).
16. Irene Morgenstern, Paul Poix and Andre Michel,
Compt.Rend. 258(11), 3036-37 (1964).

17. Therese Dupuis, Mikrochim Ichno anal. Acta., 4,737-50 (1965), (CA, 64:10728a).
18. Therese Dupuis and Vincenzo Lorenzelli compt. Rend. 259(25), 4585-8 (1964), (CA, 62:11305e).
19. Vincenzo Lorenzelli, Therese Dupuis and Jean Lecomte, Compt. Rend. 259(5), 1057-62 (1964), (CA, 62:1140f).
20. Therese Dupuis, Clement Duval and Jean Lecomte, Compt. Rend. 257(21), 3080-5 (1963).
21. Levy Clement, Claude; Morgenstern Badarau Irene; Billiet Yves and Michel Andre, C.R. Acad. Sci. Ser. C. 270(23), 1860-2 (1970), (CA, 73:70758j).
22. A.J. Nozik, U.S. Pat. 3,773,914 (1973), (CA, 80:72143y).
23. A.J. Nozik, Phys. Rev. 'B', 6(2), 453-59 (1972).
24. A.J. Nozik, U.S. Pat. 3,811,953 (1974), (CA, 81:18372e).
25. G. Haacke, U.S. NTIS, AD-A. Rep. (1975), No. 008783, (CA, 83:140388w).
26. H. Haacke, NASA Contract Rep. (1975), NASA-CR-143107, f, 1st, 1775, 661-76 (CA, 85:180082q).
27. M. Tanenbaum and H.B. Briggs, Phys. Rev. 91, 1561 (1953).
28. E. Burstein, Phys. Rev. 93, 632-33 (1954).
29. J. Stuke, Z. Phys. 137, 401-15 (1954).
30. S.M. Dodds, Materials Methods, August, 108 (1956).
31. T.S. Moss, Proc. Phys. Soc. Lond. 'B', 67, 775-82, (1954).
32. M. Skribljak, S. Dasgupta and A.B. Biswas, Acta. Cryst. 12, 1049-50 (1959).
33. M. Hassanein, J. Chem. U.A.R. 9(3), 275-280 (1966).

34. M. Tromel, *Naturwissenschaften*, 54(1), 17-18 (1967), (CA, 67:15815b).
35. J. Choisnet, A. Deschanvres and B. Raveau, *Compt.Rend.* 266c, 543 (1968).
36. M. Tromel, *Z.Anorg.Allgem.Chem.*, 371, 237-47 (1969).
37. A.H. Meitzler, J.R. Maldonado and D.B. Fraser, *Bell System Tech.J.* July/August p.953 (1970).
38. S.A. Keneman, G.W. Taylor, A. Miller and W.H. Fonger, *Appl.Phys.Lett.* 17(4), 173 (1970).
39. A.J. Nozik, U.S. Pat. 3,815,036 (1974), (CA, 81:43989u).
40. R.D. Giglia, S. African Pat. 74;06,284 (1975), (CA, 84:188573a).
41. L.C. Burton, G. Haacke, *Rec.Intersoc.Energy Convers.Eng.Conf.* 10th, 1975, 396-9, IEEE, (CA, 84:124366c).
42. G. Haacke, *Appl.Phys.Lett.* 28(10), 622-23 (1976).
43. G. Haacke, *J.Appl.Phys.*, 47 (9), 4086-89 (1976).
44. D.B. Frazer and H.D. Cook, *J.Electrochem.Soc.*, 119, 1368 (1972).
45. L.C. Burton, T. Hench and G. Storti, *J. Electrochem.Soc.*, 123(11), 1741-44 (1976).
46. J.A. Thornton and V.L. Hedgecoth, *J.Vac.Sci.Technol.* 13(1), 117 (1976).
47. A.J. Nozik, U.S. Pat. 3,957,029 (1976), (CA, 85:39229m).
48. A.J. Nozik and G. Haacke, *Brit.Pat.* 1,451,080 (1976), (CA, 86: 98915).
49. A.J. Nozik and G. Haacke, U.S. Pat.3,987,780 (1976). (CA, 86:93099c).

50. A.J. Nozik and G. Haacke, 3, 987,781 (1976), (CA, 86:93100w).
51. G. Haacke, U.S. Pat. 3,998,752 (1976), (CA, 86:63392a).
52. G. Haacke, Ann.Rev.Mater.Sci., 7,73-93 (1977).
53. G. Haacke, H. Ando, and W.E. Mealmaker, J.Electrochem.Soc. 124 (12), 1923-26 (1977).
54. P. Lloyd, Thin Solid Films, 41, 113-120 (1977).
55. P. Lloyd, R.S.R.E. Newsl.Res.Rev. 1, 9/1 - 9/4 (1977), (CA, 92:50669v).
56. G. Haacke, Appl.Phys.Lett. 30(8), 380-81 (1977).
57. R.D. Shannon, J.L. Gilson and R.J. Bouchard, J.Phys.Chem.Solids, 38, 877-81 (1977).
58. Dale Hall, J. Electrochem.Soc., 124(5), 804-807 (1977).
59. G. Haacke, L.C. Burton, U.S. NTIS, PB Rep. 1976, PB -261850 (CA, 87:26019j).
60. A. Hici and G. Haacke, U.S. Pat. 4,048,372 (1977), (CA, 87:176416a).
61. G. Haacke, W.E. Mealmaker and L.A. Siegel, Thin Solid Films, 55, 67-81 (1978).
62. W.G. Haines and R.H. Bube, J.Appl.Phys. 49, 304, (1978).
63. N. Miyata and K. Miyake, Jpn.J.Appl.Phys., 17(9), 1673-74 (1978).
64. N. Miyata, S. Nao, K. Miyake, Yamaguchi Diagaku, Kagakabu Kenkyu Hokoku, 29(1), 91-6, (1978), (CA, 90:144667d).
65. L.A. Siegel, J.Appl.Cryst., 11, 284-286 (1978).

66. N. Miyata, K. Miyake and H. Nakaoka, Yamaguchi Diagaku Kogakuka Kenkyu Kokoku, 28(2), 235-40 (1978), (CA, 89:121431n).
67. Z.V. Goriyacheva, N. Yu, A.V. Gribenyuk and O.N. Baskakova, U.S.S.R. Pat. 629,647 (1978), (CA, 90:15369j).
68. P. Lloyd, Brit.Pat. 1,519,733 (1978), (CA, 90:16154b).
69. O.P. Agnihotri, B.K. Gupta and A.K. Sharma, J.Appl.Phys. 49(8), 4540-42 (1978).
70. A. Raza, O.P. Agnihotri and B.K. Gupta, J.Phys.D., 10, 1871 (1977).
71. B.K. Gupta and O.P. Agnihotri, Solid State Commun. 23, 295 (1977).
72. N. Miyata, K. Miyake, T. Fukushima and K. Koga, Appl.Phys.Lett. 35(7), 542-543 (1979).
73. K. Miyake, N. Miyate, Ger.Offen.2,839,057 (1979), (CA, 90:196525).
74. H. Dislich, P. Hinz, Belg.Pat.872,697,(1979), (CA, 91:94434y).
75. N. Miyata, K. Miyake and S. Nao, Thin Solid Films, 58, 385-89 (1979).
76. N. Miyata and K. Miyake, Surf.Sci. 86, 384 (1979).
77. K.J.O. Mackenzie, W.A. Gerrard and F. Golestani Farad, J.Mater.Sci., 14(10), 2509-12 (1979).
78. F.P. Koffyberg and F.A. Benko, Appl.Phys.Lett. 37(3), 320-2 (1980).
79. N. Miyata, K. Miyake and Y. Yamaguchi, Appl.Phys.Lett. 37(2), 180-182 (1980).
80. N. Miyata, K. Miyake, K. Koga and T. Fukushima, J.Electrochem.Soc. 127,918 (1980).

81. Y. Yamaguchi, N. Miyata, K. Miyake,
Yamaguchi Diagaku Kenkyu Kohoku, 31(1), 105 (1980),
(CA, 94:75267s).
82. Tokyo Shibaura Electric Co.Ltd., Jpn.Kokai
Tokkyo Koko, 8135, 123 (1981), (CA, 95:106443y).
83. R.P. Hawson and M.I. Ridge, Thin Solid Films,
77, 119-25 (1981).
84. R.P. Howson, M.I. Ridge, C.A. Bishop,
Thin Solid Films, 80(1-2-3), 137-42 (1981).
85. S. Miyake, Jpn.Kokai Tokkyo Koho,
81, 134, 730 (1981), (CA, 96:61269y).
86. M. Nakao, N. Miyata, K. Miyake,
Yamaguchi Diagaku Kogakubu Kenkyu Hokoku
30(2), 325-30 (1980), (CA, 94:166111c).
87. G. Blasse Philips, Res.Rep.Suppl.
3, 1-139 (1964).
88. E. Mollwo and R. Stumpp, Z.Physik,
184, 286-92 (1965), (CA, 63:10851h).
89. H. Finkenrath, Z.Phys. 159,112-124 (1960),
(CA, 54:17073e).
90. F. Möllers and R. Memming,
Ber.Bursengas, Phys.Chem., 76,469 (1972).
91. M.S. Setty, Electronics - Information, Planning,
8(6), 436-38 (1981).
92. M.S. Setty, M.Sc. Thesis, "Electrical properties
of thick films of a vanadium phosphate glass", 1977.
93. D.P. Amalnerkar, M.S. Setty, N.R. Pavaskar
and A.P.B. Sinha, Bull.Mater.Sci., Vol.2(4),
251-264 (1980).
94. J.K. Higgins, J.E. Lewis, M. Lowe and F.V. Roue,
J. Non-crystalline Solids, 18(1), 77-93 (1975).
95. R.G. Loasby, Phys.Bulletin, 22, 75 (1971).

96. Technical Bulletin, Electro-Science Laboratories, Inc., 2211, Sherman Avenue, Pennsauken, N.J., U.S.A.
97. Thick Film Products Bulletin, Engelhard Sales Limited, Valley Road, Ginderford, Glos. GL142 PB, USA.
98. T.T. Hitch, Proc. IEEE-EIA Electronic Components Conf. May, 16-18, 1977.
99. Thick film product literature and Thick Film Microcircuitry Handbook (1 & 2), E.I. DuPont, De Nemours, USA).
100. F.T.J. Smith and S.L. Lyu, J.Electrochem.Soc., 128 (5), 1083-1088 (1981).
101. F.T.J. Smith and S.L. Lyu, J.Electrochem.Soc., 128(11), 2388-2394 (1981).
102. Z.M. Jarzebski, Phys.Stat.Sol.(a) 71 (13), 13-41 (1982).
103. M.S. Setty, Prepared by high temperature chlorination of ferrosilicon at National Chemical Laboratory, Poona-8 (India).
104. M.S. Setty and A.P.B. Sinha, Ind.J.Chem., 20A, 322-325 (1981).
105. M.S. Setty, Air drying silver paste developed at the National Chemical Laboratory, Poona-8 (India).
106. Mitsuo Wada and Yoshio Iida, Jpn.J.Appl.Phys. 8,1569 (1969).
107. Swanson and Fuyat, NBS Circular, 539, Vol.II, 27, 1953 (ASTM Card: 5-0640).
108. M. Vieltange, J.Therm.Anal. 3(3), 265 (1971).
109. R. Haul and D. Just, J.Appl.Phys.Suppl. 33(1), 487 (1962).

110. Handbook of Chemistry and Physics, 61st edition, Edtd. by Robert C. Weast, CRC Press, Inc., 1980-81.
111. Jae Shi Choi, Young Hwankang and Keu Hong Kim, J.Phys.Chem. 81(23), (2208-2211), (1977).
112. E.F. Lamb and F.C. Tompkins, Trans.Faraday Soc., 68, 1424 (1962).
113. F.P. Koffyberg, Can.J.Phys., 49, 435 (1971).
114. Wright, Proc.Phys.Soc.A, 64, 350, 949 (1951).
115. Wright Proc.Phys.Soc.B, 66, 273 (1953).
116. W.E. Morgan and J.R. Van Wazer, J.Phys.Chem., 77, 964-969 (1973).
117. Thomas A. Carlson, "X-ray photoelectron spectroscopy, Plenum Press, New York, pp.365 (1978).
118. A. Kosloff, "Screen Printing Electronic Circuits", The Science of the Times Publishing Co., U.S.A., (1968).
119. C.A. Harper, Editor, "Handbook of Thick Film Hybrid Microelectronics" (1974).
120. D.W. Hamer and J.V. Biggers, "Thick Film Hybrid Microcircuit Technology", Wiley-Interscience, New York (1972).
121. M.L. Topfer, "Thick Film Microelectronics", Van Nostrand Reinhold Company, New York, (1971).
122. R.A. Rikoski, "Hybrid Microelectronics Circuits - The Thick Film", Wiley Interscience, New York (1973).
123. C.A. Harper, Editor, "Handbook of Materials and Processes for Electronics", McGraw-Hill Book Company, New York (1970).
124. H. Finkenrath and von Ortenberg, Z.Angew.Phys., 23, 323-8 (1967).

125. W. Clarke, "An Introduction to Textile Printing", 4th edition, Newnes-Butterworths, London, pp.39 (1980).
126. Pincherlee, Proc.Phys.Soc., 64, 650, 664 (1951).
127. F.P. Koffberg, Solid State Commun., 9, 2187 (1971).

SUMMARY

The aim of the present work has been to prepare highly conductive Cd_2SnO_4 thick films by chemical doping and offer a plausible explanation for the conduction mechanism.

Thick film technology is a recent development. It is a new approach of fabricating components and devices in the field of hybrid microelectronics.

Earlier, Cd_2SnO_4 has been studied mainly as thin films obtained by sputtering, CVD, vacuum evaporation, etc. In the thin films, the high conductivity is attributed to oxygen vacancies and/or cadmium interstitials.

We have successfully adapted thick film technique for the preparation of the samples. It is amenable to material characterisation. The lead oxide dopant induction is carried out subsequent to film deposition. This is done in a novel way. Doping is effected by including the PbO with the other glass forming oxides which make the glass frit. Simultaneously, the glass provided a vitreous bond between the film and the substrate.

Cd_2SnO_4 is synthesised by solid state reaction of CdO and SnO_2 taken in the 2:1 mole ratio at $1050^\circ\text{C}/6$ hrs.

It is formulated into screen printable pastes using lead borosilicate glass frit and organic binder. The thick films are fired at 500, 600, 700, 800 and 900°C in an indigenously fabricated thick film furnace as per the required time-temperature schedule.

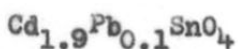
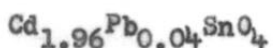
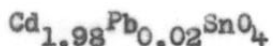
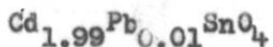
Thermogravimetric analysis of $2\text{CdO} + \text{SnO}_2$ physical mixture revealed the weight losses at 221, 300 and 368°C. These are attributed to moisture, cadmium hydroxide decomposition and cadmium oxide dissociation. The DTA curve showed two endothermic peaks corresponding to 221 and 300°C. A net loss of 2.4% is observed which is attributed to oxygen. In the case of Cd_2SnO_4 and Cd_2SnO_4 + glass samples, a gain is observed which is considered as adsorbed oxygen. This indicates that the Cd_2SnO_4 formed is deficient in oxygen and annealing of the sample at 400-1000°C is required to regain the small amount of oxygen loss. These studies have in a way produced factual evidence to the presence of oxygen vacancies which in turn are responsible for making the films highly conductive. Also, the samples heated in oxygen atmosphere showed increase in their resistance values.

X-ray studies showed that Cd_2SnO_4 has orthorhombic crystal structure with $a = 5.5458 \text{ \AA}$, $b = 9.8686 \text{ \AA}$ and

$c = 3.1890 \text{ \AA}$. They have also revealed the successful inclusion of the dopant, PbO. The crystal structure has not changed but a variation of lattice parameter values and unit cell volume is observed. The X-ray diffractograms of the films fired at $500\text{-}600^\circ\text{C}$ showed the presence of CdO lines. The a/c and b/c ratios and the unit cell volume increase with the firing temperature. This is attributed to the slow inclusion of PbO and Cd interstitials (because of CdO dissociation) in the Cd_2SnO_4 lattice. For the samples fired at $700\text{-}800^\circ\text{C}$, the ratios decrease but the unit cell volume continues to increase. The system appears to have stabilised at 900°C with the marginal increase of unit cell volume suggesting the completion of the induction of PbO.

The SEM photomicrographs of the samples show that the sintering is taking place in the samples with the increase in firing temperature ($500\text{-}900^\circ\text{C}$). The coalescing of the particles lends support to the theme that the increase in conductivity of the samples fired at 900°C is due to the higher carrier mobility which is attributed to sintering.

Conductivity measurements are carried out for the following compositions.



The log R-1000/T curves generally show two slopes corresponding to low (< 0.01 eV) and high (0.06-0.76 eV) activation energy values depending on the dopant concentration and firing temperature. The resistance increases initially with temperature for all the samples fired at 700-900°C. It falls very rapidly, including for the sample films fired at 600°C, at 84-144°C. The increase in conductivity is due to oxygen vacancies created which provide electrons for conduction. Annealing of the samples at 180°C/4 hours results in the decrease of resistance by 1-2 orders of magnitude. This is a common feature with all oxygen deficient semiconductors. The colour of all the sample films fired at 900°C is green for all dopant concentrations and are highly conducting.

Conductivity data revealed that the samples are degenerate semiconductors. Several cycles of heating-cooling

have been carried out. The room temperature resistance is reduced after every cycle. It has taken more than 5 such cycles to have almost identical curves. The XPS spectra showed the presence of two species of oxygen. Argon ion bombardment revealed the disappearance of the peaks due to adsorbed oxygen or reduction in the peak heights. This further strengthens the scheme of explaining the increase in conductivity is due to oxygen vacancies.

Thermoemf measurements indicated that all the samples are n-type semiconductors. The value of Seebeck coefficient and its dependence on temperature indicate that the samples are in a degenerate state (metal-like). A linear dependence of ' θ ' with temperature is observed. The increase in θ (-8 to $-127 \mu\text{V}/^\circ\text{K}$, 600-900°C firing temperature) is attributed to the decrease in carrier concentration. But the increase in conductivity with firing temperature leads to the conclusion that higher firing temperature results in the increase in carrier mobility. SEM results show the sintering taking place, leading to increase in contact area, in the samples, as the firing temperature is increased. This has reflected in the decrease in resistance.

The diffuse reflectance measurements are carried out for the first time in thick films of Cd_2SnO_4 , both undoped and doped. The results are similar to those of

Nozik for polycrystalline Cd_2SnO_4 bulk samples prepared under different conditions.

Burstein shift is observed in the spectra as we go from highly resistive sample ($10^6 \Omega/\text{Sq}$, yellow, fired at 500°C) to highly conductive ($80 \Omega/\text{Sq}$, green, fired at 900°C). The shift is towards UV region. The reflectance decreases from 40 to 20%. The lower reflectance value is due to the scattering effect of the free electrons. The band gap increases from 2.32 to 2.41 eV. The sample having optical energy gap and larger absorption shift has higher electrical conductivity. This indicates that the effective electron mass is small. The conduction band has high curvature with low density of states. Small carrier concentration is sufficient to saturate the energy levels in the conduction band. The low effective mass indicates high carrier mobility. Thermoemf measurements and SEM results also support the reasoning of high carrier mobility.

X-ray photoelectron spectroscopic studies revealed the presence of cadmium at the surface of the samples. The binding energy values of $\text{Cd}(3d_{5/2})$ core electrons in the samples matched with that for cadmium metal i.e. < 405.0 eV as against the value of 407.58 eV for $\text{Cd}(3d_{5/2})$ in CdO . The B.E. value corresponding to Cd

peaks varies with the preparation conditions. This shows the metallic character of the material and decrease in the ionic character of the bond. The Cd/Sn ratio seems to be dependent on the firing temperature.

(O_{1s}) peaks indicate two oxygen species. These are attributed to bound and adsorbed types. The main peak (B.E. ≈ 531.5 eV) remains unchanged. It is interesting to note that the samples (i) Cd_2SnO_4 + dopant mixture and (ii) $Cd_{1.9}Pb_{0.1}SnO_4$ fired at $500^\circ C$ do not give two peaks but only one for oxygen. The induction of Pb at higher temperatures disturbs the oxygen content. Pb itself undergoes changes in its B.E. values for $Pb(4f_{7/2})$ core electrons. It reduces from 141.86 to 138.2 eV for the sample films fired at 500 and $900^\circ C$ respectively. This indicates the increase in electron density around the lead sites.

The increase in electron density around the cation sites is visualised as coming from the loss of oxygen, i.e. the electrons bound to oxygen vacancies get delocalised to create appreciable electron density around the metal sites.

Mossbauer spectra showed the absence of divalent tin (Sn^{2+}). The samples fired at 500 and $600^\circ C$ are more covalent in character than those fired at higher temperatures.

This means that oxygen removes fewer electrons from cations. The electron density around cation is more. These results are consistent with the results of other measurements (e.g. XPS).

The results of I-V measurements (presented in Appendix I) provide supporting evidence to the conclusions drawn from the conductivity, thermal analysis and SEM w.r.t. adsorbed oxygen and sintering.

The above studies show that the thick film technique is highly suitable for the preparation of conducting coatings of Cd_2SnO_4 . Chemical doping method is successfully used to get highly conductive Cd_2SnO_4 thick films. The reason for high conductivity has been explained on the basis of oxygen vacancies, cadmium interstitials, dopant action and increase in carrier mobility because of low effective electron mass and sintering effect.

High temperature Hall mobility measurements of thick film samples of Cd_2SnO_4 would further help in understanding of the conduction mechanism.

APPLICATION OF THICK FILM TECHNIQUE FOR PRODUCING
TRANSPARENT CONDUCTORS - A POSSIBILITY

Since Cd_2SnO_4 is a good transparent conductor, thick film technique can very effectively be adapted for depositing films. Suitable organometal compounds of Cd and Sn can be formulated in the form of thixotropic pastes. These pastes are screen printed and fired at a controlled time-temperature cycle in the thick film furnace. This gives transparent films. Doping of the samples can easily be carried out to effect any desired variations in the electrical and optical properties of the deposited films. This technique is potentially economical compared to sputtering, vacuum evaporation or pyrolytic decomposition techniques.

APPENDIX - IILIST OF PUBLICATIONS OF M.S. SETTY

1. Electrical conductivity and thermoemf measurements of thick films of 70% V_2O_5 - 30% P_2O_5 semiconducting glass, Ind.J. Pure and Appl.Phys. 17, 283-286 (1979).
2. Radiosonde thermistors, Science Today (Ideas and Inventions), 55, December 1979.
3. Optoelectronic properties of cadmium sulphide thick films - Proceedings of the symposium on "Electronic Devices - Development and Future Trends", Institution of Electronics and Telecommunication Engineers, Pune Centre, (India), September, 1980.
4. Studies on thick films of photoconducting cadmium sulphide, Bull.Mater.Sci., 2 (4), 251-264 (1980).
5. Thick film materials, Technical paper, Electronics - Information and Planning, Electronics Commission, (India) 436-438, March 1981.
6. Thermogravimetric analysis of thick film materials of vanadium phosphate semiconducting glass, Ind.J.Chemistry, 20A, 322-325, April (1981).
7. Magnetic, Spectral, Thermal and Electrical properties of polychelates, Die Angewandte Makromolekulare Chemie, 97, 67-77 (1981).
8. XPS studies on thermal switching in Al-Vanadium phosphate glass-Al sandwiches (To be communicated).
9. Electrical and structural properties of V_2O_5 doped RuO_2 thick film resistors (to be communicated).
10. Silver migration studies in Pd-Ag conducting thick films (Under preparation).